APPROVAL SHEET

Title of Dissertation: Polyurethane Nanocapsules in Biomaterials

Name of Candidate: Sydney Menikheim

Master of Science, 2019

Dissertation and Abstract Approved: 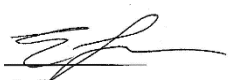

Dr. Erin Lavik

Associate Dean of Research and Faculty Development

Chemical, Biochemical, and Environmental Engineering

Date Approved: 04/30/2019

NOTE: *The Approval Sheet with the original signature must accompany the thesis or dissertation. No terminal punctuation is to be used.

ABSTRACT

Title of Document: POLYURETHANE NANOCAPSULES IN BIOMATERIALS

Sydney Danielle Menikheim, Master of Science, 2017

Directed By: Associate Dean of Research and Faculty Development, Dr. Erin Lavik, Chemical, Biochemical, and Environmental Engineering

Despite the growth in the field of self-healing materials over the past twenty years, no capsule-based self-healing systems have been trialed clinically.[1] This project aims to improve the lifespan of dental and orthopedic restorations by allowing dental resins and bone cement, respectively, to autonomously self-heal when either system experiences any type of degradation. Two different types of capsules were synthesized, one containing an initiator and one encapsulating a monomer, both in polyurethane shells. The monomer used was triethylene glycol dimethacrylate (TEGDMA). The initiator capsules synthesized contained benzoyl peroxide (BPO) and butylated hydroxytoluene. When released from the two types of nanocapsules, the encapsulated contents created a self-healing effect as the BPO initiated the TEGDMA to polymerize. The effects of the monomer capsules in epoxy resins were studied via tensile tests. The capsules reduced the strength of the resins; however, the capsules cracked during the resin fracture and a self-healing effect resulted.

POLYURETHANE NANOCAPSULES IN BIOMATERIALS

By

Sydney Danielle Menikheim

Thesis submitted to the Faculty of the Graduate School of the
University of Maryland, Baltimore County in partial fulfillment
of the requirements for the degree of
Master of Science, Chemical and Biochemical Engineering
2019

Acknowledgements

As I reflect on my project and time at the University of Maryland, Baltimore County (UMBC), I would first like to express my gratitude to Dr. Erin Lavik for her patient guidance, enthusiastic encouragement, and helpful critiques of this research work. I would next like to thank my committee members, Dr. Erin Lavik, Dr. Jennie Leach, and Dr. Doug Frey, for their continuous support through my proposal and now through my thesis defense. I would also like to extend my thanks to the entire CBEE department. I appreciate all of the lessons I have learned and all the direction I received throughout my six years at UMBC as both an undergraduate and graduate student. I would also like to thank the Naval Medical Research Unit San Antonio (NAMRU-SA) who spearheaded this project.

Next, I would like to thank Dr. Mark Zupan and his Micromaterials Characterization Lab for their help with the mechanical testing in this project. I would also like to extend my thanks to each and every person in the Lavik Lab, Nuzhat Maisha, Narendra Goud Pandala, Devorah Cahn, Justin Hosten, Abir Rauf, Grace Jones, Josh Leckron, Tobias Coombs, Catie Spencer, Adam Day, Rakan El-Mayta, and Trevor Smith, for their friendship and assistance in the lab. I would especially like to thank the undergraduate researchers who worked with me on this project, specifically Justin Hosten, Abir Rauf, and Grace Jones.

Furthermore, I would like to express my appreciation for our technician, Victor Fulda, for all of his help throughout my years at UMBC. I would also like to thank the members of the MCAC lab in addition to the Keith R. Porter Imaging Facility for their help along the way.

Lastly, I would like to thank my family and friends for all their support through my education here at UMBC. I know I would never be where I am today without their constant encouragement, patience, and understanding. I thank them for reading over all the papers I asked to be edited, listening to all the complaints I had, comforting me when I convinced myself that I would never complete my project or even come close to graduating, and supporting me in all of my academic decisions.

Table of Contents

List of Figures

Chapter 1: Introduction

1.1 MOTIVATION

Self-healing materials, those with the ability to automatically repair themselves and recover functionality without human intervention, are yet to be addressed fully and trialed clinically but have become an increasingly predominant topic of research for the past twenty years.[1] Many types of self-healing systems exist and have the potential to be used in a variety of areas in the body including neurology, orthopedics, and dentistry. The capsule-based self-healing system is one commonly studied self-healing system, with intended uses in both dental resins and bone cements.

Dental diseases are the most prevalent chronic diseases worldwide and are costly burdens to health care services.[2] Dental caries (tooth decay) is considered a major part of oral disease globally, affecting nearly 100% of the population in most countries.[3] To treat dental caries, diseased tissue is removed, and teeth are restored with appropriate materials.[4] In place of amalgams, dental resins (composites) have been increasingly used for dental restorations.[4] In addition to providing a smaller risk of toxicity, dental resins have become increasingly popular because they are aesthetically pleasing, as they are tooth-colored, and they are able to adhere to remaining tooth tissues.[4] However, durability is a major problem in posterior composites, as the typical life-span of posterior composites ranges from 3 to 10 years. Large fillings usually persist fewer than 5 years.[5] Bernardo et al. evaluated a total

of 1,748 restorations across a 7-year span and concluded that the overall survival rate of the amalgam restorations was 94.4% while that of composite restorations was 85.5%. Additionally, the risk of secondary caries was 3.5 times greater in composites than in amalgams.[6] Shrinkage stresses are the Achilles heel of composite resin restoration. Contraction stress is caused by a variety of factors, such as material formulation and polymerization factors, cavity geometry, and placement techniques. These stresses lead to many issues including, but not limited to, tooth flexure, post-operative sensitivity, and craze lines in marginal areas.[7] Micro-cracking is also highly problematic. Micro-cracks are caused by mastication forces and thermal stresses. If left untreated, this "fatal deterioration" can cause catastrophic failures in restorations.[8] For this reason, as dental resins are becoming increasingly more prevalent yet still problematic, the implantation of a capsule-based self-healing system into the resin to heal small cracks without human intervention appears to be an innovative and sustainable mechanism to reduce the number of repeat dental restorations occurring.

Similar to dental resins, bone cement, used in orthopedic restorations experiences analogous durability issues. Bone cement is a space-filler that holds the implant solidly in place.[9] It relies on close mechanical interlock between the bone surface and the prothesis.[10] In terms of orthopedics, the main role of bone cements is to increase the load carrying capacity in the prothesis-bone cement-bone system.[11] More than 500,000 hip arthroplasty procedures alone are performed every year in the United Kingdom and United States, and this number is expected to double within the next two decades.[12] Despite the growing frequency of total hip arthroplasties, the revision burden has remained unchanged, with instability causing 23% of revision cases and mechanical loosening triggering 22% of

revision cases.[12] Ultimately, the success of a cemented total joint replacement depends largely on the mechanical integrity of the bone cement.[13] Failure or fracture in the bone cement leads to loosening and failure of the prosthesis.[14] For this reason, imbedding a capsule-based self-healing system within bone cement has the potential to increase the longevity of prostheses by mitigating cracks in the cement without human intervention thus reduces the risk of revision.

Although self-healing systems promise a more sustainable society, these systems still have many barriers to overcome to even be trialed clinically. Such barriers include biocompatibility and a standardization in testing protocols to determine healing efficiency. The next logical step to better develop capsule-based self-healing systems, to be used clinically, is to establish a better comprehension of these systems both chemically and mechanically.

1.2 HYPOTHESIS

In this work, the following ideas were tested:

1. The monomer, triethylene glycol dimethacrylate (TEGDMA), and the initiator, benzoyl peroxide (BPO) and butylated hydroxytoluene, can be encapsulated separately by polyurethane (PU) nanocapsules via a poly-condensation in a two-phase system through mini-emulsions.
2. Embedding PU nanocapsules encapsulating TEGDMA in a resin will affect the mechanical properties of the resin.

3. When a resin containing PU nanocapsules encapsulating TEGDMA is cracked, the capsules will also break.
4. Adding PU nanocapsules encapsulating TEGDMA to a resin in addition to BPO will result in a self-healing effect when the capsules burst as the resin is cracked via a tensile test.
5. PU nanocapsules can be used in drug release systems. The capsules can be triggered to burst via sonication or can be used for long-term sustained drug release.

1.3 THESIS OVERVIEW

The history of self-healing materials for both dental and orthopedic uses is reviewed in chapter 2. In chapter 3, the synthesis procedure for the monomer PU capsules is discussed, and in chapter 4, the synthesis procedure for the initiator PU capsules is discussed. In these chapters the characteristics of the monomer and initiator capsules prepared are also identified. Ultimately, in these two chapters, the first hypothesis is tested. Chapter 5 includes a comparison of two types of resins. One of the resins contains monomer capsules and the other contains no monomer capsules. The effects the capsules have on the resin's mechanical properties are described. Additionally, the self-healing efficacy in the resins is also recognized. Overall, the second, third, and fourth hypotheses are trialed. In chapter 6, additional uses of PU capsules are conferred. A release study is reviewed in order to determine if the capsules can be used for drug delivery purposes. Principally, the last hypothesis is investigated. Chapter 7 includes a summary of all of the work performed in this thesis in addition to future works that need to be performed and the broader impact of the work. Chapters 3 through 6 are intended to be able to stand alone outside of this thesis.

These chapters include 4 major sections: introduction, materials and methods, results and discussion, and conclusion.

Chapter 2: Literature Review: Next Generation of Biomaterials: Self-healing

2.1 INTRODUCTION

Self-healing materials are a class of smart materials that have the autonomic ability to repair themselves and recover functionality after degradation, damage, and/or failure, without intervention.[15] Although unknown at the time, the first example of a synthetic self-healing effect in materials was utilized in ancient Roman constructions, which are still standing today.[16] The Romans used mortar as glue to bind together the bricks used to develop stone bridges and aqueducts. This mortar, which consisted of volcanic ash and lime, acted as a synthetic self-healing agent.[17] Ultimately, rain water dissolved the lime, which then seeped into other places, such as cracks in the construction. When the water vaporized, the lime was deposited in the cracks, hardened, and repaired the structures locally.[18]

Largely inspired by biological systems, self-healing approaches to combat structural failures are currently being explored, and have become an increasingly popular area of study over the last two decades.[19] The development of self-healing materials allows for autonomous repair *in situ* on the microscopic level before macroscopic failures ensue.[20] These materials can be of utmost value societally and economically, as they inspire sustainable manufacturing and construction. Self-curing properties can be integrated into many different materials including polymers and composites, asphalt and concrete, coatings, metals and ceramics, and micro-electronics.[16]

2.2 SELF-HEALING MATERIALS

First published in 1969, self-healing has been investigated substantially; however, since 2001, the rate of study and publications has significantly increased.[1, 21] When "self-healing biomaterial" was used as the key words in a web of science search, only 1 article appeared to be published in 2001; however, 70 publications were present in 2018. Today, many types of design strategies exist to form self-healing materials. These include the release of healing agents, reversible cross-linking, electrohydrodynamics, shape-memory effects, conductivity, and co-deposition.[22] These various types of self-healing systems can be generally divided into three overarching categories: intrinsic, vascular, and capsule-based.[23] Intrinsic self-healing involves healing through the inherent reversibility of bonds which acts as the healing agent. In these systems, self-healing occurs at the molecular level, and bond forming reactions develop after a source of energy induces the mobility of the molecules.[24] Vascular self-healing incorporates healing agents into the matrix through hollow micro-channels.[24] When vascular systems are damaged, self-healing agents are released; however, these networks are able to be refilled by an external source or from an undamaged connecting vascular network.[23] Capsule-based self-healing materials sequester the healing material in discrete capsules.[23] These capsules are usually microcapsules or nanocapsules. Microcapsules and nanocapsules are vesicular, hollow, spherical structures composed of a polymer matrix.[25] When the capsules are physically damaged, for example, by the propagation of a crack in the resin, the initiator and the reactants encapsulated are released and allowed to react together. Ultimately, healing occurs when the self-healing agent is released from the capsules, fills the cracks, and polymerizes; this polymerization

bonds the crack together and inhibits farther propagation of the crack.[26] Diba et al. recently redefined the characterization of these self-healing systems and separated them into merely two categories: extrinsic and intrinsic. Materials with extrinsic self-healing capacity require "external aid." This external aid includes capsules and vascular systems that contain self-healing agents to enable self-healing. Intrinsic materials can self-heal without any external aid.[27]

Self-healing systems have great aptitude in many biomedical applications that experience physiological stresses; however, self-healing materials have yet to be trialed clinically due to both technical optimization constraints as well as issues with toxicity and biocompatibility.[28] Some applications in which self-healing biomaterials would provide a crucial impact are artificial heart valves, vascular grafts, bone cements, dental implants, and intraocular lenses. These materials often experience crazes and microcracks that form to relieve internal and external stresses in high pressure areas;[20] therefore, the self-healing counterpart to these materials have the potential to be superior to the non-self-healing materials, but none have been tested clinically.

In particular, biomaterials in dentistry and orthopedics have become increasingly studied. The biomaterials that will be more thoroughly investigated in this review are dental composites and bone cements. Both types of biomaterials are commonly comprised of a methacrylate resin. Methacrylate is a monocarboxylic acid anion that forms when a proton is removed from the carboxylic acid group of the methacrylic acid. Figure 1 depicts the two-dimensional structure of a methacrylate.[29]

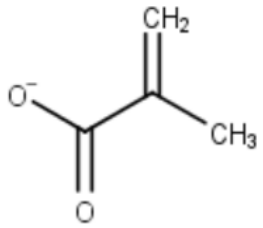

Figure 1. Methacrylate is a key component of both dental resins and bone cements.

2.3 DENTAL COMPOSITES

Arguably some of the first self-healing biomaterials to reach clinical trials, dental resins are consistently on the leading edge of novel materials in biomedical applications. Resins have been replacing traditional mercury-comprised amalgams for dental restorations, whose toxicity, both biologically and environmentally, has been debated for many years.[30] Dental resins are composite materials containing organic fillers and additives bound together with a polymer matrix used for dental reconstruction.[31] Dental resins have been conventionally formed via methacrylate chemistry, as previously mentioned, such as BisGMA (bisphenol A glycidyl dimethacrylate), TEGDMA (triethylene glycol dimethacrylate), BisEMA (ethoxylated bisphenol-A dimethacrylate), and UDMA (urethane dimethacrylate). However, the longevity of dental resins is limited.[32]

Although there are over one hundred published, peer reviewed studies pertaining to dental composites clinically, clear reasons for the failure of these composites have not been established; therefore, the capability to predict the clinical performance of dental composites has not been significantly advanced in nearly twenty years.[33] Mechanically speaking, the structural integrity of resins is compromised by one or a combination of the

following types of wear: fatigue, cracking and chipping, dislocation from the base, and the formation of wear particles.[28, 34-35] Apart from the mechanical problems of the dental resin, issues can also arise from polymerization shrinkage, polymerization-induced stress, a thermal expansion mismatch, abrasion and resistance, marginal leakage, and toxicity.[36] In one study performed by Opdam et al., the main reasons for composite failures were restoration fracture, caries (particularly secondary caries), root canal therapy, defective margin, and lack of proximal contact.[37] Out of the 290-million cavities restored each year in the United States, 200 million are replaced due to failed restorations.[38] This is problematic not only because failed restorations are expensive, but also because their failure can lead to life-threatening conditions. If a crack forms in the composite, one must obtain an entirely new composite; if the crack is left untreated, infection under the filling can develop.[39] To combat the frequent failures in dental composites and reduce the risk of infection, a variety of cutting edge biomaterial innovations are being trialed.[40]

Some current research thrusts related to the development of sustainable dental resins include stress-reducing materials, degradation resistant materials, and as previously stated, self-healing materials.[33] These improvements would limit the formation of gaps in resins resulting from stress generation at the bond interface.[41] The intent behind developing stress-reducing materials is to modify the polymer network so that it simultaneously reduces stress and enhances mechanical properties and monomer conversion in the resin.[41] To design degradation resistant materials, alternative resin chemistries have been proposed altogether. One study performed by Bacchi et al. formulated composite materials modified with thio-urethane additives to access the degree of conversion, reaction kinetics, bulk

mechanical properties, and polymerization shrinkage and stress.[41] Modified chemistries have also been trialed. Methacrylamide monomers have demonstrated more stability in aqueous environments, unlike the traditionally used vinyl bonds and methacrylate monomers. Several bisacrylamides have been evaluated as potential crosslinkers for dental resins.[42] Additionally, other chemistries, such as thiol vinyl sulfone polymerization, vinyl ether homopolymerization, and azide-alkyne click polymerization, have been evaluated as alternatives for the conventional methacrylate chemistry in dental resins.[43-45]

2.4 BONE CEMENTS

Similar to dental composites, bone cements, specifically polymethyl methacrylate (PMMA), are attractive biomaterials in which to implement self-healing properties. First used about 60 years ago, PMMA is a matrix used to bind the stem of an implant to the surrounding boney tissue.[46-47] Bone cement is not a glue but instead more of a space-filler that holds the implant solidly in place.[9] It relies on close mechanical interlock between the bone surface and the prothesis.[10] In terms of orthopedics, the main roles of bone cements are to increase the load carrying capacity in the prothesis-bone cement-bone system (also known as the construct).[11] Ultimately, the bone cement transfers stress from the prothesis to the bone cement and to the bone.[48] More specifically, PMMA bone cement is a two component thermoset that does not require post-polymerization modifications.[28] Methyl methacrylate is a methyl ester of methacrylic acid; it is a reactive resin whose polymerized form is used as a cement in areas such as dentistry, orthopedic surgery, and ophthalmology.[29] Figure 1 depicts the two-dimensional structure of methyl methacrylate.

Bone cement is in high demand, as the number of hip and knee arthroplasties in 2017 were over 1.6 million, of which 966,000 were knee replacements.[49] Kim et al. analyzed data in the Nationwide Inpatient Survey from 1997 to 2004 and described the recent trend of hip and knee replacements in the United States. This finding can be seen in Figure 2.[50] Although the predictions are a bit higher than the statistics reported in 2017 for primary total knee replacements, the trends in this graph do portray the rapid increase in the amount of hip and knee arthroplasties in the past 20 years.

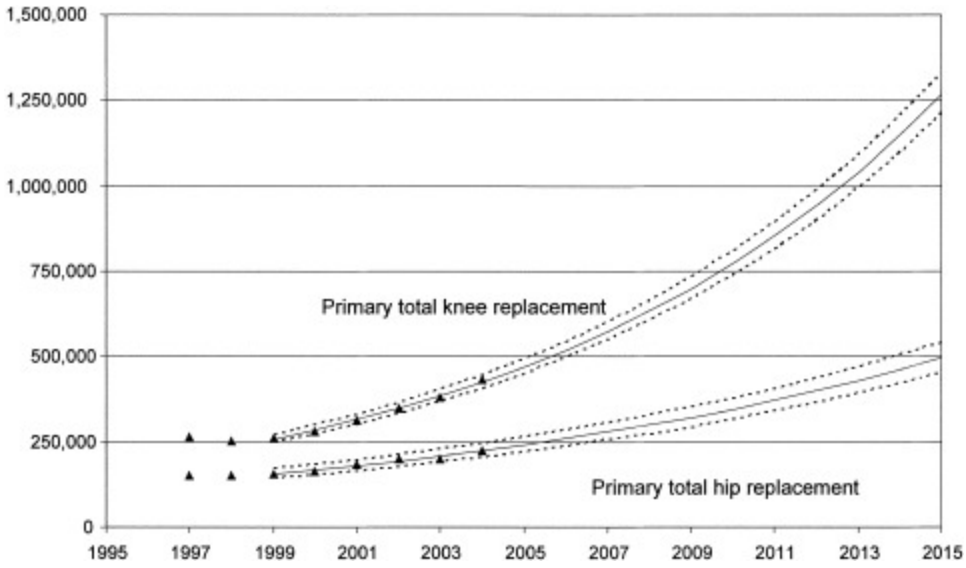

Figure 2. This figure portrays the trends in primary total knee replacement and primary total hip replacement between the years 1997 and 2004 in the United States. The trend in this graph predicted a rapid increase in primary total hip and knee replacements in the United States from 1995 to 2015.[50]

Though bone cement continues to be largely coveted, bone cement has a plethora of drawbacks including but not limited to chemical and thermal necrosis of the bone,

shrinkage of the cement during polymerization, a large stiffness mismatch between the cement and the adjoining bone, weak zones which consist of the interfaces between the bone cement and the prothesis and the bone cement and the bone, and cement particle interaction with the surrounding tissues.[11, 51-54] Mechanical failure in bone cement is postulated to be one of the main causes of mechanical failure in protheses, especially hip arthroplasties.[55] Hill et al. stated that a successful total hip replacement has a lifetime of 10 to 20 years with over 75% of failures caused by aseptic loosening, which is directly related to cement mantle failure.[56] Aseptic loosening is "a multifactorial phenomenon involving interfacial failure, bond failure, bone remodeling, and cement failure.[53] Bone cement failure can be caused by joint loosening, microcrack formation and accumulation through cyclic loading, and creep under compression.[28] It is important to note that PMMA, as an acrylic cement, is reasonably strong in compression but since it is a brittle material, it is prone to fracture resulting from tensile stresses.[57] Mechanical failure in the bone cement can result in an increase in cement particles which interact with the surrounding tissues and can contribute to an inflammatory response, increased bone destruction, and accelerated prothesis loosening (which frequently requires correction via revision surgery).[58]

Improvements to bone cement have been made; these improvements can be separated into 3 distinct categories: changing the cement mixing methodologies, reinforcing the existing cements, and developing new formulations.[48] Modern mixing techniques have been utilized to reduce porosity, a suspected cause of fatigue failure in the bone cement. These techniques include mixing the cement in a vacuum and centrifuging the mixture during curing.[59] A review by Arora et al. concluded that there are many bone cement additives

including but not limited to steel fibers, glass fibers, carbon fibers, and titanium fibers; however, none of these additives perfectly enhance strength without inducing adverse effects. The authors suggest that mechanical strength and interface integrity should be improved through the use of rubber-toughened cements, amphiphilic bonders, and increased trabecular bone concentrations. The field of nanotechnology also holds promise.[60] In terms of new formulations for bone cement, there are other types of commercially available bone cement such as calcium phosphate cements (CPCs) and glass polyalkenoate cements (GPCs); however, there formulations have low mechanical strength. [10]

2.5 CAPSULE BASED SELF-HEALING SYSTEMS

Conceivably the most curious type of resin which has been limitedly explored in dental and orthopedic systems is the implication of self-healing materials in resins. It is hypothesized that if the microcracks are healed when the crack first forms, then catastrophic failure in the resin can be avoided, ultimately reducing the need for revisions.[61] Self-healing resins have proven to be able to self-repair when degraded or damaged to avoid complete failure in the composite and are thus highly sustainable. One self-healing material that has been frequently trialed to improve the longevity of dental resins and bone cements is the capsule-based self-healing system. The capsules in these self-healing systems are tiny particles that contain core materials encapsulated by coatings or shells.[62] Ultimately, the approaching crack bursts the embedded capsules, which then release healing agents into the crack via capillary action.[8] This results in polymer crosslinking and

repair in the damaged resin.[40] The same type of capsule-based self-healing system can be used in both dental resins and bone cements theoretically because both of these resins experience similar types of failure. This type of healing is classified as extrinsic self-healing because it relies on the release of healing liquids from embedded capsules.[27]

Tremendous strides have been made in the generation of self-healing materials, particularly for capsule-based self-healing systems; however, much is still to be learned to better optimize this technology for all self-healing systems. It is important to note that all the materials involved in the system must be carefully engineered to ensure proper bursting of the capsules when needed. It is important for the capsules to not prematurely rupture before the propagation of a crack but to rupture in a timely matter in the presence of a crack. To warrant this, the encapsulation procedure must be chemically compatible with the healing agent. Furthermore, the capsule walls need to be resistant enough to withstand the physical stresses they must endure when implanted into a material but also adhere to the composite material to burst during the onset of composite fracture.[15] Capsule characteristics can vary depending on the intended system. These capsule characteristics include resultant morphology, average size, size distribution, shell thickness, mechanical properties, content and reactivity of encapsulated agent, and shelf-life.[15, 63-64] These characteristics are reliant on solvent types and amount, surfactant type and amount, temperature, pH, agitation rate, reaction time, and mode of addition of the oil phase to the aqueous phase.[63]

Controlling the size of the self-healing capsules has proven to be extremely important. The size of the capsules strongly depends upon the application of the self-healing system.

Larger capsules contain a bigger volume of healing chemicals and allow bigger cracks to be healed. Conversely, large capsules negatively influence the propagation of cracks as well as the roughness of the material's surface; therefore, it has proven more beneficial to use smaller, nano-sized capsules. Although the nano-sized capsules are limited in their healing ability due to the reduction in the volume of the healing agents that can be delivered from one capsule, the smaller capsules are thought to more efficiently heal nano-sized cracks in the material in which they are implanted before the cracks can propagate into more sizeable cracks.[24]

The choice of capsule shell material is also an important aspect of the self-healing system. Perhaps the most common material is urea-formaldehyde (UF). This material displays good thermal stability; however, it has its drawbacks. Aggregated nanoparticles debris have reportedly formed when synthesizing UF microcapsules; these nanocapsule aggregates could potentially act as crack initiation sites. Furthermore, the rough agglomerated nanocapsules on the surfaces of the microcapsules could decrease the adhesion of the capsules to the composite in which it is added. Lastly, the rubbery and thin capsule walls threaten the containment of the self-healing material before the onset of a crack in the composite.[15, 64]

Other capsule shell materials that have been successfully synthesized include melamine-formaldehyde (MF), melamine-urea-formaldehyde (MUF), and polyurethane (PU).[15, 62, 65-67] Melamine-formaldehyde is thermally stable up to 69°C and has reportedly had a shell thickness up to 30.0 μm. Due to the high thermal stability of the crosslinked MF and the

formation of a smooth surface, MF capsules with dicyclopentadiene has proven to have better thermal stability when compared to UF capsules encapsulating dicyclopentadiene.[62] Liu et al. observed that MUF microcapsules showed narrow size distribution with shell thickness ranging from 700 to 900 nm. The capsules appeared to have neat outer surfaces with minor roughness and were thermally stable up to 300°C. Overall, Lui et al. reported that capsules composed of MUF had superior properties compared to those made of UF used for self-healing systems to date. Additionally, the synthesis of MUF microcapsules was noted to be significantly easier than that of UF.[67] PU is a commonly used polymer. The shell thickness has been found to be roughly uniform and in the micrometer range (1-15 μm); this acts as an appropriate barrier to premature leakage and to prevent premature rupture.[68] It has been used in the health field for nearly half a century and is one of the most popular groups of biomaterials applied to medical devices.[69] Specifically, PU are block copolymers, made of two or more polymeric blocks attached by covalent bonds. Due to their block-copolymer character, polyurethanes have a wide range of versatility in terms of their physical properties and ability to biodegrade. Proven to be biocompatible, PU is formed by the chemical reaction between isocyanates, that have more than one reactive isocyanate group (-NCO), and alcohols, with two or more reactive hydroxyl (-OH) groups per molecule; this reaction forms repeating urethane groups.[69] The thermal stability in polyurethanes is also thermally stable in the body, as the thermal decomposition temperature for urethane linkages ranges from 150 to 250°C.[70]

There are two overarching categories used to organize self-healing capsule-based systems: dual and mono capsule self-healing systems.[1] A comparison of these capsule systems is

shown in Figure 3. Dual capsule self-healing systems contain two sets of capsules, one set containing the monomer and the other set comprising the hardener/polymerizer/catalyst.[1, 63] Mono capsule self-healing systems include only one set of capsules. These capsules can incorporate a range of healing agents, such as reactive chemicals, suspension solvents, low melting point metals, and monomers (with catalysts suspended freely in the matrix). These mono capsule systems also include all-in-one capsules where both the monomer and required catalyst are either held in the core of the capsule, separated by layers, or are encapsulated in separated smaller spheres that are stored within a larger sphere. These capsules are also susceptible to rupture during crack formation. When the capsule cracks, the healing agent is released and the self-healing is achieved,[1] as shown in Figure 4.[8, 71]

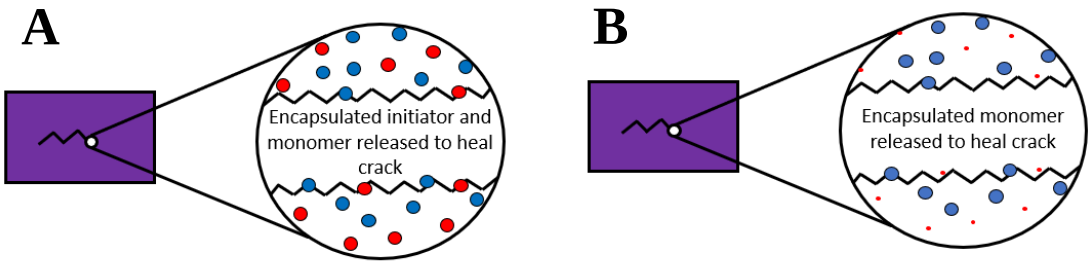

Figure 3. (A) The dual capsule based self-healing system contains 2 sets of capsules, one with the monomer and one with the initiator. (B) The mono capsule based self-healing system only contains one set of capsules.

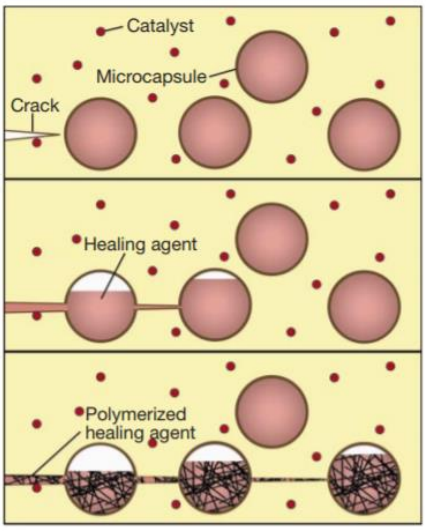

Figure 4. This image depicts microcapsules with healing agents added to a composite matrix containing catalyst throughout the composite as in a mono capsule self-healing system. From top to bottom of this image, one can see a crack forming in the matrix. In the second box, the crack ruptures the capsule and releases the self-healing agent. Then, in the bottom box, the healing agent comes into contact with the catalyst and polymerization occurs.[8]

For use in biological systems, the most important factor to examine is the biocompatibility of the self-healing system; if the system effective in healing a crack but toxic, its usefulness is futile. Self-healing material formulations proposed for a biomedical application must pass both ASTM and ISO standards for mechanical and biocompatibility characterization of the materials.[72] The first recognized self-healing capsule-based system in polymer composites, a mono capsule-based system, consisted of dicyclopentadiene encapsulated in a poly (urea-formaldehyde) shell that formed a microcapsule (50 to 200 um). Grubb's catalyst was used to initiate the polymerization of the dicyclopentadiene. This first-generation self-healing system relied on ring opening metathesis polymerization and

proved to self-heal efficiently in an epoxy matrix, yielding up to 75% recovery in toughness in the matrix. Until 2001, the only successful crack healing methods reported required some form of manual intervention.[8] For dental use, Wertzberger et al. characterized the self-healing system consisting of encapsulated dicyclopentadiene and Grubb's catalyst and achieved a recovery of 57% of the virgin fracture toughness of the composite.[73] Biggs et al. further studied the dicyclopentadiene/Grubb's catalyst system and demonstrated significantly lower crack propagation rates in Surgical Simplex P, a commercially available PMMA bone cement, specimens with the self-healing system compared to the specimens without the self-healing system.[74] However, high cost and toxicity concerns curbed the use of both dicyclopentadiene and the Grubb's catalyst in dental composites.[75-76]

Another, more recent, study developed nanocapsules with triethylene glycol dimethacrylate (TEGDMA) liquid encapsulated in polyurethane. In this study, no self-healing effect was reported since no catalyst for polymerization was present.[77] When microcapsules with polymerizable TEGDMA with N,N-dihydroxyethyl-p-toluidine (DHEPT) healing liquid in poly (urea-formaldehyde) shells were prepared by Wu et al. in a mono capsule self-healing system with benzoyl peroxide (BPO), the catalyst, freely added to the resin, self-healing efficiency showed that about 65% of the virgin fracture toughness could be achieved when using 15% microcapsules. The microcapsules also

proved to have low cellular cytotoxicity.[75] Figure 5 shows an optical image of the microcapsules synthesized by Wu et al.

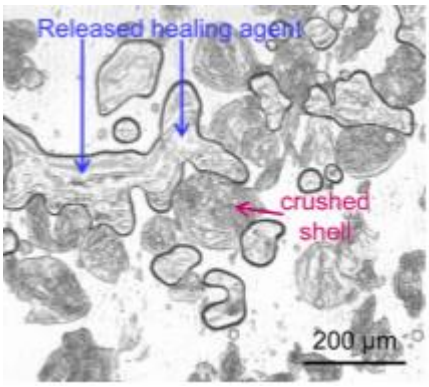

Figure 5. This figure displays an optical image of crushed microcapsules and the healing liquid films being released from the capsules.[75]

Wilson et al. developed an example of a dual capsule self-healing system to be used in bone cement. UF microcapsules containing BPO were embedded in epoxy vinyl ester resin samples. When a mixture of acrylic monomers and tertiary amine activators were injected into a cracked plane of the sample after initial fracture, an estimated 80% healing efficiency was recorded in preliminary tests. This study focused on the free-radical-initiated polymerization of acrylates because after investigation, this chemistry stands out as "the most attractive chemistry for designing a self-healing system for bone cements." Unfortunately, a dual capsule self-healing system was not fully developed in this study since the main objective was to determine the peroxide initiator best suited to the diverse demands of various self-healing systems.[54] However, in 2013, using the findings from Wilson et al., Dailey et al. created a dual UF microcapsule self-healing system, shown in Figure 6. The initiator capsules contained BPO, and the monomer/activator capsules contained 4'-methylenebis(N,N-dimethylaniline) (MBDMA) (the tertiary amine),

trimethylol-propane ethoxylate triacrylate (TMPET) (an acrylate monomer), and bisphenol A ethoxy-late diacrylate (Bis-EMA) (an acrylate monomer). When tested, this system restored approximately 75% of the original fracture toughness at room temperature in an EVE matrix. Although initially intended for use in bone cement, the possible applications for this system have not been fully explored.[78]

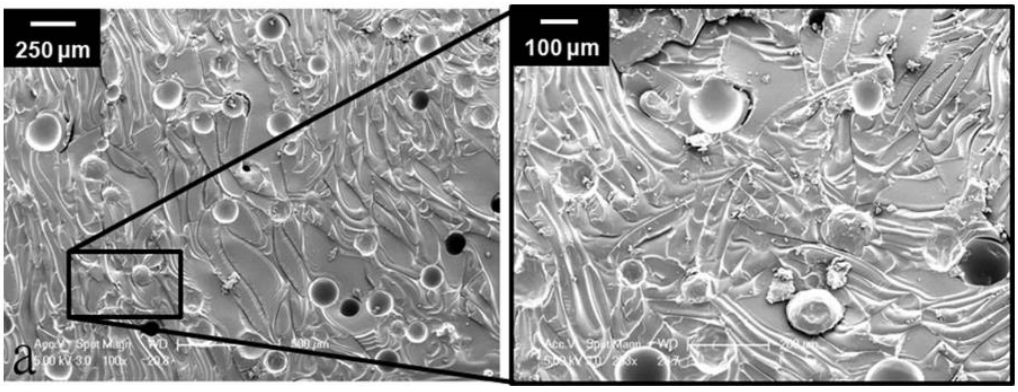

Figure 6. This SEM image portrays the healed fracture plane for the dual UF microcapsule self-healing system (10 wt % capsules loadings).[78]

Thus far, more mono capsule self-healing systems have been developed. In 2015, Gladman et al. developed a thermoplastic solvent-healing method for bone cement. In this single, biofriendly capsule approach, microencapsulated solvent was embedded in Simplex P bone cement. In this approach, the self-healing polymerization does not rely on chemical reactions or external stimuli, and the capsules can be added as an independent component of the bone cement formulation.[79] Brochu et al. also fabricated a capsule-based self-healing system using only materials that are currently in clinical use. This system encapsulated the water reactive healing agent, 2-octul-cyanoacrylate (OCA) tissue adhesive, in PU microcapsules. The capsules were then dispersed in a matrix of Palacos R PMMA bone cement.[72] Like Gladman's system, this is a catalyst free self-healing bone cement system.

The most recent mono capsule self-healing system intended for use in either dental composites or bone cements was the model published by Huyang et al. in 2016. The self-healing dental composite contained a healing powder, strontium fluoroaluminosilicate particles, and a healing liquid, aqueous solutions of polyacrylic acids. The powder was freely present throughout the composite; however, the healing liquid was encapsulated in silica microcapsules. When the microcapsule cracks, the healing liquid is released, interacts with the healing powder, and reacts to form glass ionomer cements (GIC) within the crack. Figure 7 depicts the self-healing steps in this model.[80]

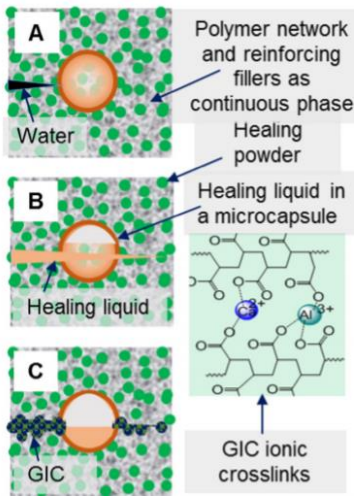

Figure 7. This image portrays the self-healing dental composite developed by Huyang et al. (A) A crack forms, and water enters the composite. (B) A microcapsule is broken due to the propagation of the crack, and the healing liquid is released. (C) The healing liquid and healing powder react to form GIC.[80]

2.6 CONCLUSION

Moving forward, it is necessary to investigate the use of capsule self-healing systems further, both dual and mono capsule-based systems testing both microcapsules and nanocapsules. For capsule based self-healing systems to be used clinically, they must first reach clinical trials. This means the systems must be biocompatible, implying they must be synthesized with only non-toxic materials. The greatest challenges currently arise from a lack of standard protocols for reliable and comparative quantification of the self-healing properties.[27] However, this statement alone creates yet another challenge in the field. Self-healing systems are intended for various areas of use in biological systems. Even when comparing the same areas in one species, differences can arise. These dissimilarities result from the individuality of each organism. For example, when developing self-healing systems for dental resins in the mouth, it is important to account for the fact the oral environment can vary from person to person. These disparities result from not only bacteria cultures present but even the alignment of the teeth in the mouth.[81-82] Despite this, a model must be devised for each area intended for self-healing usage. The model must test the self-healing system both statically and dynamically. An example of such a device is the Rub&Roll, "an in vitro fatigue and/or wear simulator enabling controlled application of force, speed, type of liquids, and duration, to mimic challenges representative for the human oral environment."[83]

Despite the growth in the self-healing material field over the past twenty years, to date, no capsule-based self-healing systems for biomaterials have been trialed clinically. Capsule-

based self-healing systems have the capability to have a significant effect in many areas in today's world, including, but not limited to, biomechanics and construction. These capsules, if optimized well, can exhibit high shell strength while rupturing under external force and releasing the healing agent to the damaged area without any human intervention.[84] The most relevant reason to use materials that can heal themselves is the necessity of reliable and durable materials. Self-healing materials can overcome current limitations and prevent the significant failures that are currently commonplace in structures that experience high physiological stresses, including, but not limited to, dental composites and bone cements. Ultimately, self-healing materials reduce the cost for restorations and creates a more sustainable society.

Chapter 3: Synthesizing Polyurethane Capsules that Encapsulate Triethylene Glycol Dimethacrylate

3.1 INTRODUCTION

The idea of self-healing materials stems from nature, specifically in the way living multicellular organisms are able to freely repair themselves without external intervention.[85] These materials, if utilized correctly, could create a more sustainable society. Self-healing materials are a rapidly emerging class of materials with applications intended for use in a wide range of industries including but not limited to civil, electrical, aerospace, and medicine.[86] This study will focus on creating a self-healing system for clinical usages for utilizations in both dental resins and bone cements. Both dental resins and bone cements experience breakdown in structural integrity.[28, 34-35, 55]

Specifically, in this study, we present the first phase of the development of a dual capsule self-healing system to be used in both dental resins and bone cements. The self-healing system can potentially be implemented into both of these biomaterials because they are very similar. Both types of biomaterials are commonly comprised of a methacrylate resin.

In this dual capsule self-healing system, the healing agents, the monomer and the initiator, will be stored separately in nanocapsules. This capsule-based system allows for the localization of reactivity within the crack in the resin.[85] Inclusion of hollow capsules filled with the healing agent may influence the tensile and compressive strength of resin. Moreover, after release of the healing agent, spherical, cylindrical or tubular holes remain in the structure. Therefore, capsule dimensions need to be small enough in order not to

change the properties of the structure too much.[1] For this reason, nanocapsules are being synthesized to house the self-healing agents. In general, spherical capsules will have less influence on the mechanical properties as their shape reduces the stress concentrations around the void left from empty capsules.[87]

The capsules will be dispersed throughout the resin in high concentrations.[85] This will ensure that when a crack propagates through the resin, the capsules will burst, releasing the healing agents which will polymerize to heal the crack.[85] Figure 8 presents a depiction of the dual capsule self-healing system in a dental resin. This dual capsule-based self-healing system holds the potential to significantly extend the lifetime of the materials by preventing and repairing failures which are caused by the accumulation of microcrack formation.[86]

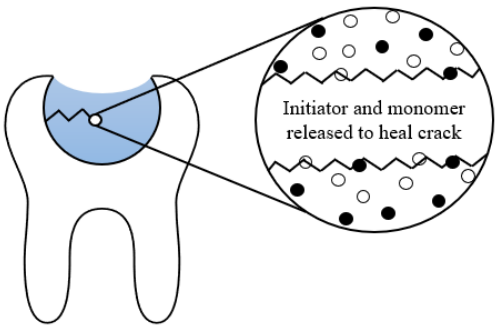

Figure 8. When the capsules are physically damaged by the propagation of a crack in the resin, the (encapsulated) initiator and the monomers are released and allowed to react together. This results in polymer crosslinking and repair in the damaged dental resin.[40]

The dual capsule self-healing system consists of polyurethane (PU) nanocapsules that encapsulate the initiator and monomer. PU has been chosen to encapsulate the monomers because PUs have been used in the health field for nearly half of a century and are one of

the most popular groups of biomaterials applied to medical devices.[69] PU is also very compatible with blood.[88] Due to their block-copolymer character, polyurethanes have a wide range of versatility in terms of their physical properties and ability to biodegrade. Polyurethane, through the years, has proven to be extremely biocompatible as well as thermally stable in the body.[69] Triethylene glycol dimethacrylate (TEGDMA) is the monomer of choice. Benzoyl peroxide (BPO) is employed as the initiator. The self-healing aspect of the composite is comprised of a two-part monomer-initiator polymerization system made solely from materials that are classified by the U.S. Food and Drug Administration as Generally Recognized as Safe (GRAS) to eliminate complications concerning biocompatibility.[75] In this chapter, we focus on the encapsulation of TEGDMA in a PU nanocapsule shell.

3.2 MATERIALS AND METHODS

3.2.1 Materials

All materials were obtained from commercial suppliers and used without further purification. Sodium dodecyl sulfate (SDS) (BP166, Fisher Scientific) and 99% pure hexadecane (AC120465000, ACROS Organics) are the surfactant and costabilizer, respectively, used to form the PU nanocapsules. Isophorone diisocyanate (IPDI) 98% (AC427602500, ACROS Organics) and 1,6-hexanediol (HDOH) 97% (AAA1243930, ACROS Organics) are the reactants from which PU is formed. Triethylene glycol dimethacrylate (TEGDMA) 95% (261548, Sigma Aldrich) is the monomer encapsulated in the PU nanocapsules. Fluorescein (free acid, dye content 95%) (F2456, Sigma-Aldrich) was the fluorescent molecule that was encapsulated in the PU shell and used to quantify

the total mass that the PU nanocapsules can encapsulate. Phosphate buffered solution (PBS) was used when determining the amount of fluorescein encapsulated. One PBS tablet (P4417, MilliporeSigma) dissolved in 200 mL of deionized water yielded 0.01 M phosphate buffer, 0.0027 M potassium chloride, and 0.137 M sodium chloride, pH 7.4, at 25 °C.

3.2.2 Preparation of Monomer Capsules

PU nanocapsules encapsulating TEGDMA were synthesized following procedures previously published in literature.[89-90] PU nanocapsules were formed via a poly-condensation in a two-phase system through mini-emulsions. Specifically, hexadecane (HD) and deionized (DI) water formed the two phases, an oil phase and an aqueous phase. SDS was used as the surfactant to confer colloidal stability. In this reaction, SDS helped to control the equilibrium between the rates of fusion and fission during sonication, which ultimately dictated the size of the droplets that form.[90]

Once the 70 mL of DI water, 1.145 mL of HD, and 0.88 g of surfactant (SDS) were mixed together at 300 rpm and 40°C for 1 hour, 2.094 mL of IPDI and 6.1 mL of TEGDMA was slowly dripped into the mixture and stirred; this step began the synthesis of the nanocapsules. It is important to note that IPDI is hydrophobic. By dripping the IPDI and monomer into the solution, the IPDI was evenly distributed throughout the oil phase. As the IPDI and TEGDMA entered the pre-emulsification solution, the stirring speed was increased to 400 rpm. Once the IPDI and TEGDMA were fully injected into the beaker, the solution was left to mix at 400 rpm and 40°C for 10 minutes. During this step, the solution turned an opaque white. Next, the solution was sonicated with a 130-Watt

Ultrasonic Processor with Thumb-actuated Pulser at an amplitude of 38% to break up any IPDI molecules that had aggregated. During this step, emulsions formed, and the solution looked like milk. While sonication was still progressing, an aqueous solution of 5.9 g of HDOH and 10 mL of DI water was dripped into the system. Because of the high reactivity of the isocyanate, the IPDI reacted immediately with the HDOH at the interface of the two phases.[90] The synthesis process is portrayed in Figure 9, and Figure 10 shows a flow diagram to summarize the reaction.

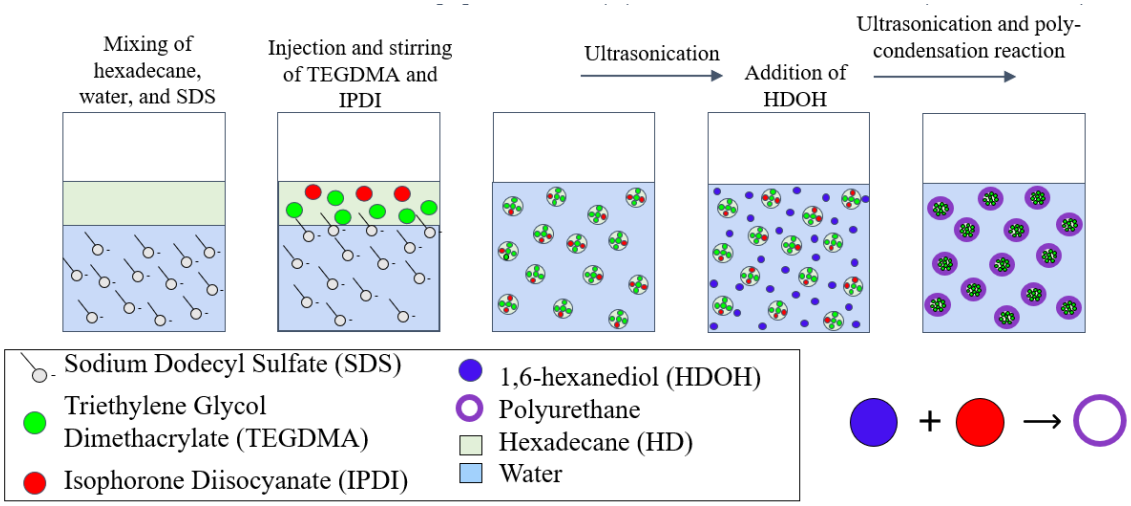

Figure 9. The synthesis method for the monomer capsule is depicted. Note that the SDS is a surfactant. It acts as a stabilizing agent and is always present; however, it is not depicted fully in each step to avoid cluttering the image.

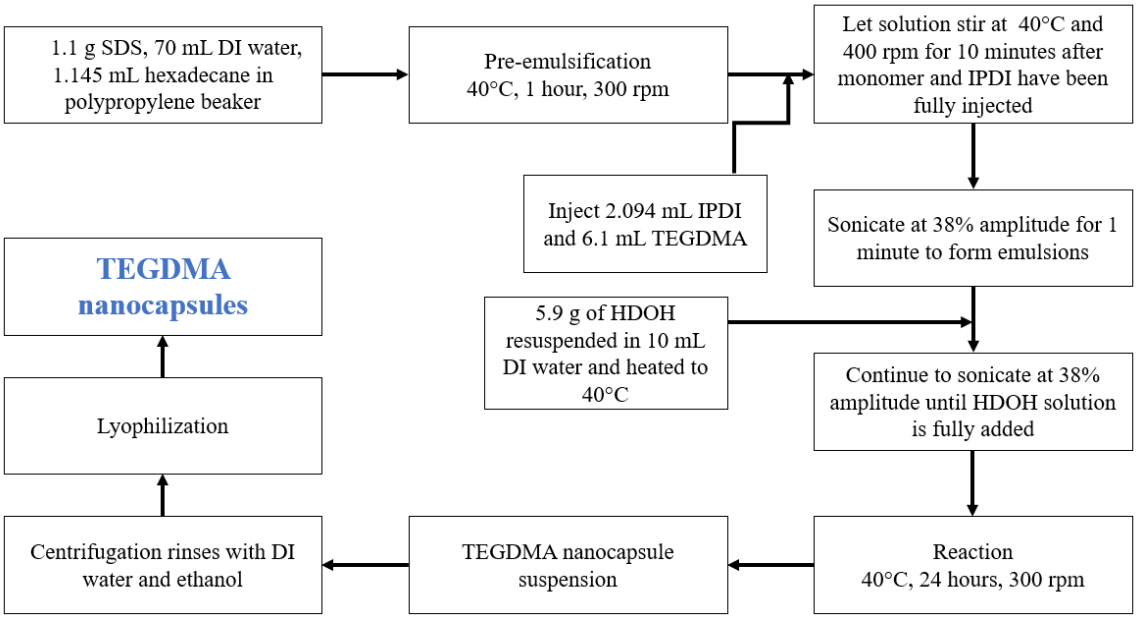

Figure 10. This flow diagram summarizes the synthesis method for the monomer capsules.

After sonication, the solution was left to react for 24 hours at 40°C and mixed at 300 rpm. After 24 hours, much of the solvent had evaporated and a clear, viscous solution with a solid, white sphere was left in the beaker. The solution was washed to rid it of excess reactants or other contaminants. First, the solution was centrifuged in DI water at 4,500 rpm and 4°C for 30 minutes. After the centrifugation, a hard, white substance appeared at the bottom of the centrifuge tube, a small semi-transparent layer was above the solid layer, and a cloudy, transparent water layer with an oily disk was on top. The disk and the water were removed, and fresh DI water was added to the centrifuge tube. The solution was vortexed and again centrifuged at 4,500 rpm and 4°C for 30 minutes. After the second wash, the solid, white pellet again appeared at the bottom of the centrifuge tube. The water layer was also present with a smaller oily disk on top. The water (supernatant) was again removed and replaced with fresh DI water. The solution was vortexed and centrifuged at 4,500 rpm and 4°C for 20 minutes. After this centrifugation, layers similar to those after

the second wash appeared. The supernatant was removed, and new DI water was added. The solution was vortexed and centrifuged at 4,500 rpm and 4°C for 20 minutes for a fourth and final time. After this centrifugation, the centrifuge tube contained mostly clear water and a sticky, solid, white substance at the bottom. The supernatant (the water) was again removed and the pellet was resuspended in fresh DI water; however, the pellet did not resuspend well. The partially resuspended pellet was then frozen in liquid nitrogen and lyophilized.

3.2.3 Characterization of Nanocapsules

Capsule morphology and size. A vacuum sputter coater (Denton Desk II) was used to deposit a 20 nm layer of gold palladium onto the nanocapsule samples placed on carbon tape on a specimen stub for scanning electron microscopy (SEM) imaging using the Nova NanoSEM 450 from FEI. The surface morphology of the capsules was examined as well as the diameters of the capsules.

Capsule size and zeta potential. The Malvern ZetaSizer (Nano ZS90) was used to determine the diameter and zeta potential of the nanocapsules via dynamic light scattering (DLS). The nanocapsules were placed in a 1mg/mL solution of 190 proof ethanol for sizing. This solution was pipetted into a cuvette (14955129, Fisher Scientific) which was placed into the ZetaSizer. The capsules were placed in a 1mg/mL solution of 10 mM potassium chloride (KCl) to determine the zeta potential. To measure the zeta potential, the solution was inserted into a folded capillary zeta cell (Malvern Store, DTS1070) which was placed in the ZetaSizer. Both the size and zeta readings were performed in triplicates.

Capsule molecular components and structures. Fourier-transform infrared (FT-IR) (PerkinElmer Frontier Optica) spectroscopy was used to produce spectrum to identify the molecular components and structures within the capsules. Gel Permeation Chromatography (GPC) (Viscotek, VE 2001) was used to measure the molecular weight of the PU in the capsules. The GPC column (PL1110-6504) is of the Agilent Plgel MIXED family. Its phase is MIXED-D, its inner diameter is 7.5mm, its length is 300 mm, and its particle size is 5 μm. To measure the molecular weight polyurethane, the capsule samples were first crushed via mortar and pestle. Then, 10 mg of the crushed sample was resuspended in 1 mL of tetrahydrofuran (THF). This solution was filtered with PTFE membrane syringe filters (Fisher, 09-720-002) into GPC vials (VWR, 89239-024) which were placed in the GPC for characterization.

3.3 RESULTS AND DISCUSSION

3.3.1 Optimization of Polyurethane Capsules

Polyurethane reaction. In order to optimize the monomer capsules, first the reaction to form PU was optimized. PU is formed by the chemical reaction between a di/poly isocyanate and a diol or polyol; this reaction forms repeating urethane groups, as shown in Figure 11.[69]

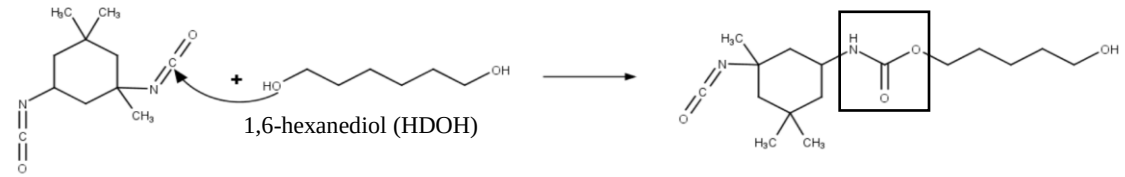

Figure 11. This reaction scheme depicts the nucleophilic attack that occurs as the positively charged carbon atom in the IPDI is attacked by the negatively charged oxygen atom in the HDOH molecule. The key is to form a urethane linkage as shown in the product molecule.

To form the PU nanocapsules, a 5:1 ratio of HDOH to IPDI was used to ensure end capping of the IPDI resulted during the reaction. To minimize the size distribution of the PU nanocapsules in the system, the amount of surfactant was varied. For SDS, the critical micelle concentration is 6 to 8 mM. This is the concentration of SDS in a bulk phase, in this case water, above which micelles start to form. In this particular formulation, with a total of 80 mL of DI water, this means a mass of 0.138 g of SDS or greater must be added in order to form micelles. GUO et al. in "The Role of Surfactant and Costabilizer in Controlling Size of Nanocapsules Containing TEGDMA in Miniemulsion" stated that a typical recipe to obtain PU nanocapsules encapsulating TEGDMA included 0.88 g of SDS and 0.88 g of HD.[90] Torini et al. reported preparing the miniemulsions with 0.66 g SDS and 0.66 g of HD.[89] The basic recipe for the preparation of miniemulsions is based on the dispersion of HD in the aqueous phase with the surfactant, SDS; however, the amount of HD and surfactant must be varied depending on what is being encapsulated.[89] Figure 12 shows the peak 1 average diameter sizes for the monomer capsules when the amount of SDS was varied. This graph compares the varying amount of surfactant used when the

amount of TEGDMA, hexadecane, water, IPDI, and HDOH were held constant. Note that the peak 1 value was used in Figure 12 due to the fact that large aggregates of capsules and/or polymerized TEGDMA had skewed the DLS readings in some samples since these particles were in the micrometer size range. The peak 1 has the largest percent intensity and is therefore the most abundant size encountered.

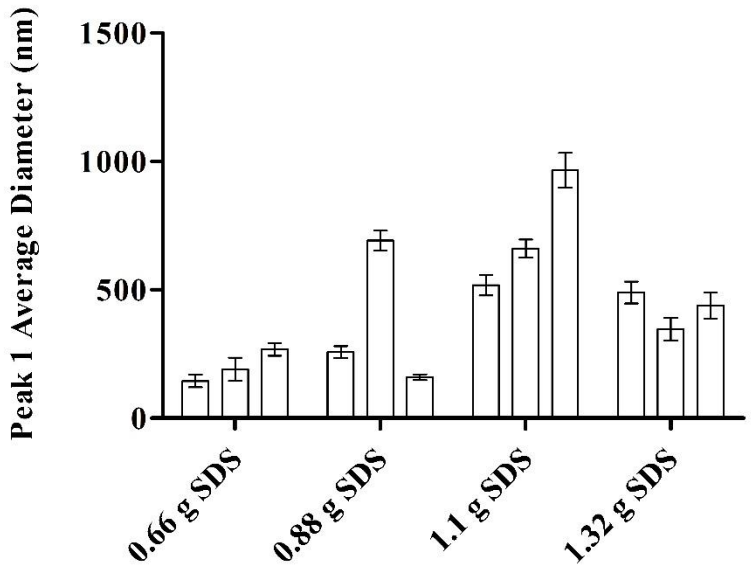

Figure 12. This figure depicts the average peak 1 diameter size in nanometers for the monomer capsules. In each synthesis, only the amount of surfactant changed. Three replicates were performed in each set; these are displayed as the three bars in each group. The error bars on each bar represent the standard deviation from the three DLS readings performed for each sample when sizing the particles.

In the reaction, the surfactant was anionic and provided stable miniemulsions.[89] The costabilizer allowed for the buildup of an osmotic pressure in the droplets which provided stability against Ostwald ripening.[89] During the reaction, to form both the monomer and

initiator nanocapsules, a stable miniemulsion was first obtained when the IPDI was added to the pre-emulsification solution and sonicated. Then, the HDOH was dissolved in the external phase and added to the miniemulsion. This addition leads to the reaction between the IPDI and HDOH at the interface of the two non-miscible phases (the water and oil phases).[89] From Figure 12, it is clear that the reactions were not easily repeatable. The bar graphs do not display a distinct, consistent trend in the size of the particles.

3.3.2 Monomer Capsule Characteristics

Currently, monomer capsules have been effectively synthesized. Figure 13 shows the SEM images of two different batches of monomer capsules made using an identical method. These capsules were made with 0.88 g of SDS. The size data for the monomer capsule samples are shown in Figure 14. Figure 15 shows the zeta potential data for the two samples. The FT-IR data for the two samples is shown in Figure 16, and the GPC data for the samples is shown in Figure 17.

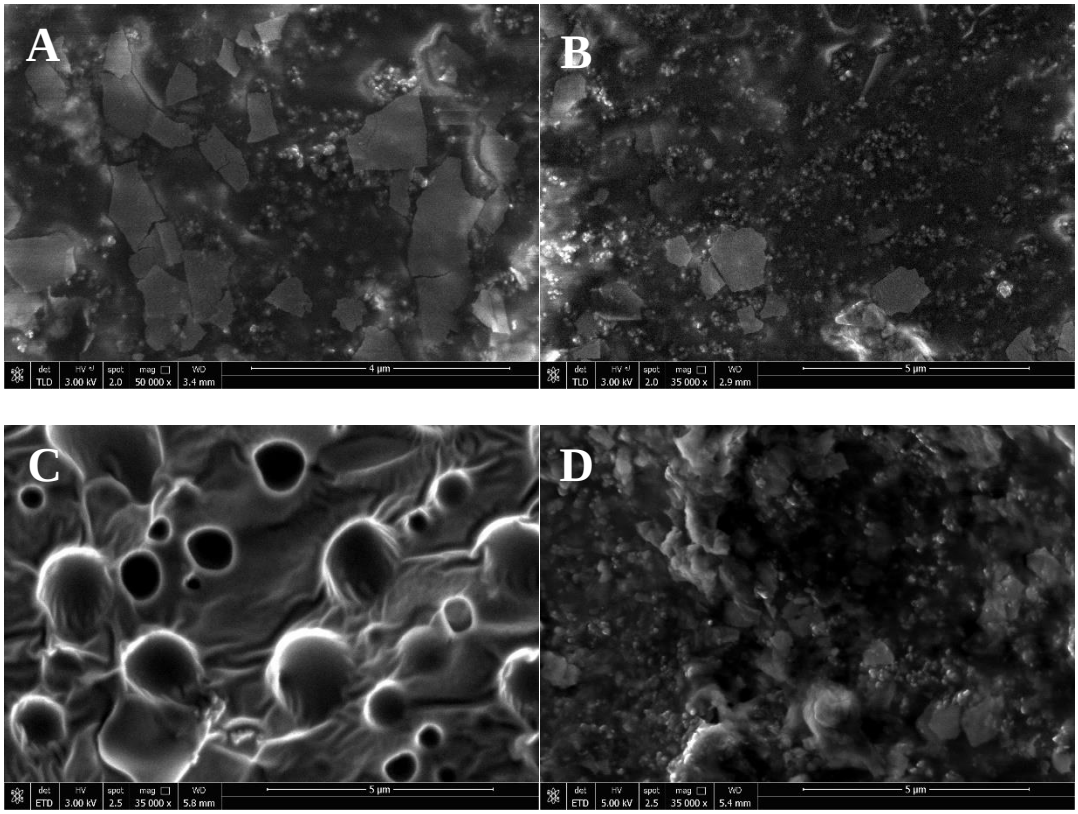

Figure 13. Images A and B are SEM images of monomer nanocapsules encapsulating TEGDMA from one sample. Images C and D are SEM images of monomer nanocapsules encapsulating TEGDMA from a different sample. Both samples were made following the same procedure with 0.88 g of SDS. The particles are the small white dots, especially evident in Images A, B, and D. The monomer particles appear to be trapped in the excess TEGDMA. This is especially evident in Image C.

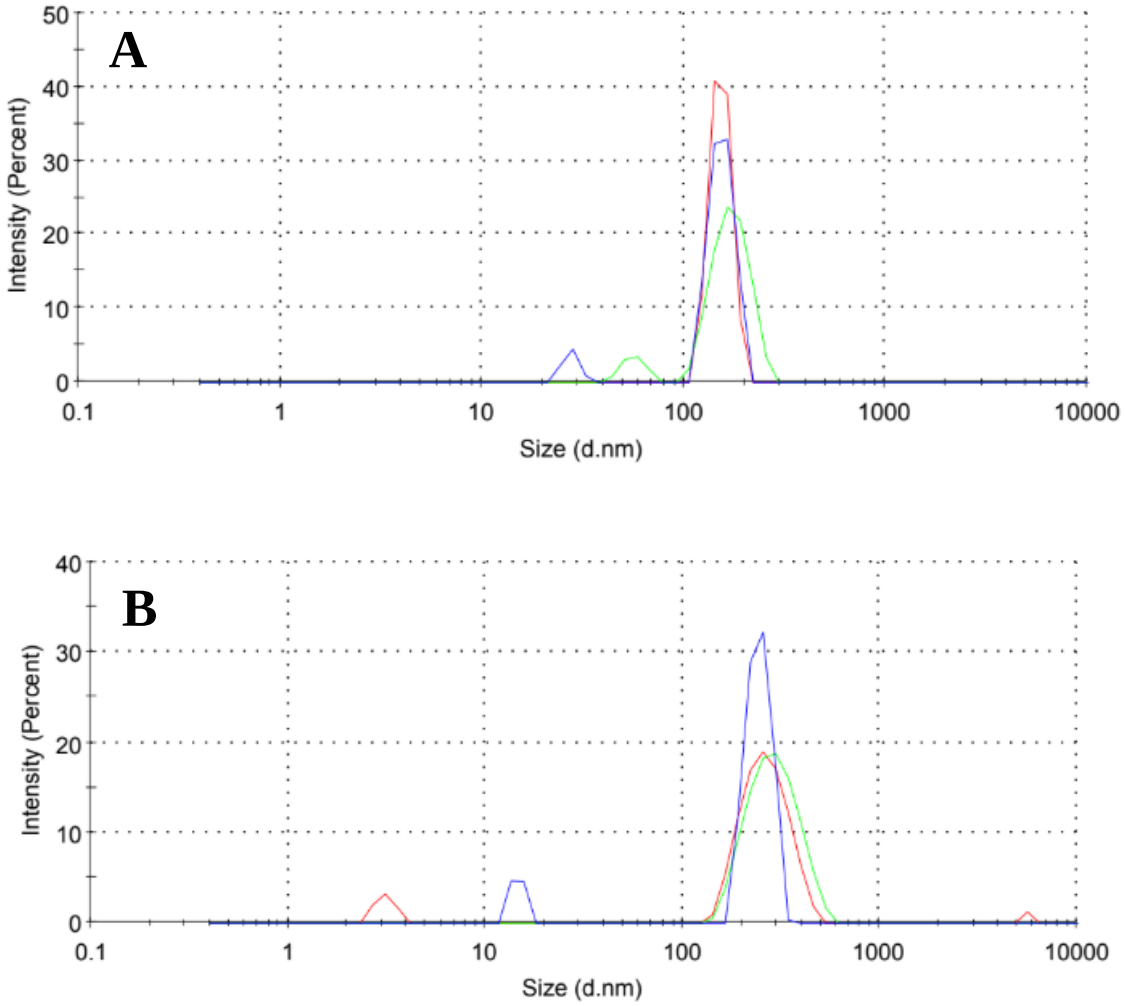

Figure 14. (A) The average diameter of the capsules shown in Figure 13 A and B is 299.6 nm, and the polydispersity index is 0.644. This information was collected using DLS. (B) The average diameter of the capsules shown in Figure 13 C and D is 260.2 nm, and the polydispersity index is 0.539. This information was also collected using DLS.

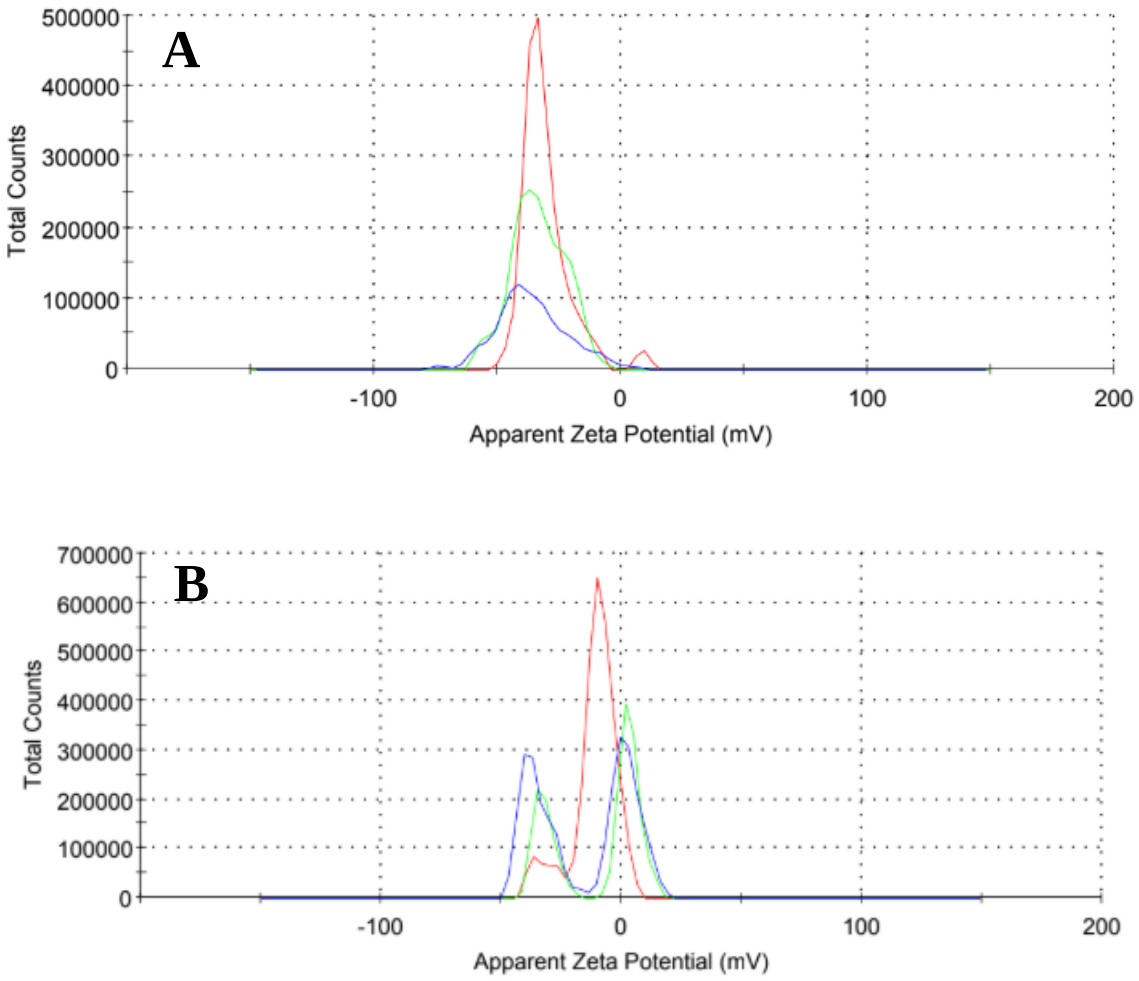

Figure 15. (A) The average zeta potential of the capsules shown in Figure 13 A and B is -33.4 mV, and the standard deviation is 11.9 mV. This information was collected using DLS. (B) The average zeta potential of the capsules shown in Figure 13 C and D is -17.1 mV, and the standard deviation is 18.2 mV. This information was collected using DLS.

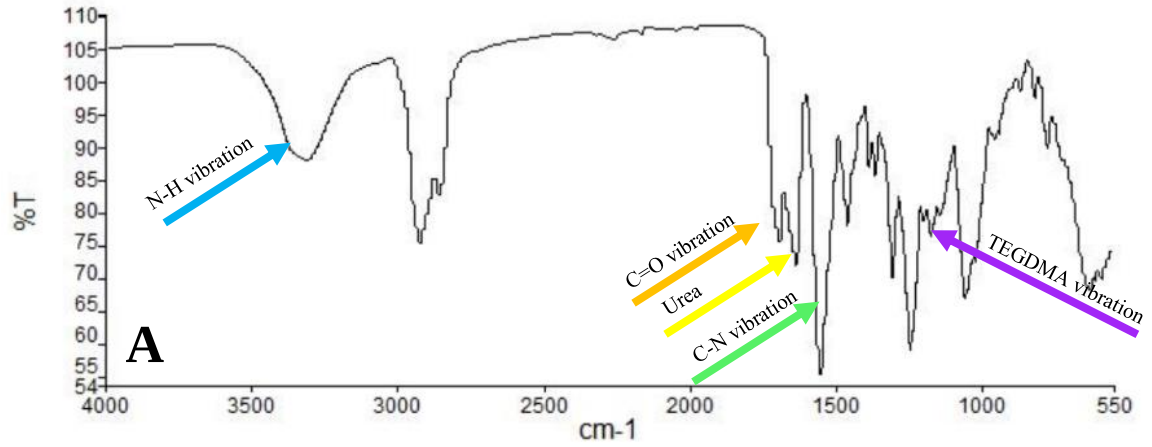
%T
cm-1
A
N-H vibration
C=O vibration
Urea
C-N vibration
TEGDMA vibration

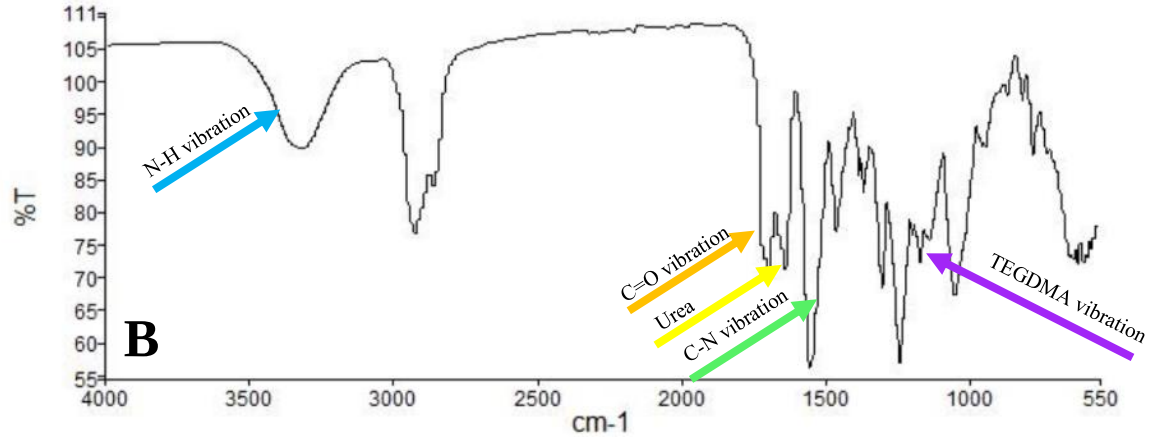
%T
cm-1
B
N-H vibration
C=O vibration
Urea
C-N vibration
TEGDMA vibration

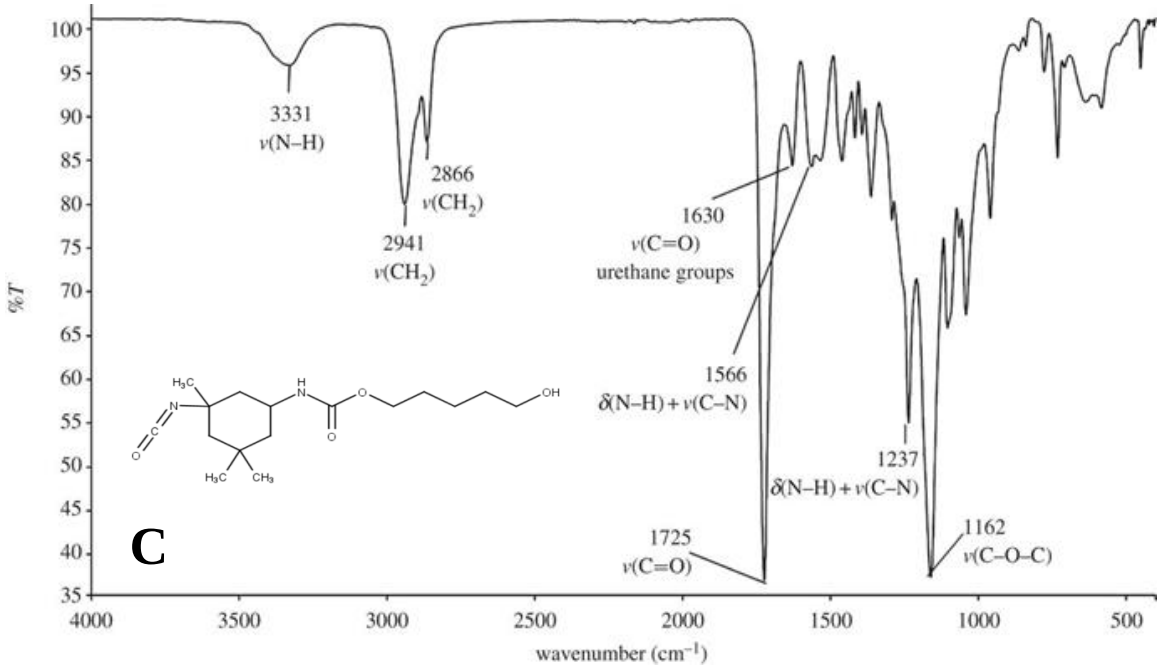
%T
wavenumber (cm⁻¹)
C
3331
ν(N–H)
2941
ν(CH2)
2866
ν(CH2)
1630
ν(C=O)
urethane groups
1566
δ(N–H) + ν(C–N)
1237
δ(N–H) + ν(C–N)
1725
ν(C=O)
1162
ν(C–O–C)

Figure 16. (A) The peaks obtained from FT-IR for the monomer nanocapsules shown in Figure 13 A and B are shown. (B) The peaks obtained from FT-IR for the monomer nanocapsules shown in Figure 13 C and D are shown. (C) The peaks obtained from PU found in literature are shown for comparison in addition to the urethane molecule itself. Overall, a lower transmittance percentage corresponds to a high population of bonds which have vibrational energies corresponding to the incident light. The purple highlighting represents the peaks associated with TEGDMA, present only in the monomer capsules. The green highlighting represents the C-N vibration in the urethane present in each capsule. The yellow highlighting symbolizes the urea carbonyl present in each capsule. The orange shows the C=O vibration present in each capsule. Lastly, the blue depicts the N-H vibration present in each capsule.[77, 91-93]

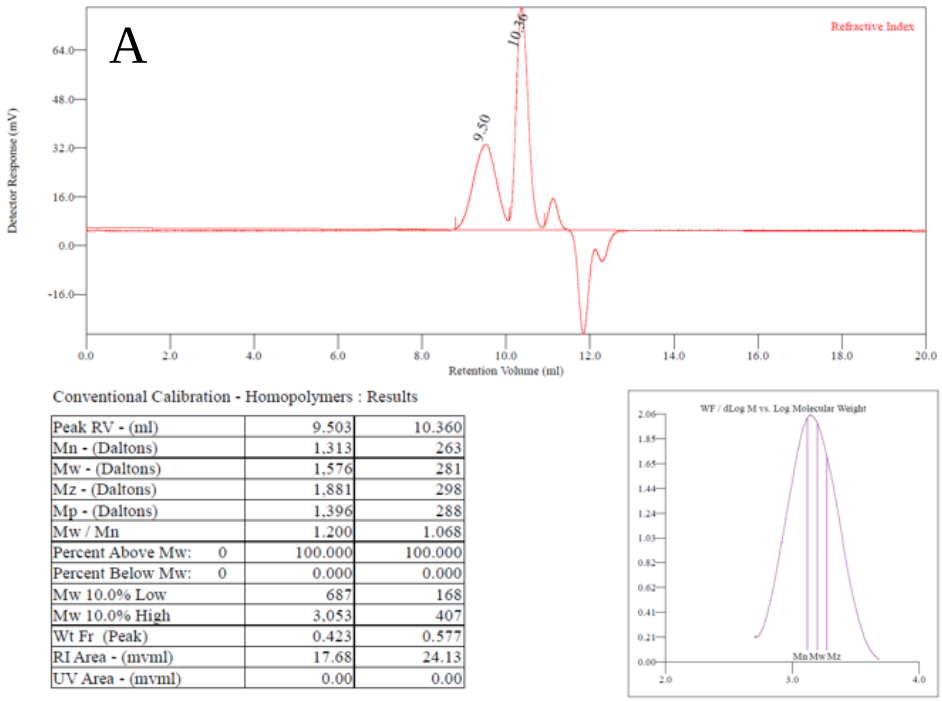

Peak RV - (ml)	9.503	10.360
Mn - (Daltons)	1,313	263
Mw - (Daltons)	1,576	281
Mz - (Daltons)	1,881	298
Mp - (Daltons)	1,396	288
Mw / Mn	1.200	1.068
Percent Above Mw: 0	100.000	100.000
Percent Below Mw: 0	0.000	0.000
Mw 10.0% Low	687	168
Mw 10.0% High	3,053	407
Wt Fr (Peak)	0.423	0.577
RI Area - (mvml)	17.68	24.13
UV Area - (mvml)	0.00	0.00

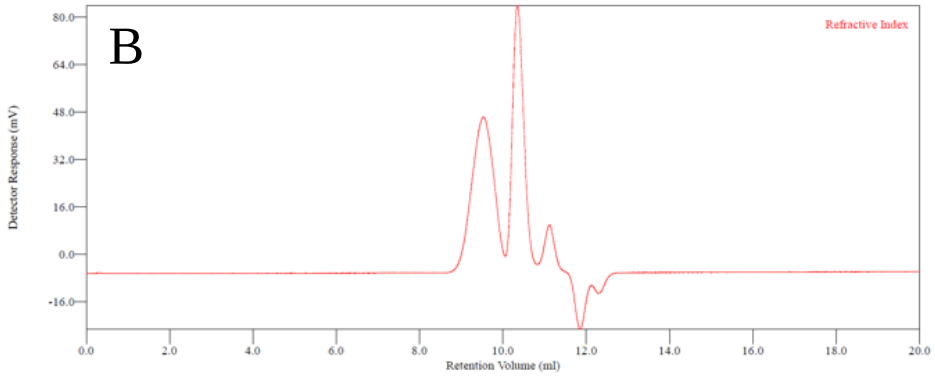

Conventional Calibration - Homopolymers : Results

Peak RV - (ml)	9.520	10.340
Mn - (Daltons)	1,294	287
Mw - (Daltons)	1,471	296
Mz - (Daltons)	1,667	306
Mp - (Daltons)	1,354	299
Mw / Mn	1.137	1.029
Percent Above Mw: 0	100.000	100.000
Percent Below Mw: 0	0.000	0.000
Mw 10.0% Low	750	214
Mw 10.0% High	1,948	403
Wt Fr (Peak)	0.507	0.493
RI Area - (mvml)	24.88	24.20
UV Area - (mvml)	0.00	0.00

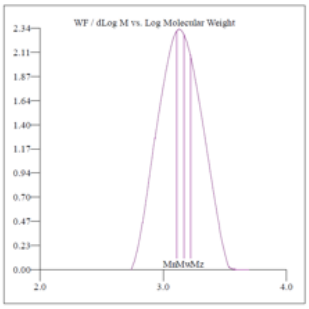

Figure 17. The GPC column's operating range is 200 to 400,000 Da. (A) The GPC data shows the molecular weight of the PU shell. The peak at 9.50 mL represents polyurethane. The number average molecular weight (Mn) is 1,313 Da, and the weight-average molecular weight (Mw) is 1,576 Da. The polydispersity (Pd=Mw/Mn) of the PU is 1.2. The peak at 10.36 mL represents butylated hydroxytoluene. This is the stabilizer in the THF. The last peak is a solvent peak. (B) The GPC data shows the molecular weight of the PU shell. The peak at 9.52 mL represents polyurethane. The number average molecular weight (Mn) is 1,294 Da, and the weight-average molecular weight (Mw) is 1,471 Da. The polydispersity (Pd=Mw/Mn) of the PU is 1.137. The peak at 10.340 mL represents butylated hydroxytoluene. Again, this is the stabilizer in the THF. The last peak is a solvent peak.

The molecular weight averages determined by GPC differ in meaning. The number average molecular weight (Mn) is the statistical average molecular weight of all the polymer chains

in the sample. It is defined in Equation 1 in which M_i is the molecular weight of the chains and N_i is the number of chains of that molecular weight. Unlike the number average molecular weight, the weight-average molecular weight (Mw) considers the molecular weight of a chain in determining contributions to the molecular weight average. Mw is defined in Equation 2. The polydispersity index (PDI) measures the broadness of a molecular weight distribution of a polymer. The PDI can range from 1 to 2. A PDI of 1 means all of the polymer chain lengths are equal and thus the polymer is very uniform. A larger PDI means a broader molecular weight distribution and less uniformity.

$$Mn = \frac{\sum N_i M_i}{\sum N_i} \qquad \textit{Equation 1}$$

$$Mw = \frac{\sum N_i {M_i}^2}{\sum N_i M_i} \qquad \textit{Equation 2}$$

According to the characteristics of the two monomer capsule samples, these capsules have nearly identical characteristics. This means the capsules have a PU shell and encapsulate TEGDMA.

According to Ouyang et al., TEGDMA within the nanocapsules is characterized through FT-IR with two characteristic absorption peaks, one around 1637 cm^{-1} for the C=C group and one at 1171 cm^{-1} for the C-O-C group. Both of these peaks are present in the spectra in Figure 16.[77] Further confirmation of the presence of TEGDMA within the capsules is found in Chapter 5 during the self-healing tests.

3.3.4 Self-Healing Reaction

Despite the difficulty TEGDMA presented during encapsulation, TEGDMA was the monomer of choice because it has proven to have a long shelf-life yet be reactive with fast kinetics when needed.[24] It is important for the healing liquid to have a relatively low viscosity to flow and fill the cracks of the resin matrix; TEGDMA is able to flow and has previously been used as a dental monomer with acceptable biocompatibility.[75] Additionally, TEGDMA can form a polymer via free-radical initiation by using a peroxide initiator (and a tertiary amine accelerator to speed the reaction).[24]

BPO was selected as the initiator because it is the best performing initiator across a wide range of evaluation criteria including reactivity, physical properties, and phases all studied by Wilson et al.[54] To produce the intended healing effect, BPO initiates the polymerization of TEGDMA via free-radical polymerization.[94-97] This reaction scheme can be seen in Figure 18. Note that although this figure depicts a free radical polymerization, a type of chain growth polymerization, the reaction is not a stereotypical chain growth polymerization. The end group of the TEGDMA (highlighted with a box in the figure) is the only part of the molecule that is able to stabilize the radical. For this reason, to form the polymer, only the end groups are able react with each other. This means the end groups with radicals must align to react. It also means the radicals are easily quenched. Thus, long chains do not form from this polymerization. Instead, polymer networks are formed, as shown in Figure 19.

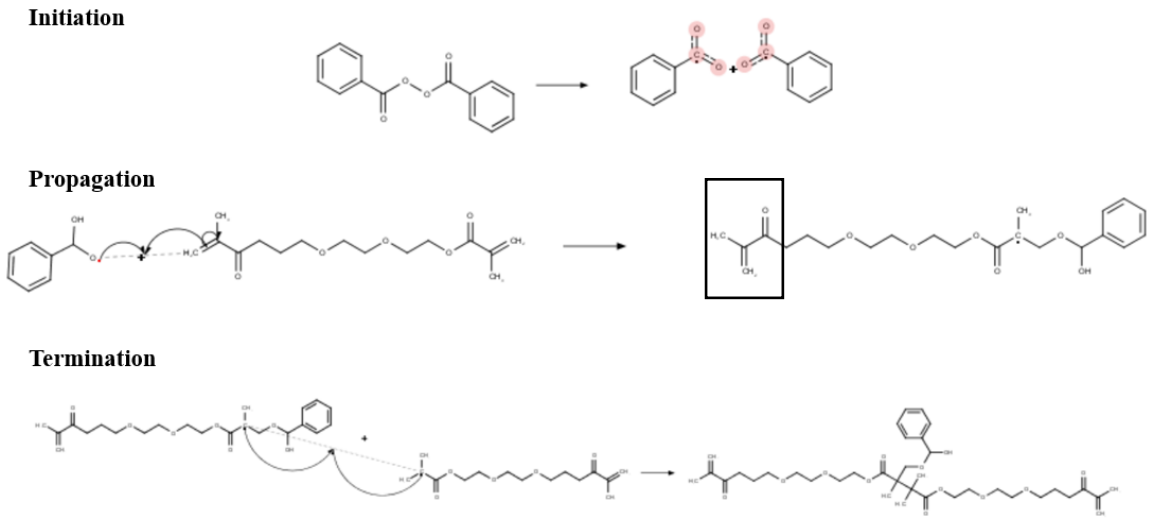

Figure 18. The reaction scheme depicts the polymerization of TEGDMA. There are three parts to the reaction mechanism: initiation, propagation, and termination. During initiation, a free radical is formed. This step leads to the propagation of the reactive intermediate, in this case TEGDMA, which is continuously regenerated during the course of the chemical chain reaction. During termination, the formation of reactive intermediates ceases, and the chain propagation step ends, effectively bringing the reaction to a halt. [94-97]

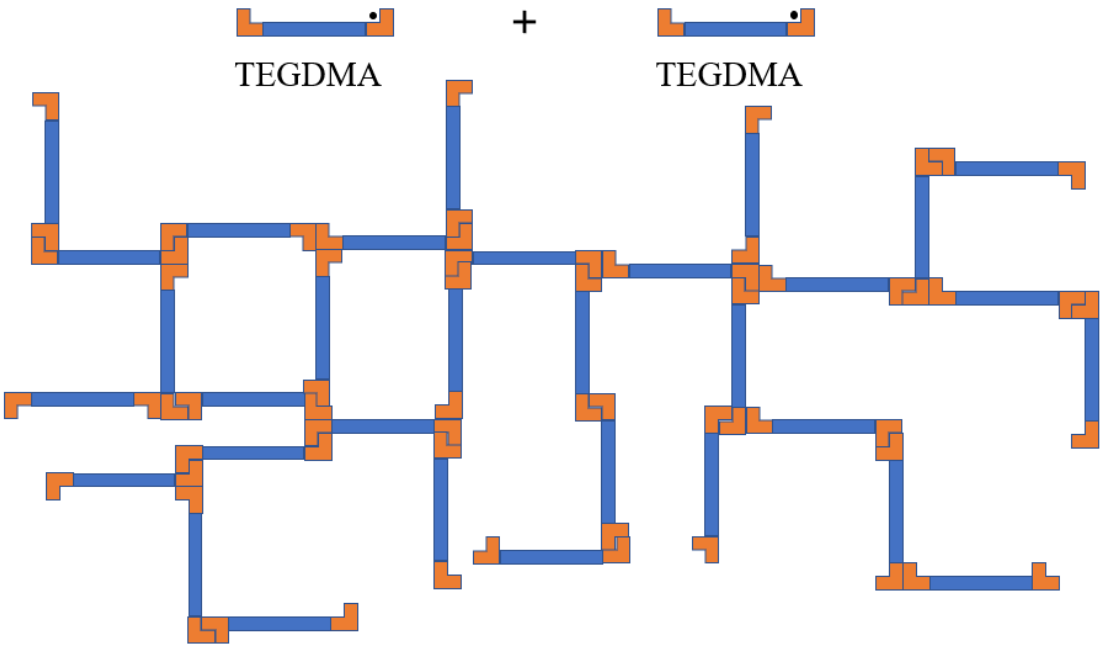

Figure 19. The schematic shows the free radical polymerization of the TEGDMA. Polymer networks form during polymerization.

To stabilize the BPO to ensure free radicals are not formed prior to its release from the capsule, butylated hydroxytoluene is used. This compound scavenges the free radical species that are responsible for peroxide formation and acts as an effective suppressor to peroxide formation.[98] Figure 20 shows the stabilization of BPO via butylated hydroxytoluene.

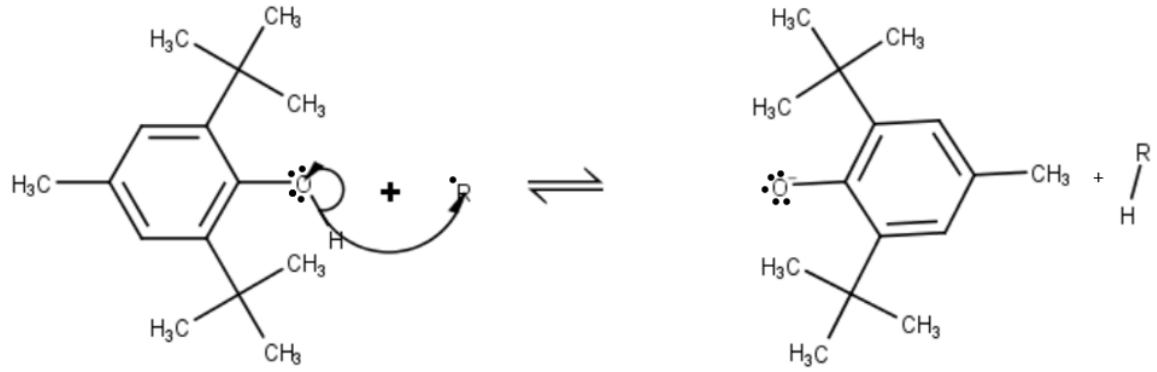

Figure 20. This mechanism shows the effective suppression of the free radical species that forms from BPO.

To accelerate the polymerization of TEGDMA in hopes to speed the healing process, 4-(N,N-dimethylamino)phenethyl alcohol (DMPOH) was added to the monomer capsule as an accelerator. Out of all the tertiary amine accelerators, DMPOH was chosen because of its good solubility and stability in TEGDMA.[99] DMPOH also has better biocompatibility than DHEPT, used by Wu et al.[100] Furthermore, DMPOH proved to have the highest accelerating ability when compared with other potential amines, such as trimethylaluminum (TMA) and 2-(dimethylamino) ethyl methacrylate (DMAEMA).[101] When DMPOH was added to the monomer capsules, it was hypothesized that the TEGDMA polymerized before the capsules even encapsulated it. This can be seen through the SEM images in Figure 21. As the amount of DMPOH was decreased, the amount of polymerized TEGDMA also appeared to decrease. For the time being, we decided to eliminate the use of DMPOH in the capsules until the amount of excess TEGDMA in the samples was reduced. TEGDMA is still able to polymerize without the inclusion of DMPOH in the reaction as DMPOH is merely an accelerator.

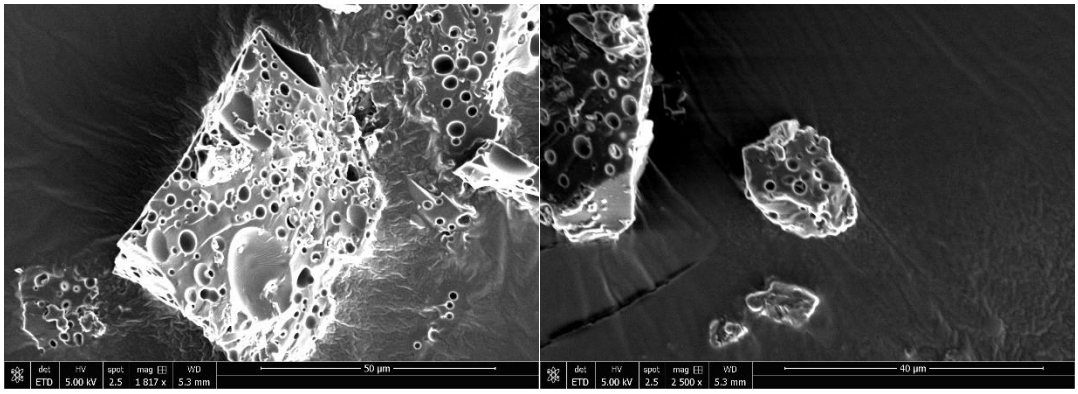

Figure 21. The SEM images support the hypothesis that adding DMPOH to the monomer capsules ultimately caused the TEGDMA to polymerize before the capsule could form around the liquid TEGDMA. In these images, the capsules are not present. A molar ratio of 1:200 moles of DMPOH to TEGDMA was added in the synthesis to produce this sample.

3.4. CONCLUSION

PU capsules that encapsulate TEGDMA were synthesized via a poly-condensation in a two-phase system through mini-emulsions. The capsules are one part of the dual capsule self-healing system. It was determined that 0.88 g of SDS is the optimal amount of surfactant needed to form nanocapsules near the 200 nm size range with a low PDI. The monomer capsules can be synthesized with consistency in size, zeta potential, and chemical composition over multiple batches; however, the samples contained excess TEGDMA that inhibited the identification of the pure monomer capsules. The encapsulation of BPO will be examined in the next chapter. In theory, the encapsulated contents, when released from the two types of nanocapsules, will be able create the self-healing effect as the BPO initiates the TEGDMA to polymerize.

Chapter 4: Synthesizing Polyurethane Capsules that Encapsulate Benzoyl Peroxide

4.1 INTRODUCTION

In order to create a dual-capsules self-healing system, the initiator and monomer must be separately encapsulated in polyurethane (PU) nanocapsules. Chapter 3 discussed the encapsulation of triethylene glycol dimethacrylate (TEGDMA); this chapter focuses on the encapsulation of the initiator, benzoyl peroxide (BPO) with butylated hydroxytoluene.

4.2 MATERIALS AND METHODS

4.2.1 Materials

All materials were obtained from commercial suppliers and used without further purification. Sodium dodecyl sulfate (SDS) (BP166, Fisher Scientific) and 99% pure hexadecane (AC120465000, ACROS Organics) are the surfactant and costabilizer, respectively, used to form the PU nanocapsules. Isophorone diisocyanate (IPDI) 98% (AC427602500, ACROS Organics) and 1,6-hexanediol (HDOH) 97% (AAA1243930, ACROS Organics) are the reactants from which PU is formed. Benzoyl peroxide (BPO) (S25672, Fisher Scientific) is the initiator that is encapsulated. Butylated hydroxytoluene, 99%, FCC (W218405, Fisher Scientific) is the stabilizer that is encapsulated with the initiator to prevent the BPO from reacting prematurely.

4.2.2 Preparation of Initiator Capsules

PU nanocapsules encapsulating BPO and butylated hydroxytoluene were synthesized referencing the same procedures previously published in literature to encapsulate TEGDMA.[89-90] Again, the PU nanocapsules were formed via a poly-condensation in a two-phase system through mini-emulsions. Specifically, hexadecane (HD) and deionized (DI) water again formed the two phases, an oil phase and an aqueous phase. SDS was again used as the surfactant to confer colloidal stability.[90]

Once the 70 mL of water, 1.145 mL of HD, and 1.1 g of SDS were mixed together at 300 rpm and 40°C for 1 hour, 0.05 g BPO, and 0.005 g butylated hydroxytoluene, resuspended in 2.094 mL of IPDI, were slowly dripped into the mixture and stirred; this step began the synthesis of the nanocapsules. By dripping the IPDI and initiator mixture into the solution, the IPDI was evenly distributed throughout the oil phase. As the IPDI solution entered the pre-emulsification solution, the stirring speed was increased to 400 rpm. Once the IPDI solution was fully injected into the beaker, the solution was left to mix at 400 rpm and 40°C for 10 minutes. During this step, the solution remained clear. Next, the solution was sonicated with a 130-Watt Ultrasonic Processor with Thumb-actuated Pulser at an amplitude of 38% to break up any IPDI molecules that had aggregated. During this step, emulsions formed, and the solution looked like milk. While sonication was still progressing, an aqueous solution of 5.9 g of HDOH and 10 mL of DI water was dripped into the system. Because of the high reactivity of the isocyanate, the IPDI reacted immediately with the HDOH at the interface of the two phases.[90] The synthesis process is portrayed in Figure 22, and Figure 23 shows a flow diagram to summarize the reaction.

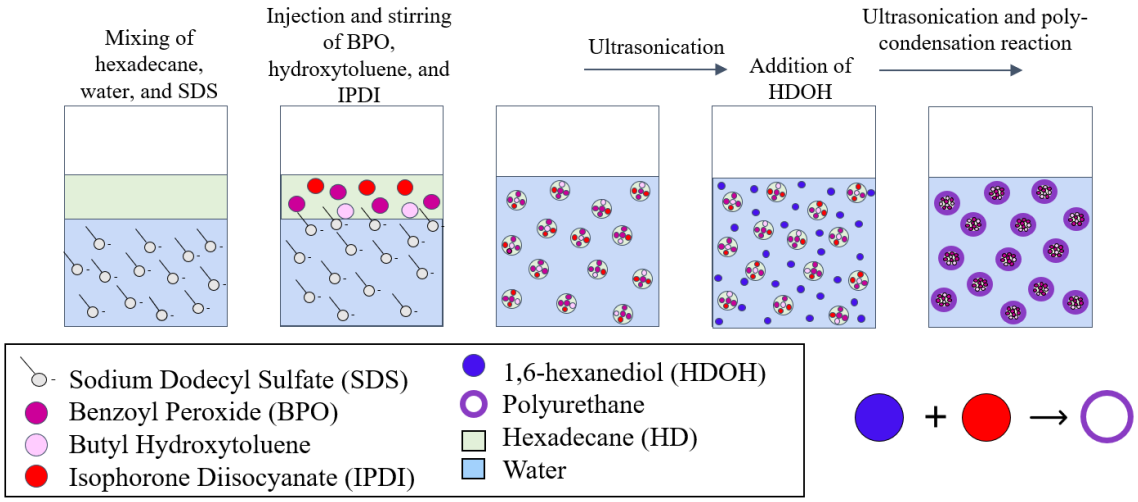

Figure 22. The synthesis method for the initiator capsule is depicted. Note that the SDS is a surfactant. It acts as a stabilizing agent and is always present; however, it is not depicted fully in each step to avoid cluttering the image. The BPO is the initiator and the butylated hydroxytoluene is the stabilizer for the initiator; the stabilizer ensures that the BPO does not react prematurely.

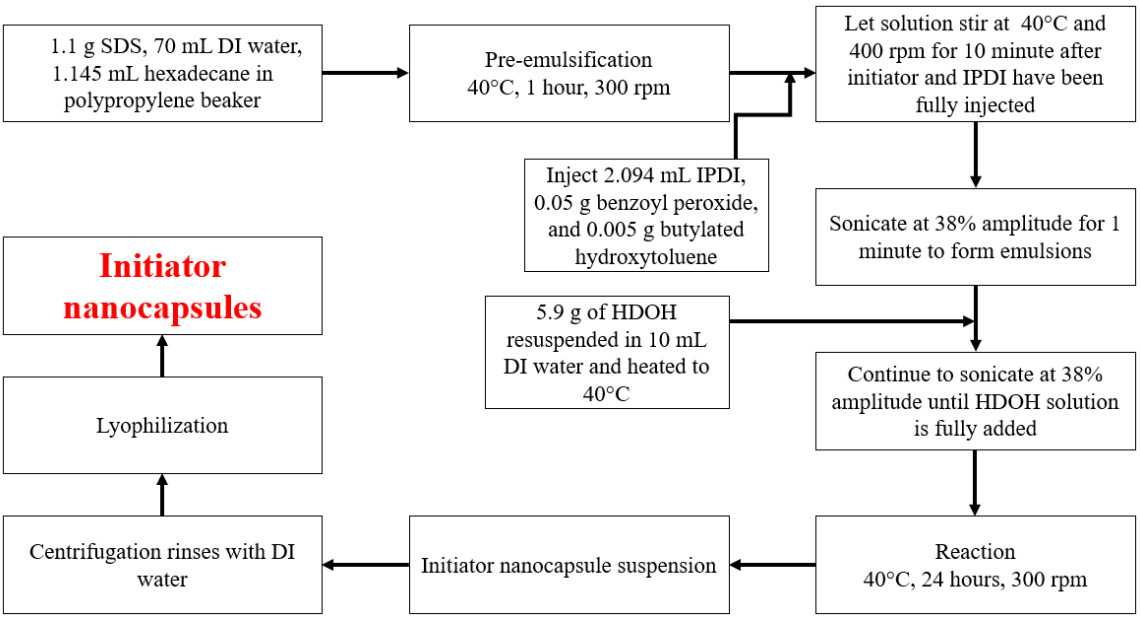

Figure 23. This flow diagram summarizes the synthesis method for the initiator capsules.

After sonication, the solution was left to react for 24 hours at 40°C and mixing at 300 rpm. After 24 hours, much of the solvent had evaporated and a clear, viscous solution was left in the beaker. The solution was poured into a centrifuge tube and centrifuged with DI water for a total of 5 times at 10,000 rpm and 4 °C for 20 minutes each run. After each run, a distinct white pellet formed at the bottom of the tube. Additionally, after each run, the supernatant was discarded, new DI water was added to the tube, and the pellet was resuspended. After the fifth centrifugation period, the supernatant was again discarded, new DI water was added, and the pellet was then resuspended. The resuspended pellet was frozen in liquid nitrogen and lyophilized. When fully dry, the capsules appeared to be a white powder.

4.2.3 Characterization of Nanocapsules

Capsule morphology and size. A vacuum sputter coater (Denton Desk II) was used to deposit a 20 nm layer of gold palladium onto the nanocapsule samples placed on carbon tape on a specimen stub for scanning electron microscopy (SEM) imaging using the Nova NanoSEM 450 from FEI. The surface morphology of the capsules was examined as well as the diameters of the capsules.

Capsule size and zeta potential. The Malvern ZetaSizer (Nano ZS90) was used to determine the diameter and zeta potential of the nanocapsules via dynamic light scattering (DLS). The nanocapsules were placed in a 1mg/mL solution of 190 proof ethanol for sizing. This solution was pipetted into a cuvette (14955129, Fisher Scientific) which was placed into the ZetaSizer. The capsules were placed in a 1mg/mL solution of 10 mM potassium chloride (KCl) to determine the zeta potential. To measure the zeta potential, the solution was inserted into a folded capillary zeta cell (Malvern Store, DTS1070) which was placed in the ZetaSizer. Both the size and zeta readings were performed in triplicates.

Capsule molecular components and structures. Fourier-transform infrared (FT-IR) (PerkinElmer Frontier Optica) spectroscopy was used to produce spectrum to identify the molecular components and structures within the capsules. Gel Permeation Chromatography (GPC) (Viscotek, VE 2001) was used to measure the molecular weight of the PU in the capsules. The GPC column (PL1110-6504) is of the Agilent Plgel MIXED family. Its phase is MIXED-D, its inner diameter is 7.5mm, its length is 300 mm, and its particle size is 5 μm. To measure the molecular weight polyurethane, the capsule samples were first crushed via mortar and pestle. Then, 10 mg of the crushed sample was resuspended in 1 mL of tetrahydrofuran (THF). This solution was filtered with PTFE

membrane syringe filters (Fisher, 09-720-002) into GPC vials (VWR, 89239-024) which were placed in the GPC for characterization. Hydrogen-1 Nuclear Magnetic Resonance (^{1}H-NMR) spectroscopy was used to further determine the structures of the capsules and the encapsulated contents. To perform this NMR, the capsule samples were resuspended in deuterated dimethyl sulfoxide (DMSO) at a concentration 0f 1 mg/mL

4.3 RESULTS AND DISCUSSION

4.3.1 Optimization of Polyurethane Capsules

To form the PU nanocapsules, like the monomer capsules, a 5:1 ratio of HDOH to IPDI was used to ensure end capping of the IPDI resulted during the reaction. To minimize the size distribution of the PU nanocapsules in the system, the amount of surfactant was varied. For SDS, the critical micelle concentration is 6 to 8 mM. This is the concentration of SDS in a bulk phase, in this case water, above which micelles start to form. In this particular formulation, with a total of 80 mL of DI water, this means a mass of 0.138 g of SDS or greater must be added in order to form micelles. GUO et al. in "The Role of Surfactant and Costabilizer in Controlling Size of Nanocapsules Containing TEGDMA in Miniemulsion" stated that a typical recipe to obtain PU nanocapsules encapsulating TEGDMA included 0.88 g of SDS and 0.88 g of HD.[90] Torini et al. reported preparing the miniemulsions with 0.66 g SDS and 0.66 g of HD.[89] The basic recipe for the preparation of miniemulsions is based on the dispersion of HD in the aqueous phase with the surfactant, SDS; however, the amount of HD and surfactant must be varied depending on what is being encapsulated.[89] Figure 24 shows the peak 1 average diameter sizes for the initiator capsules when the amount of SDS was varied. This graph compares the varying amount of surfactant used

when the amount of BPO, butylated hydroxytoluene, hexadecane, water, IPDI, and HDOH were held constant. Note that the peak 1 value was used in Figure 24 due to the fact that large aggregates of capsules had skewed the DLS readings in some samples since these particles were in the micrometer size range. The peak 1 has the largest percent intensity and is therefore the most abundant size encountered.

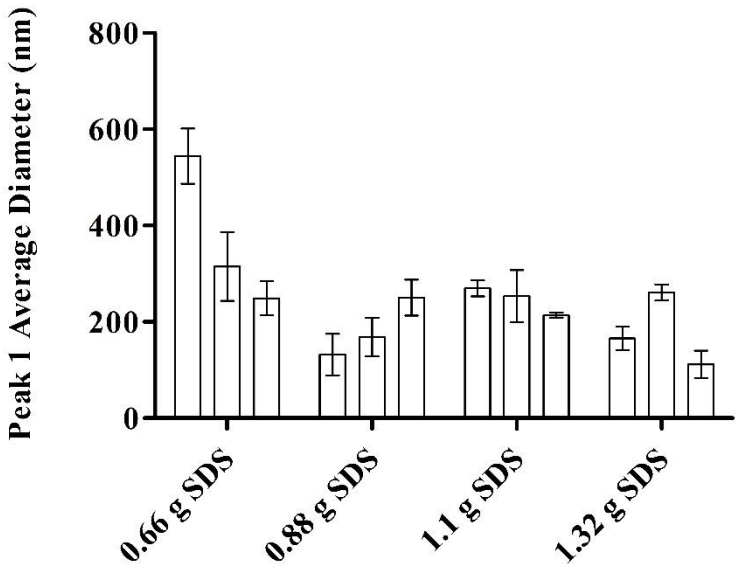

Figure 24. This figure depicts the average peak 1 diameter size in nanometers for the initiator capsules. In each synthesis, only the amount of surfactant changed. Three replicates were performed in each set; these are displayed as the three bars in each group. The error bars on each bar represent the standard deviation from the three DLS readings performed for each sample when sizing the particles.

3.3.2 Initiator Capsule Characterization

Initiator capsules have also been effectively synthesized. Figure 25 shows the SEM images of two different batches of initiator capsules made using an identical method. These capsules were made with 1.1 g of SDS. The size data for the initiator capsule samples are

shown in Figure 26. Figure 27 shows the zeta potential data for the two samples. The FT-IR data for the two samples is shown in Figure 28, the GPC data for the samples is shown in Figure 29, and the NMR data is shown in Figure 30.

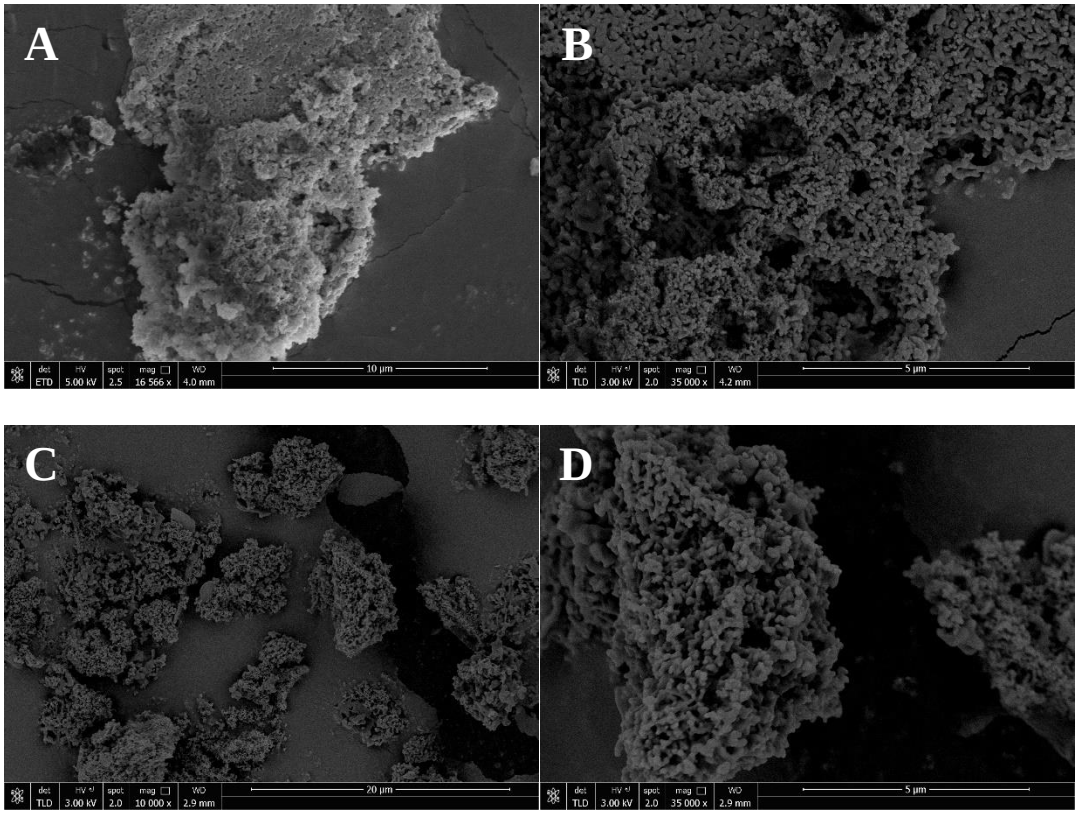

Figure 25. Images A and B are SEM images of initiator nanocapsules encapsulating BPO and butylated hydroxytoluene from one sample. Images C and D are SEM images of initiator nanocapsules encapsulating BPO and butylated hydroxytoluene from a different sample. Both samples were made following the same procedure with 1.1 g of SDS.

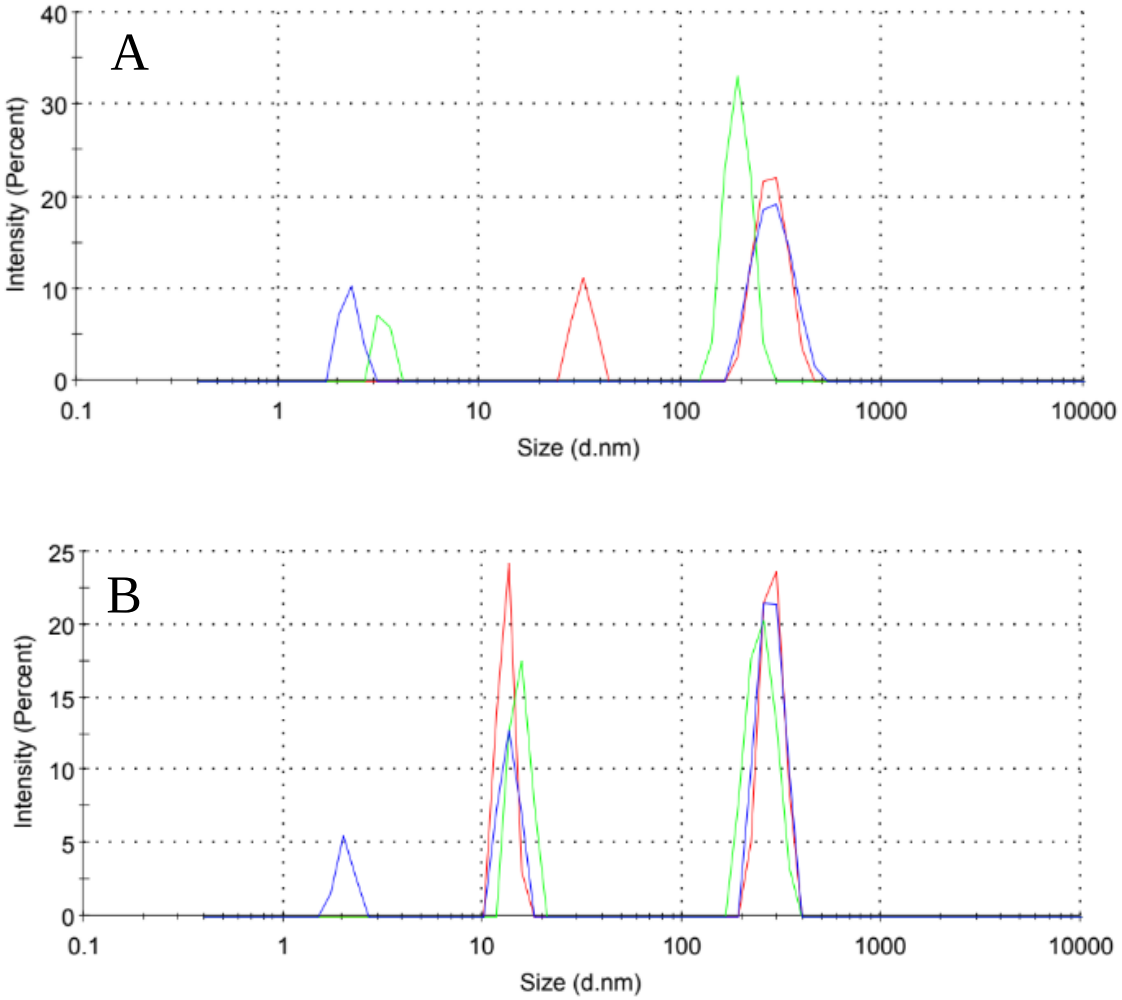

Figure 26. (A) The average diameter of the capsules shown in Figure 25 A and B is 327.4 nm, and the polydispersity index is 0.680. This information was collected using DLS. (B) The average diameter of the capsules shown in Figure 25 C and D is 258.5 nm, and the polydispersity index is 0.717. This information was collected using DLS. Here, there were no large capsules or aggregates that skewed the data so the overall average diameter is a good representation of the size of the sample.

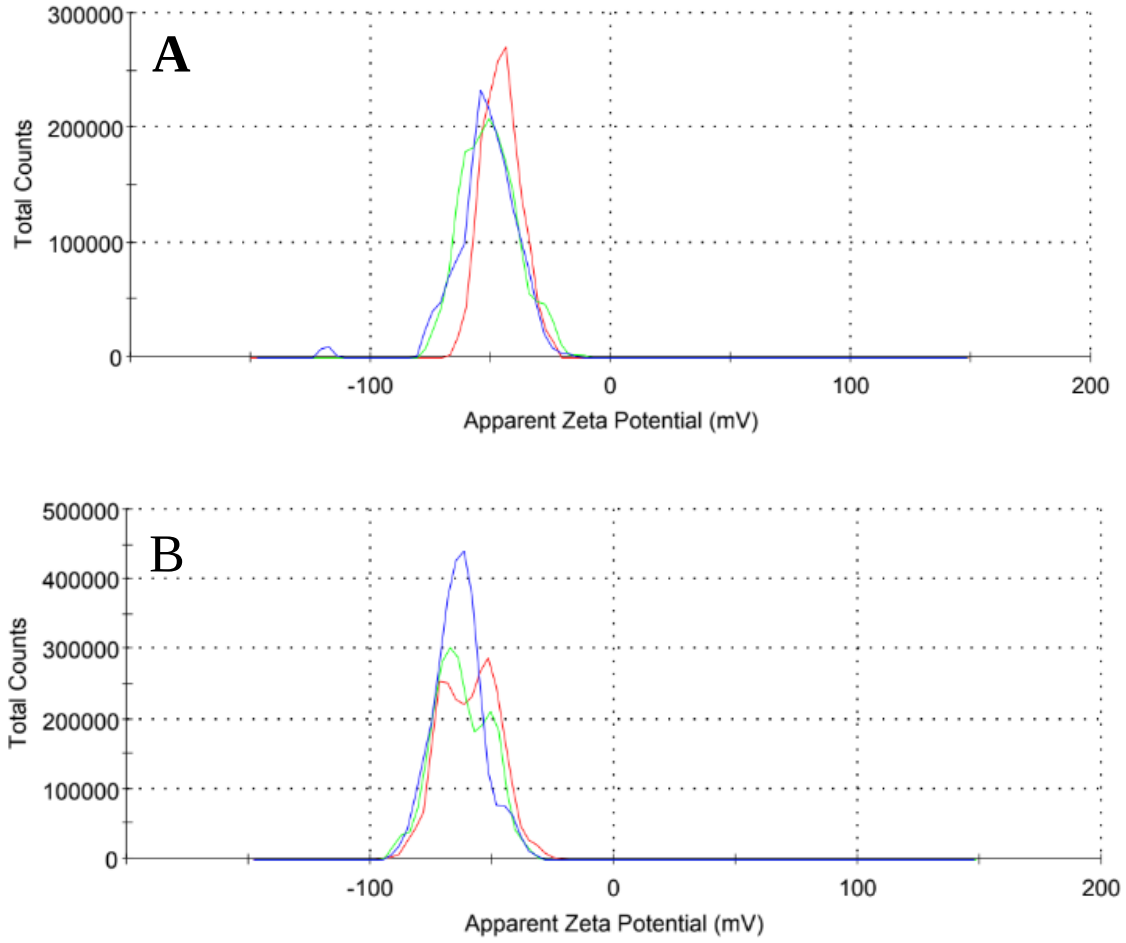

Figure 27. (A) The average zeta potential of the capsules shown in Figure 25 A and B is -49.4 mV, and the standard deviation is 11.0 mV. This information was collected using DLS. (B) The average zeta potential of the capsules shown in Figure 25 C and D is -61.9 mV, and the standard deviation is 11.1 mV. This information was also collected using DLS.

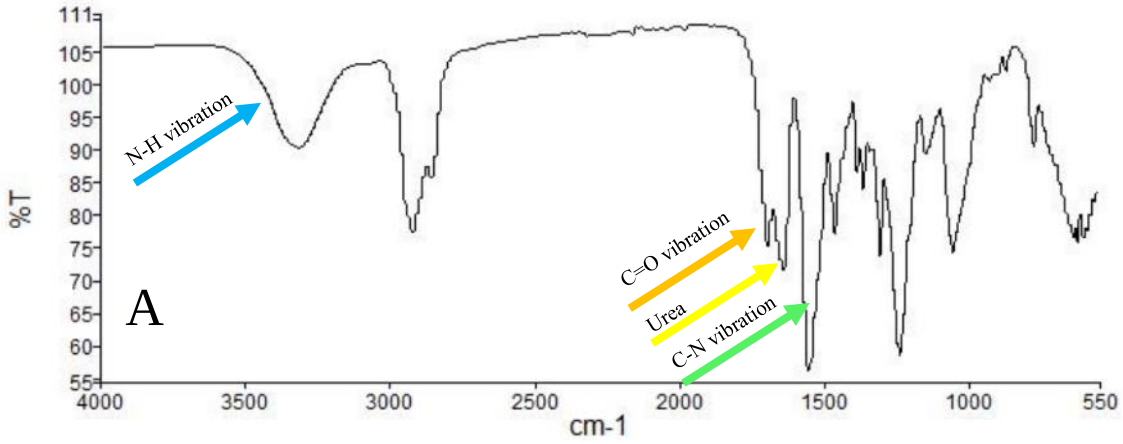
N-H vibration
C=O vibration
Urea
C-N vibration
A
%T
cm-1

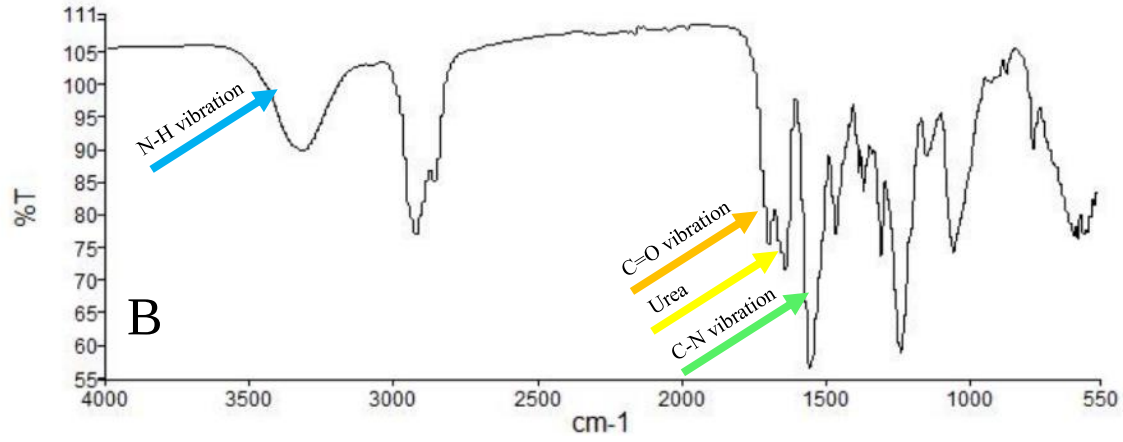
N-H vibration
C=O vibration
Urea
C-N vibration
B
%T
cm-1

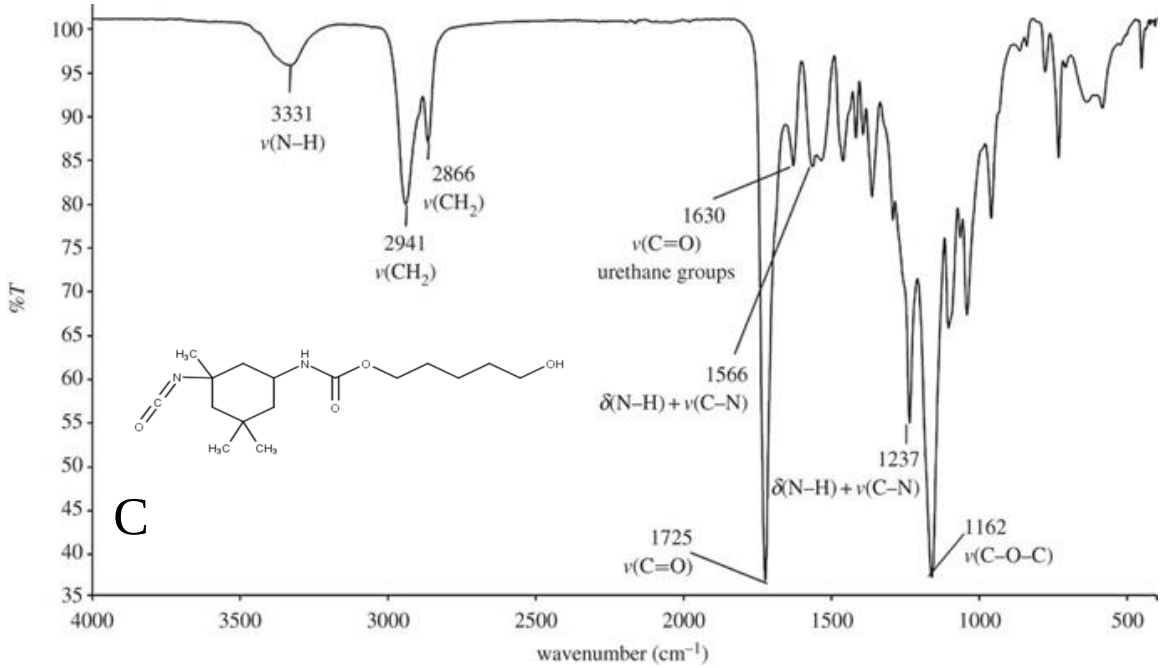
3331
ν(N–H)
2866
ν(CH2)
2941
ν(CH2)
1630
ν(C=O)
urethane groups
1566
δ(N–H) + ν(C–N)
1237
δ(N–H) + ν(C–N)
1725
ν(C=O)
1162
ν(C–O–C)
C
%T
wavenumber (cm−1)

Figure 28. (A) The peaks obtained from FT-IR for the initiator nanocapsules shown in Figure 25 A and B are portrayed. (B) The peaks obtained from FT-IR for the initiator nanocapsules shown in Figure 25 C and D are displayed. (C) The peaks obtained from PU found in literature are shown for comparison in addition to the urethane molecule itself. A lower transmittance percentage corresponds to a high population of bonds which have vibrational energies corresponding to the incident light. The green highlighting represents the C-N vibration in the urethane present in each capsule. The yellow highlight symbolizes the urea carbonyl present in each capsule. The orange shows the C=O vibration, present in each capsule. Lastly, the blue depicts the N-H vibration present in each capsule.[77, 91-93]

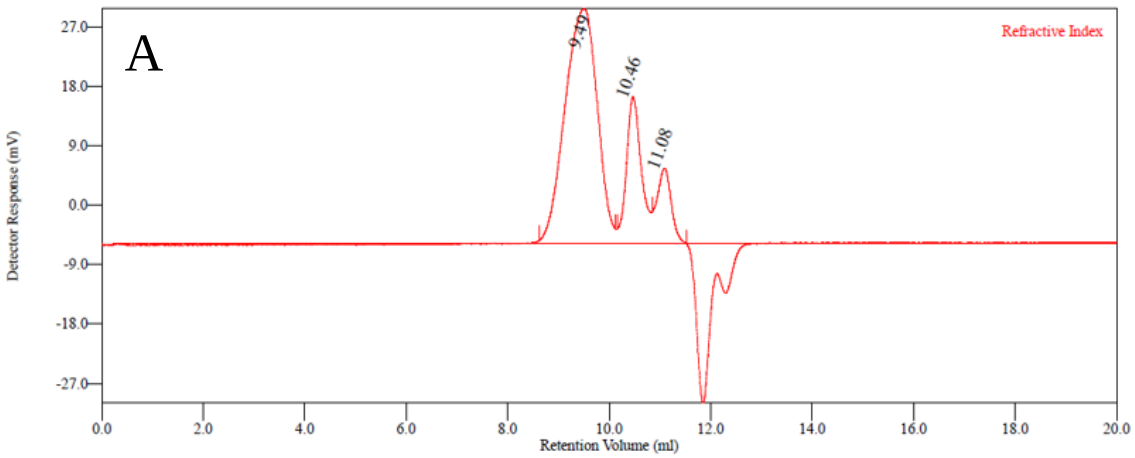

Conventional Calibration - Homopolymers : Results

Peak RV - (ml)	9.487	10.460	11.080
Mn - (Daltons)	1,411	215	66
Mw - (Daltons)	1,804	233	71
Mz - (Daltons)	2,294	251	75
Mp - (Daltons)	1,438	238	68
Mw / Mn	1.278	1.084	1.073
Percent Above Mw: 0	100.000	100.000	100.000
Percent Below Mw: 0	0.000	0.000	0.000
Mw 10.0% Low	691	131	42
Mw 10.0% High	3,875	364	104
Wt Fr (Peak)	0.698	0.204	0.098
RI Area - (mvml)	26.32	7.70	3.71
UV Area - (mvml)	0.00	0.00	0.00

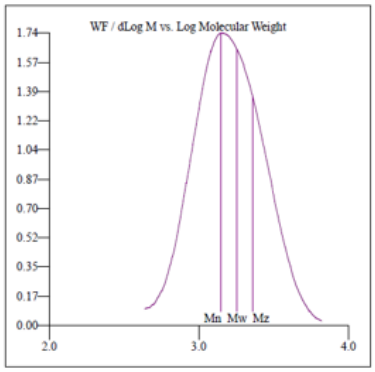

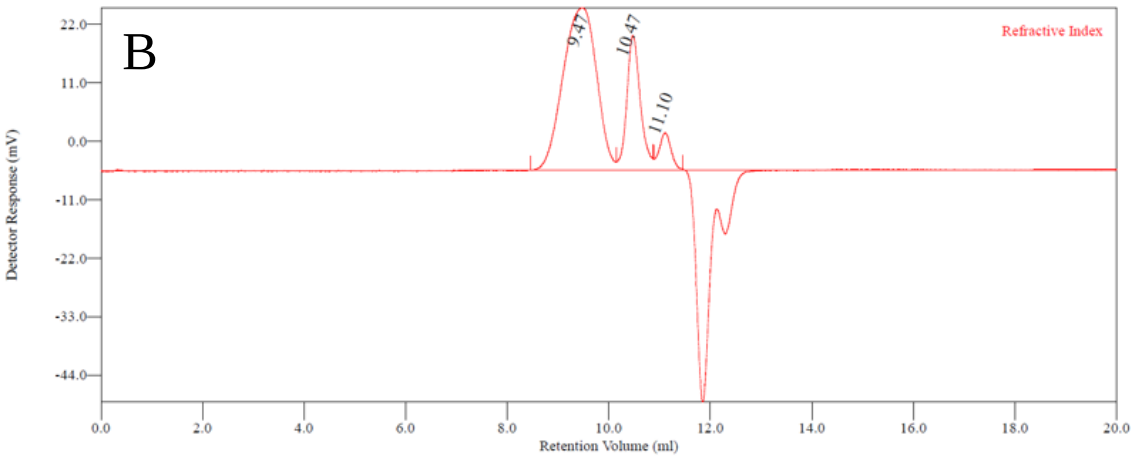

Conventional Calibration - Homopolymers : Results

Peak RV - (ml)	9.467	10.467	11.100
Mn - (Daltons)	1,443	213	63
Mw - (Daltons)	1,858	229	67
Mz - (Daltons)	2,384	244	71
Mp - (Daltons)	1,495	234	65
Mw / Mn	1.287	1.073	1.059
Percent Above Mw: 0	100.000	100.000	100.000
Percent Below Mw: 0	0.000	0.000	0.000
Mw 10.0% Low	700	132	42
Mw 10.0% High	3,999	342	98
Wt Fr (Peak)	0.703	0.238	0.059
RI Area - (mvml)	23.51	7.96	1.98
UV Area - (mvml)	0.00	0.00	0.00

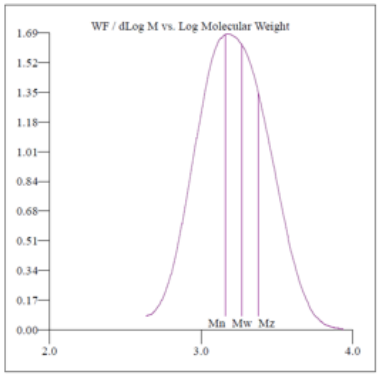

Figure 29. The GPC column's operating range is 200 to 400,000 Da. (A) The GPC data shows the molecular weight of the PU shell. The peak at 9.487 mL represents PU. The number average molecular weight (Mn) is 1,411 Da, and the weight-average molecular weight (Mw) is 1,804 Da. The polydispersity (Pd=Mw/Mn) of the PU is 1.278. The peak at 10.46 mL represents butylated hydroxytoluene. This is the stabilizer in the THF. The last peak is a solvent peak. (B) The GPC data shows the molecular weight of the PU shell. The peak at 9.467 mL represents PU. The number average molecular weight (Mn) is 1,443 Da, and the weight-average molecular weight (Mw) is 1,858 Da. The polydispersity (Pd=Mw/Mn) of the PU is 1.287. The peak at 10.467 mL represents butylated hydroxytoluene. Again, this is the stabilizer in the THF. The last peak is a solvent peak.

A

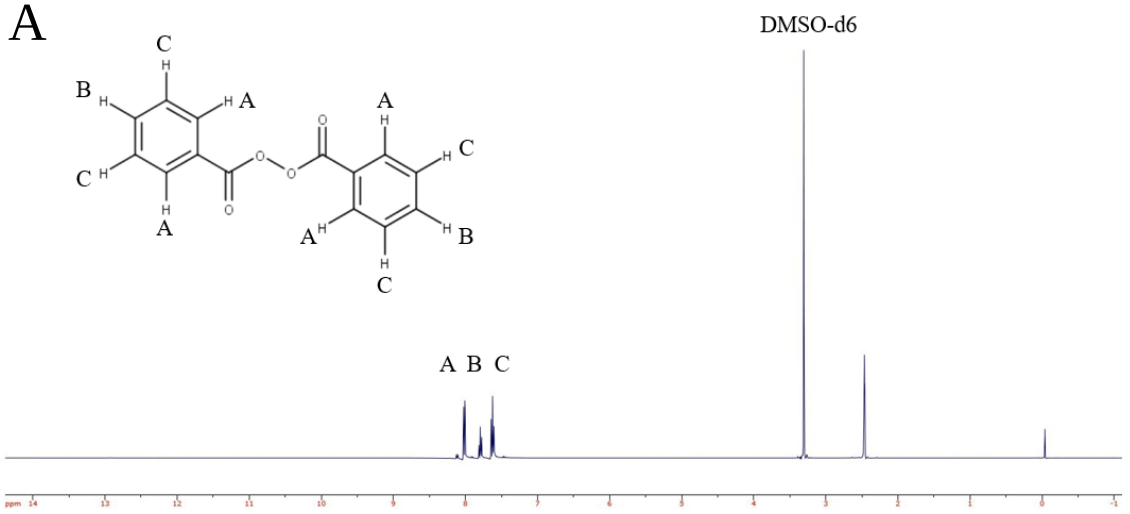

B

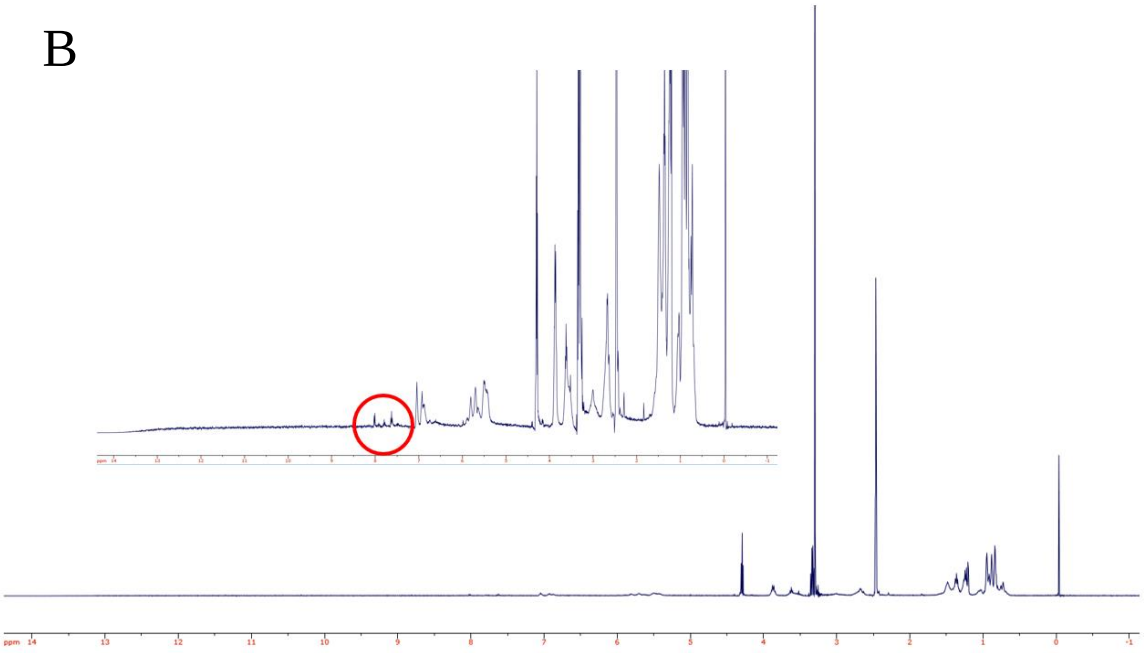

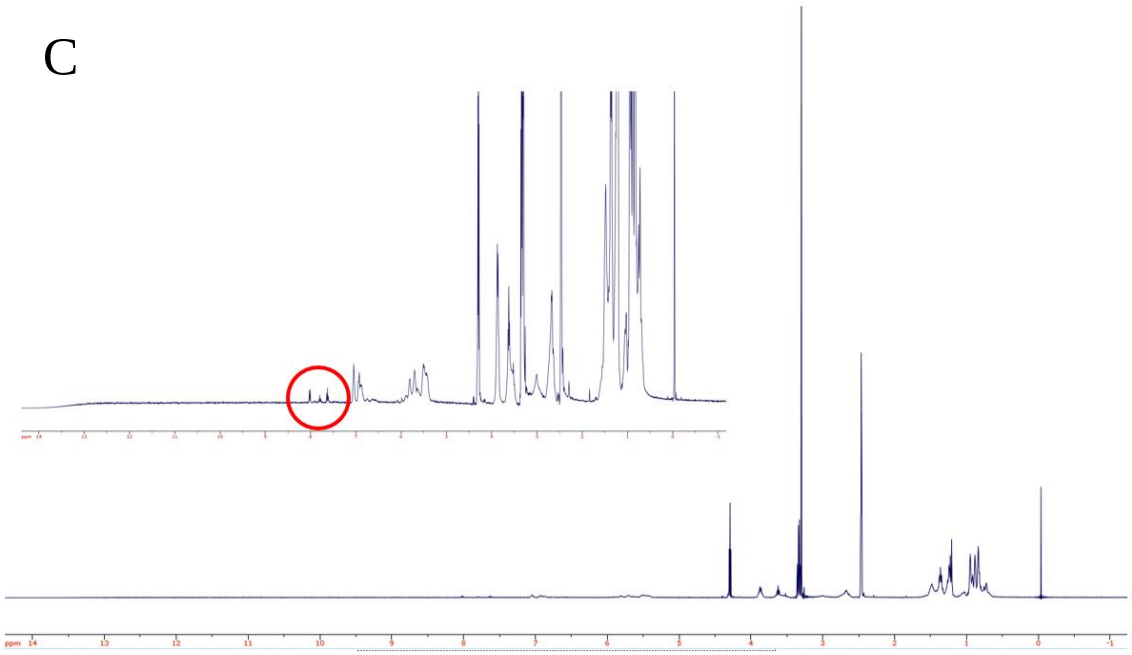

Figure 30. (A) The ^{1}H NMR spectrum for BPOis shown. The letters A, B, and C are used to designate the various protons and their resulting peaks. (B) The ^{1}H NMR spectrum for the sample shown in Figure 25 A and B is present. The red circle in the spectrum designates the peaks that prove BPO is present in the capsules. (C) The ^{1}H NMR spectrum for the sample shown in Figure 25 C and D is present. The red circle in the spectrum designates the peaks that prove BPO is present in the capsules.

According to the characteristics of the two initiator capsule samples, these capsules have nearly identical characteristics although the first sample is about 70 nm larger in diameter than the second sample. Overall, however, the capsules have a PU shell and encapsulate BPO and butylated hydroxytoluene.

4.4 CONCLUSION

The initiator capsules have been synthesized; they are composed of PU and encapsulate BPO and butylated hydroxytoluene. It was determined that 1.1 g of SDS is the optimal amount of surfactant needed to form nanocapsules with around the 300 nm size range with low PDI. These capsules can be synthesized with consistency in size, zeta potential, and chemical composition over multiple batches. Now, along with the monomer capsules synthesized in Chapter 3, the dual-capsule self-healing system has been completely synthesized. Next, the mechanical properties and healing efficiency of the system must be determined.

Chapter 5: Examining the Mechanical Properties and Healing Capacity of Polyurethane Capsules Encapsulating TEGDMA

5.1 INTRODUCTION

Ultimately, for a capsule-based self-healing system to be effective, the capsules must break as a crack propagates through the resin. A proper combination of nanocapsule and matrix properties are required. If the shell is too thick, the capsules will not rupture when a crack propagates; however, if the shell is too thin, the capsules will be too fragile. This lack of rigidity will either allow the self-healing materials to diffuse out of the capsule or will cause the capsules to rupture prematurely. Both of these properties ultimately undermine the efficacy of a self-healing system.[102]

Mechanically speaking, the capsules must be more brittle than the resin in order for self-healing to be effective. However, even when the capsule is more brittle than the matrix in which it is placed, the interface between the capsules and the resin must be examined. The interfacial region is the region beginning at the point in the fiber at which properties differ from those of the bulk filler and ending at the point in the matrix at which the properties become equal to those of the bulk matrix.[103] The interface between the matrix and the capsules can have a significant effect on the mechanical properties of the resulting composite material as well as the ability for the capsules to rupture when a crack forms in the matrix.[103]

Key mechanical parameters for efficient healing agent release include the elastic stiffness, the fill content, and the burst strength of the capsules.[102] Identifying the elastic modulus of

the capsule is very important. It is also important to investigate the rupture force and trigger sensitivity.[104]

In this section, we investigated the ability of the capsules to rupture when a crack forms in the resin. This had been done by loading the capsules into various resins in a dog bone mold. Then, the molds were broken via tension testing and a three-point bend. When the mold broke, the fracture surface was examined via scanning electron microscopy (SEM) to determine how the fracture affected the capsules in the resin. Once it was proven that the capsules do indeed crack, the self-healing efficiency of the system was examined.

5.2 MATERIALS AND METHODS

5.2.1 Materials

All materials were obtained from commercial suppliers and used without further purification. Sodium dodecyl sulfate (SDS) (BP166, Fisher Scientific) and 99% pure hexadecane (AC120465000, ACROS Organics) are the surfactant and costabilizer, respectively, used to form the polyurethane (PU) nanocapsules. Isophorone diisocyanate (IPDI) 98% (AC427602500, ACROS Organics) and 1,6-hexanediol (HDOH) 97% (AAA1243930, ACROS Organics) were the reactants from which PU was formed. Triethylene glycol dimethacrylate (TEGDMA) 95% (261548, Sigma Aldrich) was the monomer encapsulated in the PU nanocapsules. Benzoyl peroxide (BPO) (S25672, Fisher Scientific) was the initiator used in the self-healing reaction testing. Butylated hydroxytoluene, 99%, FCC (W218405, Fisher Scientific) is the stabilizer that is encapsulated with the initiator to prevent the BPO from reacting prematurely. The resin used was the West System Epoxy Resin; this resin was formed with 105 epoxy resin and

209 extra slow hardener. 190 proof ethanol (04-355-454, Fisher) was also used to form the resins.

5.2.2 Preparation of Capsules

The monomer capsules were prepared the same way described in chapter 3. The initiator capsules were created the same way described in chapter 4.

5.2.3 Preparation of Resins

West System Epoxy Resin. To prepare the epoxy resin, a 4:1 ratio of 105 epoxy resin part 1 was added to the 209 extra slow hardener and mixed together in a paper cup. Then, the monomer capsules were added. The total capsule mass was 3 weight percent of the 105 epoxy resin. The capsules were resuspended in 190 proof ethanol in order for the capsules to be well dispersed throughout the resin. The mixture was then poured into dog bone molds (shown in Figure 31) and heated with a heat gun. The resin was allowed to dry for 24 hours. At that point, the dog bones were removed from the mold and placed in an oven at 200°C for twenty minutes to further harden the resin by removing the ethanol from the resin through evaporation.

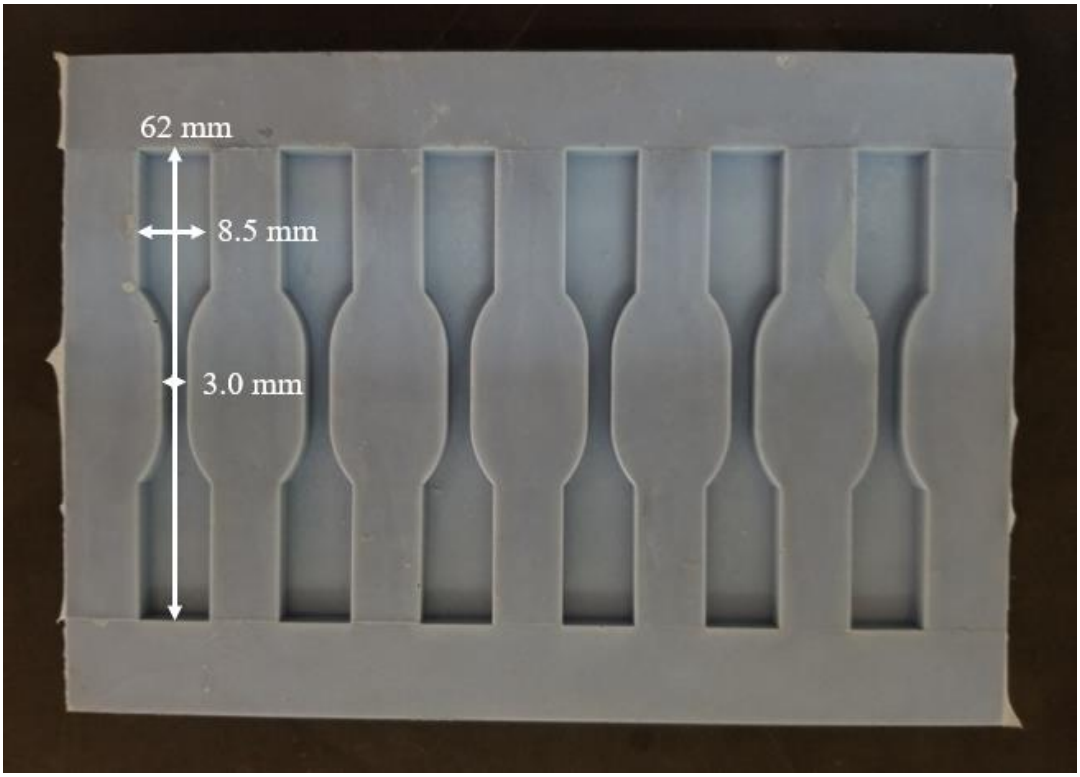

Figure 31. The mold was used to make the dog bone samples for tensile tests. The dimensions of the sample molds are shown in the image.

Blank West System Epoxy resins were also prepared in order to compare the resins with capsules. To prepare the epoxy resin, a 4:1 ratio of 105 epoxy resin part 1 was added to the 209 extra slow hardener and mixed together in a paper cup. 190 proof ethanol was also added to the mixture to create the same consistency as the resin with capsules. The mixture was then poured into a dog bone mold (shown in Figure 31) and heated with a heat gun. The resin was allowed to dry for 24 hours. At that point, the dog bones were removed from the mold and placed in an oven at 200°C for twenty minutes to further harden the resin by removing the ethanol from the resin through evaporation.

For self-healing efficiency testing, West System Epoxy resins were created with the monomer capsules and BPO. To create these resins, a 4:1 ratio of 105 epoxy resin part 1

was added to the 209 extra slow hardener and mixed together in a paper cup. Then, the capsules were added. The total monomer capsule mass was 3 weight percent of the 105 epoxy resin. The capsules were resuspended in 190 proof ethanol in order for the capsules to be well dispersed throughout the resin. Lastly, 0.5 g of BPO was added to the mixture. The mixture was then poured into the dog bone molds and heated with a heat gun. The resin was allowed to dry for 24 hours. At that point, the dog bones were removed from the mold and placed in an oven at 200°C for twenty minutes to further harden the resin by removing the ethanol from the resin through evaporation. A total of four of these samples containing monomer capsules and BPO were created.

A total of 6 other samples were made for self-healing testing. These samples were prepared the exact same way that the 4 resins with monomer capsules and BPO; however, in these resins, the initiator capsules were used in place of BPO. The total initiator capsule mass was 3 weight percent of the 105 epoxy resin.

Polishing the Dog Bones. Before fracturing the dog bones, the surface defects in the samples were removed to ensure the samples did not fracture prematurely. First, the samples were milled to smooth the convex sides of the samples. The samples were then polished using 320, 600, 800, and 1200 grit SiC paper (Allied High Tech Products) on a polishing table. The sanding paper was waterproof, and polishing was performed with water flowing. Polishing was performed with increasing grit because the higher grit created finer and finer scratches which caused less damage to the sample but also removed less impurities.

5.2.4 Fracturing the Capsules

Tension Test. The tension test is one of the most fundamental and common types of mechanical testing. This test applies a pulling force to a material with an axial force until the sample breaks and measures the specimen's response to the stress.[105] The tension test was performed on a universal testing instrument (Instron electromechancial universal testing system, 3300 series) using a strain rate of 10^{-3} s^{-1}. A complete profile of tensile properties was obtained. This data resulted in a stress/strain curve which revealed the point of failure, the modulus of elasticity, yield strength, the ultimate tensile stress, and strain to fracture.

To perform the test, the dimensions of the gauge region of the dog bone sample were first determined. Then, reflective tape was placed at the edge of the gauge region. The reflective tape was used to measure length of the gauge region. Then, the sample was placed in the grips of the machine. During the testing, the grips moved apart until the sample snapped. A laser extensometer performed the strain and elongation measurements during the testing. Figure 32 shows the set-up for the tension test.

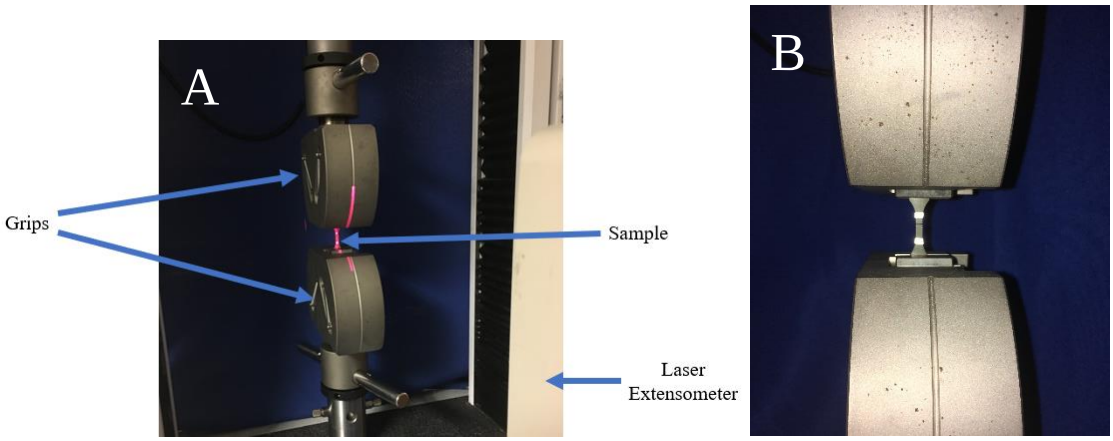

Figure 32. This figure depicts the tension test performed in which tensile forces are applied to a sample until the sample breaks. (A) This image depicts the grips for a tension test in a universal testing machine. (B) This image depicts the sample after the test is complete.

5.2.5 Determining Self-healing Efficiency

Tensile Test. During this test, the monomer capsules was placed in the resin with the BPO initiator. The test proceeded as described above, however, when the resin broke, the two halves were placed back into the dog bone mold (shown in Figure 31) and left for 48 hours to heal. Then, a second tensile test was performed on the healed resin samples.

5.3 RESULTS AND DISCUSSION

5.3.1 Capsule Characterization Results.

Before adding the monomer capsules to the various resins, the capsules were thoroughly characterized. Figure 13 shows the SEM images of the monomer capsule samples added to the resin. These capsules were made with 0.88 g of SDS. The size data for the monomer capsule samples are shown in Figure 14. Figure 15 shows the zeta potential data for the two samples. The FT-IR data for the two samples is shown in Figure 16, and the GPC data

for the samples is shown in Figure 17. All of this data is present in Chapter 3. Furthermore, the initiator capsules were also characterized. All of the characterization for the initiator capsules is present in Chapter 4.

5.3.2 Mechanical Testing

West System Epoxy Resin. A total of 24 samples were prepared. Twelve samples were made using the West System Epoxy resin with monomer capsules, and twelve blank West System Epoxy resins were prepared. The mechanical properties of the resin with the monomer capsules were compared to those of blank resins in order to determine how the capsules affect the resin properties.

From the tensile tests, the displacement in the specimen was measured within the straight central portion of the constant cross section over the gauge length, L_i. The strain, ε_{ENGR}, of the specimen was determined by computing the change in the gauge length divided by the original length, as seen in Equation 3. The axial force that had to be applied to achieve the displacement rate varied as the test proceeded; however, this force was recorded and called the load. This force, P, was divided by the cross-sectional area, A_i, of the gauge region to obtain the stress, σ_{ENGR}, in the specimen. This is shown in Equation 4.[105]

$$\varepsilon_{ENGR} = \frac{\Delta L}{L_i} \qquad \textit{Equation 3}$$

$$\sigma_{ENGR} = \frac{P}{A_i} \qquad \textit{Equation 4}$$

Stress and strain, based on the initial (non-uniform) dimensions A_i and L_i, are known as engineering stress and strain. It was necessary to find the true stress and strain and thereby account for the changing gauge length and cross-sectional area as the test proceeded. True strain, ε_T, is found via Equation 5, and true stress, σ_T, is found via Equation 6.[105]

$$\varepsilon_T = \ln(1 + \varepsilon_{ENGR}) \qquad \textit{Equation 5}$$

$$\sigma_T = \sigma_{ENGR}(1 + \varepsilon_{ENGR}) \qquad \textit{Equation 6}$$

Stress-strain curves were made to compare the mechanical properties of the two types of resins. The stress-strain curves were made by plotting the true stress versus the true strain for each sample.

Figure 33 and Figure 34 show the stress/strain curve of the blank resin and the resin with the embedded capsules, respectively.

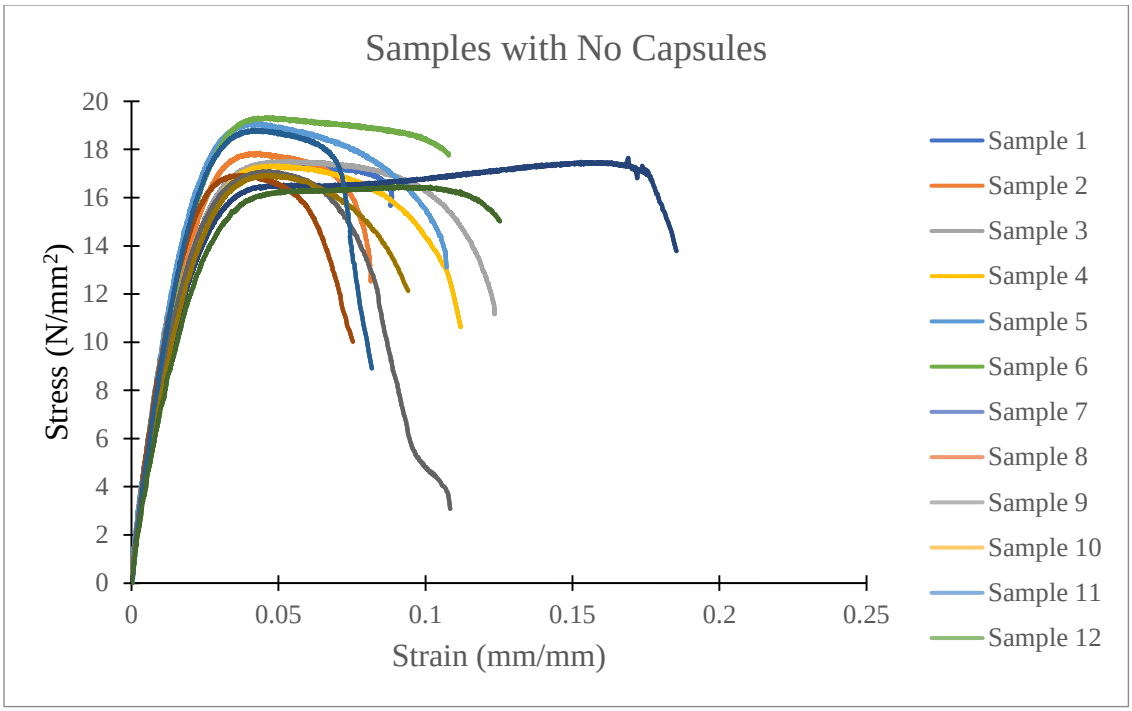

Figure 33. This figure depicts the stress/strain curves from 12 samples of blank resin. These samples were prepared at the same time and with the same conditions.

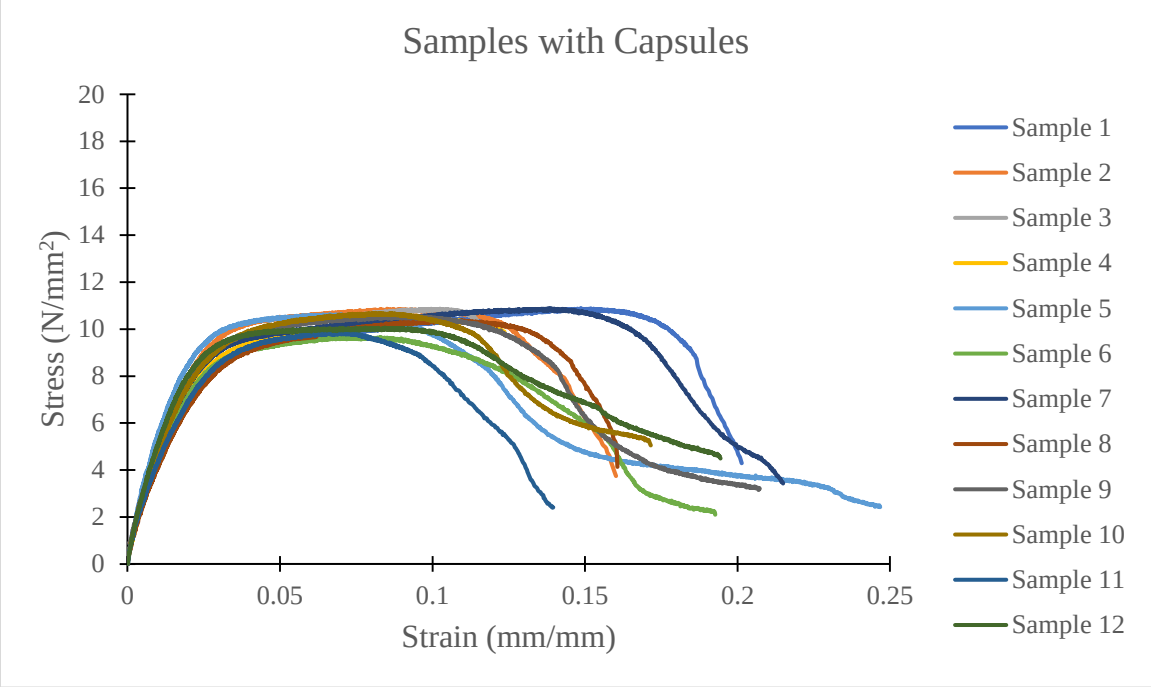

Figure 34. This figure depicts the stress/strain curves from 12 samples of resin with capsules. These samples were prepared at the same time and with the same conditions. This curve, compared to that in Figure 33, suggests that the resins with capsules are weaker than those without capsules.

From the stress-strain curves, the elastic modulus, E, 0.2% offset yield strength, the ultimate tensile strength (UTS), and the strain to failure of the resin samples were determined to compare the two sets of samples. Figure 35 shows an overview of how each of these properties was determined.

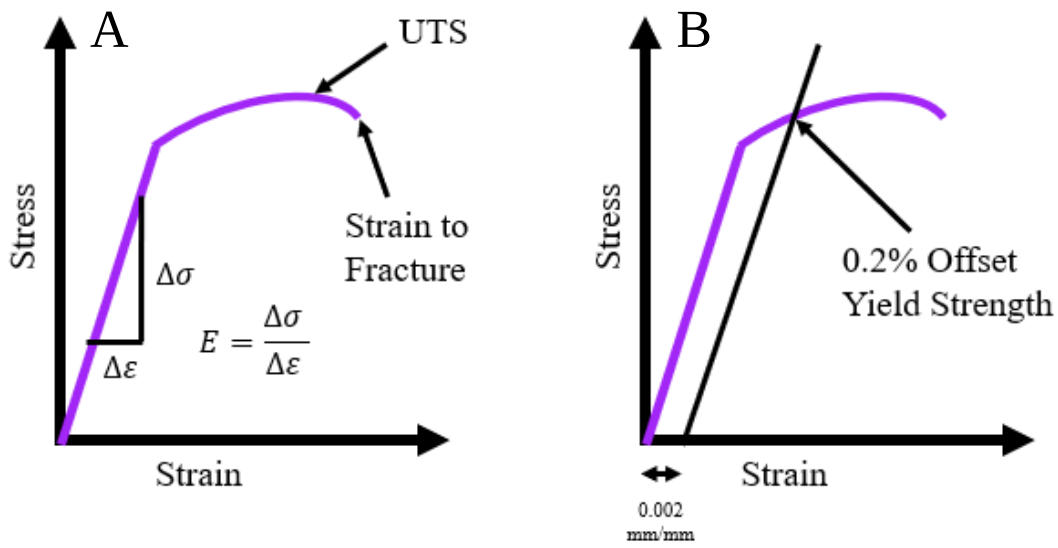

Figure 35. (A) A stress-strain curve is depicted. The elastic modulus, E, is shown in addition to the UTS and strain to failure. (B) The stress-strain curve is again depicted; however, in this graph, how to determine the 0.2% offset yield strength is shown. The 0.2% offset yield strength is determined by drawing through the point of the horizontal axis of strain=0.2%, a line parallel to the initial straight-line portion of the stress-strain curve. The 0.2% offset yield strength is the stress at which the created line intersects the stress-strain curve. Note that the line used to determine the offset and intersect the curve is parallel to the elastic modulus.[105]

Tables 1 and 2 show the elastic moduli, the 0.2% offset yield strength, the UTS, and the strain to fracture for the samples without capsules and the samples with capsules, respectively.

Table 1. The mechanical properties for the resin samples without capsules are shown.

	Samples with No Capsules			
	Elastic Modulus (N/mm^2)	0.2% Offset Yield Strength (N/mm^2)	Ultimate Tensile Strength (N/mm^2)	Strain to Fracture (mm/mm)
Sample 1	836.6	12.008	17.4	0.0885
Sample 2	809.8	13.2	17.9	0.0814
Sample 3	848.9	11.3	17.5	0.123
Sample 4	801.1	11.1	17.3	0.112
Sample 5	947.6	13.3	19.1	0.107
Sample 6	852.3	14.1	19.3	0.108
Sample 7	786.3	11.0	17.6	0.185
Sample 8	987.2	11.3	16.9	0.0753
Sample 9	813.6	12.5	17.1	0.108
Sample 10	742.6	12.6	17.0	0.0941
Sample 11	882.8	14.2	18.8	0.0818
Sample 12	695.8	11.7	16.5	0.125
Average	**833.7 +/- 80.4**	**12.4 +/- 1.1**	**17.7 +/- 0.9**	**0.107 +/- 0.0294**

Table 2. The mechanical properties for the resin samples with capsules are shown.

	Samples with Capsules			
	Elastic Modulus (N/mm^2)	0.2% Offset Yield Strength (N/mm^2)	Ultimate Tensile Strength (N/mm^2)	Strain to Fracture (mm/mm)
Sample 1	368.1	7.9	10.9	0.201
Sample 2	470.6	7.3	10.9	0.160
Sample 3	420.1	7.2	10.9	0.114
Sample 4	423.4	6.8	10.4	0.123
Sample 5	501.6	8.1	10.6	0.247
Sample 6	417.4	6.9	9.7	0.193
Sample 7	461.0	6.8	10.9	0.215
Sample 8	365.6	7.1	10.4	0.161
Sample 9	428.4	7.2	10.6	0.207
Sample 10	431.8	7.7	10.7	0.172
Sample 11	381.0	7.2	9.9	0.140
Sample 12	397.4	8.7	10.1	0.194
Average	**422.2 +/- 41.3**	**7.4 +/- 0.6**	**10.5 +/- 0.4**	**0.177 +/- 0.0395**

Figure 36 shows macro-sized images of the broken dog bone structures. Figure 37 and Figure 38 compare the fracture surface of the two resin systems via SEM imaging.

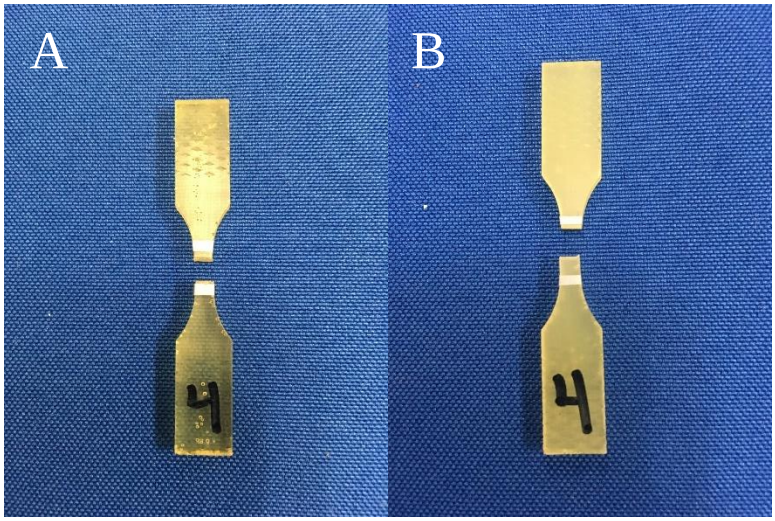

Figure 36. (A) The broken West System Epoxy resin without monomer capsules is shown. Voids (air bubbles) are present in this sample near the number 4; however, the voids did not affect the testing since they are not in the gauge region. (B) The broken West System Epoxy resin with monomer capsules is shown. Because of the capsules, this resin is less transparent than the resin in A.

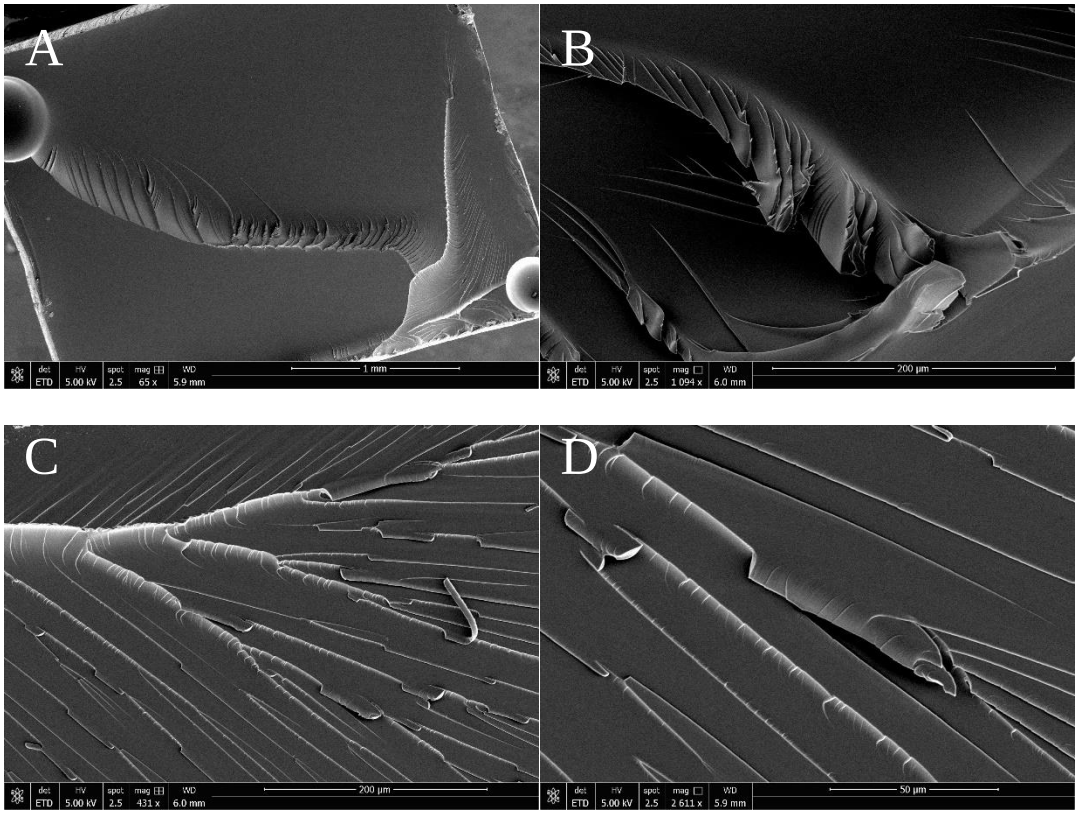

Figure 37. (A-D) The images show the fracture surface on samples of the West System Epoxy resins without monomer capsules. (A) This SEM image portrays the entire fracture surface of one sample. The two sphere-like figures in the top left corner and bottom right corner of the image are voids (air bubbles) that were present in sample. (B) This image shows a closer view of the area at which the fracture occurred in another sample. (C-D) These SEM images present a third sample without monomers. D presents a zoomed in image of the same fracture present in C.

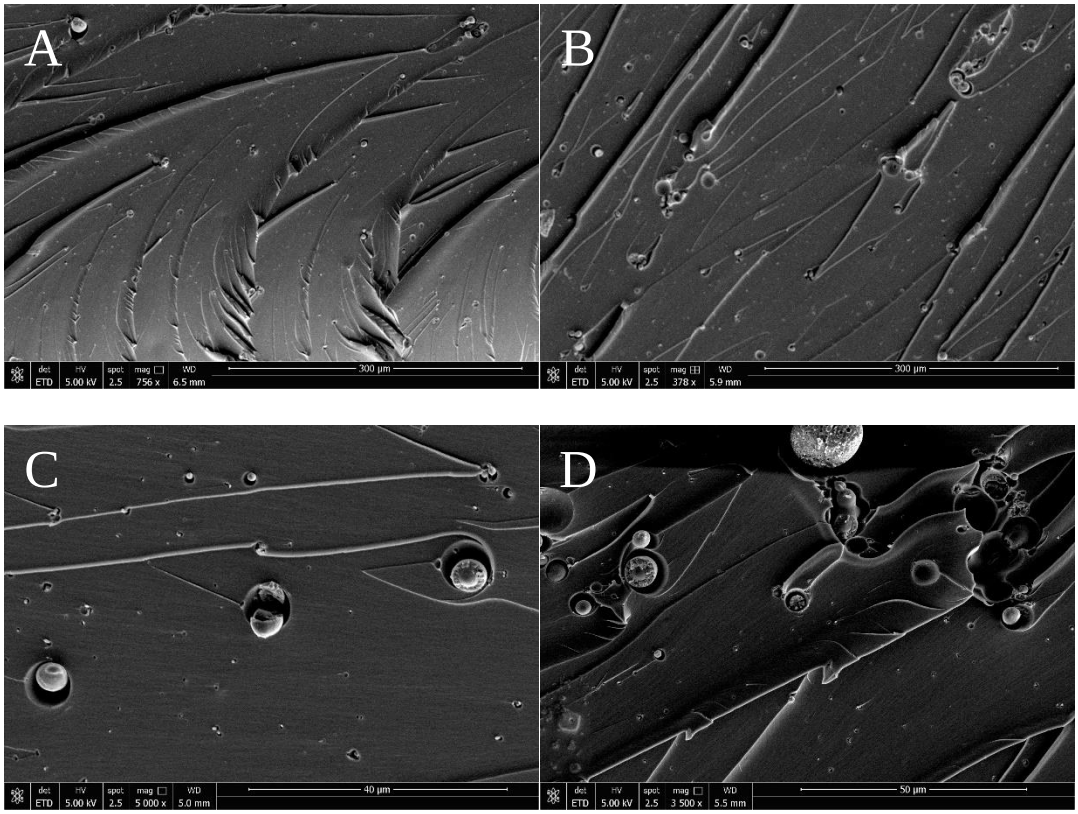

Figure 38 (A-D) The images show the fracture surface in different samples made with the West System Epoxy resin with monomer capsules. (A-B) These SEM images show fracture surfaces from two different samples at a lower magnification. The capsules, especially larger capsules, are evident in the surface and cause a rougher surface. (C-D) These SEM images show fracture surfaces from two other samples at a higher magnification. In these images, it is evident that some of the larger capsules have cracked. The white dots in these images are the nanocapsules.

As shown in Figure 38, the monomer capsules did break during the resin fracture No self-healing resulted because the initiator was not present. Figure 39 shows more magnified SEM images of the broken capsules. In these images, the insides of the capsules are hollow since the TEGDMA was released from the capsules. It was evident that the larger capsules,

those in the micrometer range, appeared to break more than the capsules in the nano-size range.

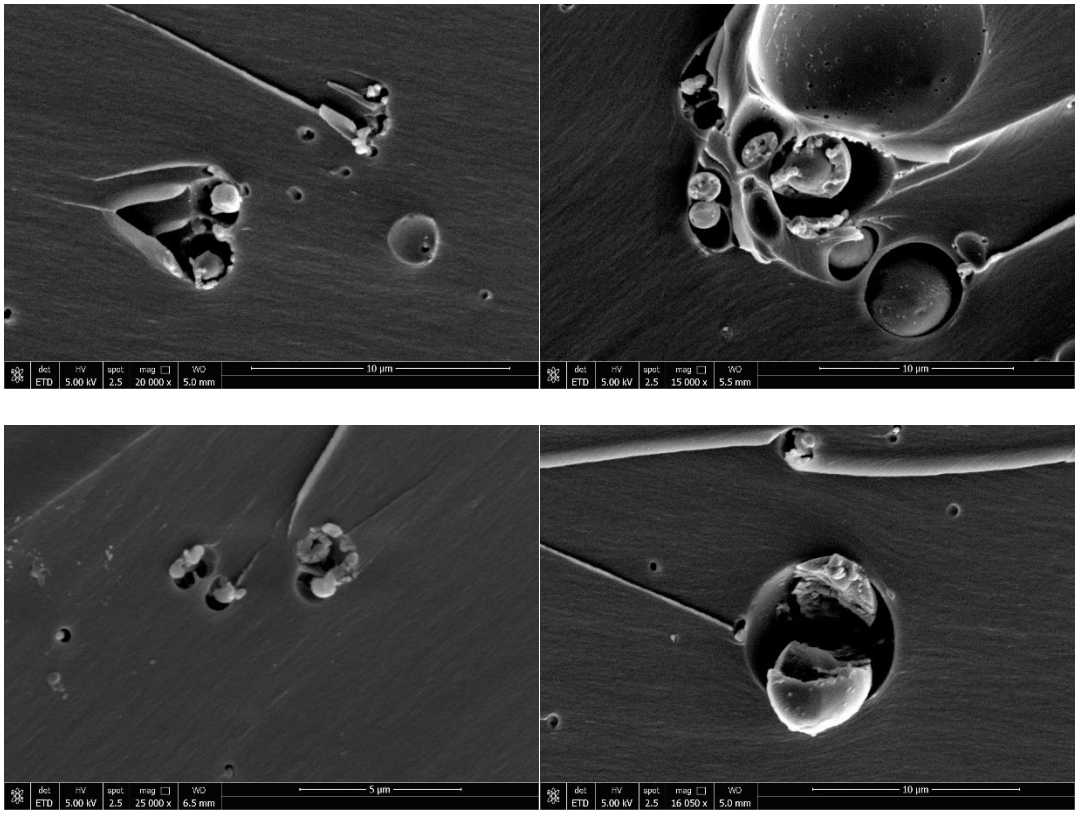

Figure 39. Broken monomer capsules at the fracture surface in the West System Epoxy resin are shown.

From this data, it is apparent that the capsules decreased the strength of the resin. The resins with the capsules had elastic moduli about half of that compared to the resin without capsules. This is also true when comparing the 0.2% offset yield strength and the UTS between the two sample types. The strain to fracture value is relatively consistent between the two samples. Overall, these comparisons mean that the resins with the capsules are more likely to break than the resins without the capsules. This is not the intended conclusion considering the fact that these capsules are intended to be placed in resins to

reduce resin fracture by healing a propagating nano and micro-sized cracks in the resin. To confirm these results, a different resin system should be used in the comparison.

If this in fact is true and adding capsules to any type of resin results in weaker resins, the outside of the capsules could be coated in order to reduce the size of the interface region, the area at which the resin surface meets the PU surface of the capsules.

5.3.3 Self-healing Efficiency

West System Epoxy resins with monomer capsules and BPO were prepared. These samples were tested with a tensile test. Figure 40 shows the results of the tensile test on the samples with monomer capsules and BPO before the self-healing. Table 3 shows the elastic moduli, the 0.2% offset yield strength, the UTS, and the strain to fracture from the samples shown in Figure 40. Only 2 of the 4 samples showed any sign of healing after 48 hours. Figure 41 shows the results of the tensile test on the 2 healed samples, and Table 4 shows the elastic moduli, the 0.2% offset yield strength, the UTS, and the strain to fracture from the samples shown in Figure 41.

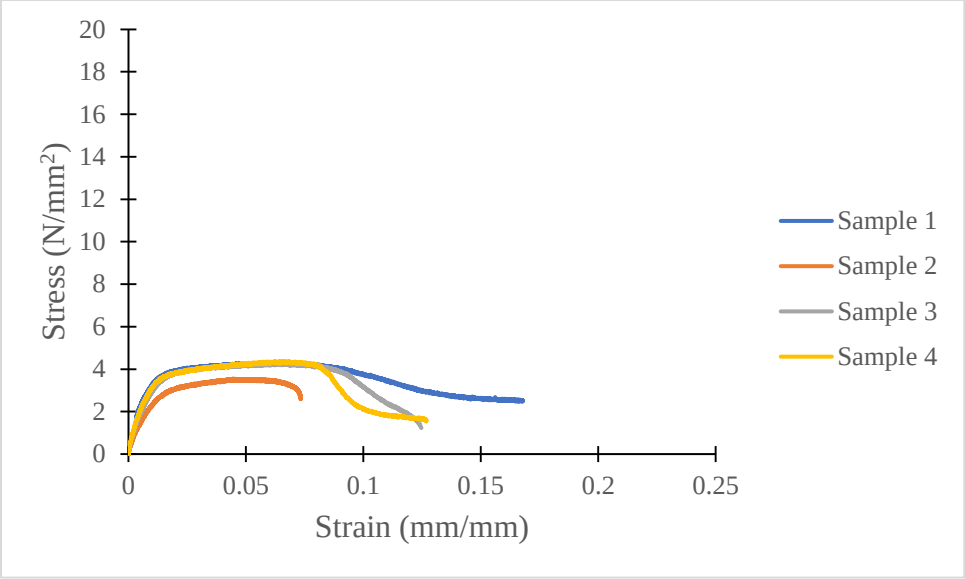

Figure 40. This figure depicts the stress/strain curves from 4 samples of resin with the monomer capsules and BPO prior to self-healing. These samples were prepared at the same time and with the same conditions.

Table 3. The mechanical properties for the resin samples before self-healing are shown.

	Pre-Self-Healing			
	Elastic Modulus (N/mm^2)	0.2% Offset Yield Strength (N/mm^2)	Ultimate Tensile Strength (N/mm^2)	Strain to Fracture (mm/mm)
Sample 1	408.8	3.3	4.3	0.168
Sample 2	217.2	2.8	3.6	0.0733
Sample 3	288.2	3.5	4.3	0.125
Sample 4	322.6	3.5	4.4	0.127
Average	**309.2 +/- 79.6**	**3.3 +/- 0.3**	**4.2 +/- 0.4**	**0.123 +/- 0.0388**

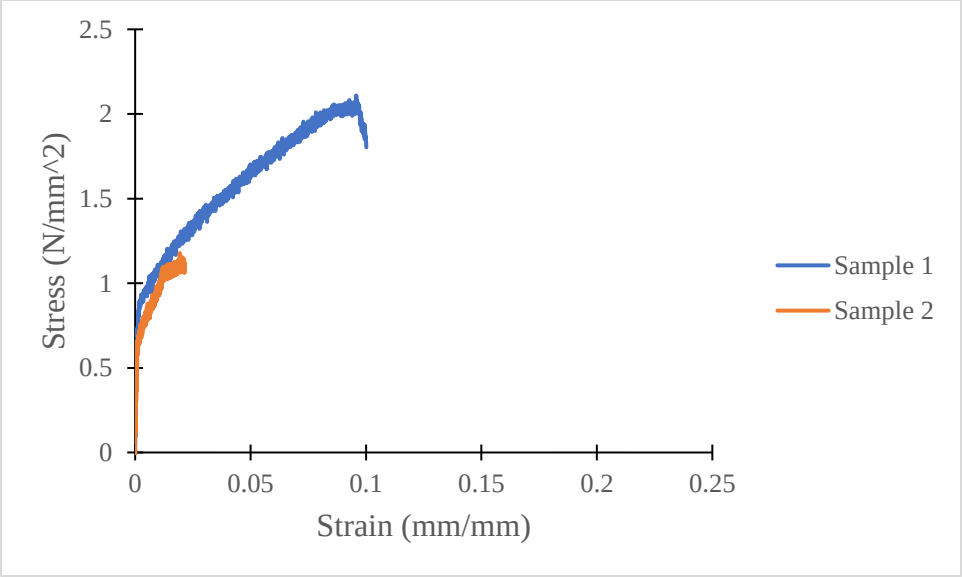

Figure 41. This figure depicts the stress/strain curves from 2 of the 4 samples of resin with the monomer capsules and BPO after self-healing. These samples were prepared at the same time and with the same conditions. Note the y-axis has a much smaller range in this graph to assure readability.

Table 4. The mechanical properties for the resin samples after self-healing are shown.

		Post Self-Healing		
	Elastic Modulus (N/mm^2)	0.2% Offset Yield Strength (N/mm^2)	Ultimate Tensile Strength (N/mm^2)	Strain to Fracture (mm/mm)
Sample 1	508.1	0.9	2.1	0.100
Sample 2	615.5	0.7	1.2	0.0118
Average	**561.8 +/- 75.9**	**0.8 +/- 0.1**	**1.6 +/- 0.6**	**0.0559 +/- 0.0624**

Figure 42 depicts one of the samples before any tensile test was performed. During the tensile test, this sample fractured like the samples seen in Figure 36.

Figure 42. The image shows one of the samples containing both the monomer capsules and BPO before any tensile tests were performed. Notice the large clumps that appear in the resin are the BPO.

West System Epoxy resins with monomer capsules and initiator capsules were also prepared. These samples were tested with a tensile test. Figure 43 shows the results of the tensile test on the samples with monomer capsules and initiator capsules before the self-healing. Table 5 shows the elastic moduli, the 0.2% offset yield strength, the UTS, and the strain to fracture from the samples shown in Figure 43. Only 2 of the 6 samples showed any sign of healing after 48 hours. Figure 44 shows the results of the tensile test on the 2 healed samples, and Table 6 shows the elastic moduli, the 0.2% offset yield strength, the UTS, and the strain to fracture from the samples shown in Figure 44.

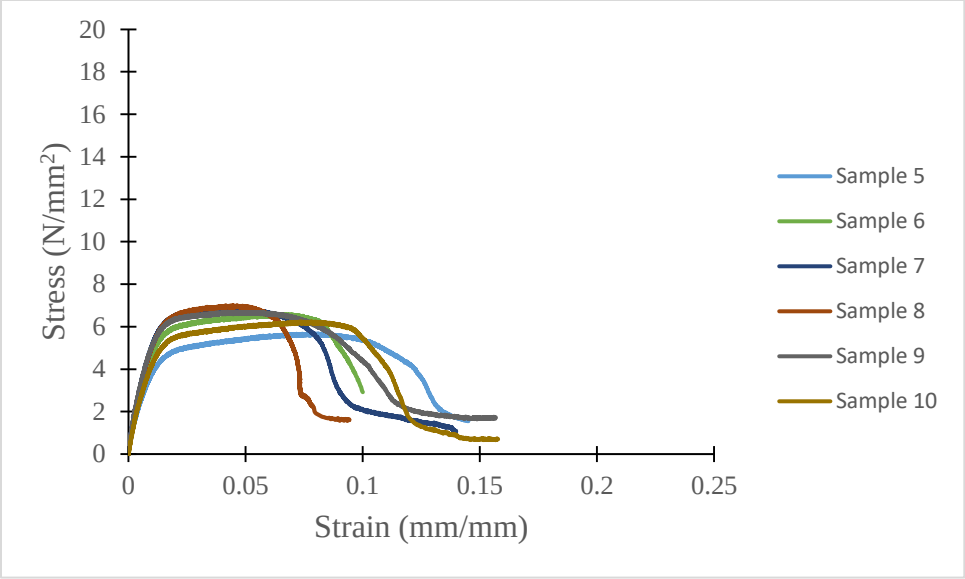

Figure 43. This figure depicts the stress/strain curves from 6 samples of resin with the monomer capsules and initiator capsules prior to self-healing. These samples were prepared at the same time and with the same conditions.

Table 5. The mechanical properties for the resin samples before self-healing are shown.

	Pre-Self-Healing			
	Elastic Modulus (N/mm^2)	0.2% Offset Yield Strength (N/mm^2)	Ultimate Tensile Strength (N/mm^2)	Strain to Fracture (mm/mm)
Sample 5	366.6	4.5	5.7	0.145
Sample 6	511.4	5.3	6.6	0.100
Sample 7	512.5	5.6	6.8	0.140
Sample 8	506.2	5.8	7.0	0.0943
Sample 9	505.3	5.7	6.7	0.156
Sample 10	427.2	4.7	6.2	0.157
Average	**471.5 +/- 61.0**	**5.3 +/- 0.5**	**6.5 +/- 0.5**	**0.132 +/- 0.0278**

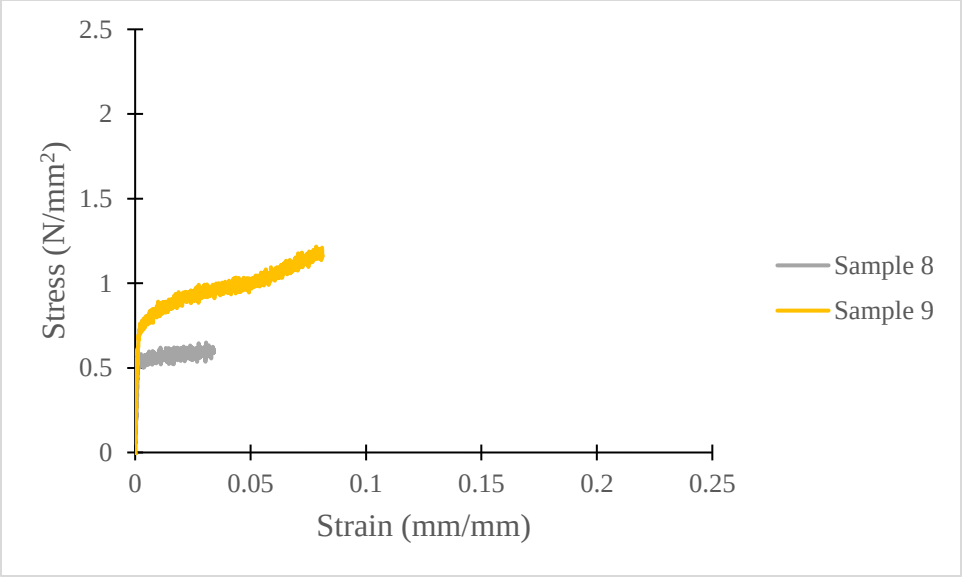

Figure 44. This figure depicts the stress/strain curves from 2 of the 6 samples of resin with the monomer capsules and initiator capsules after self-healing. These samples were prepared at the same time and with the same conditions. Note the y-axis has a much smaller range in this graph to assure readability.

Table 6. The mechanical properties for the resin samples after self-healing are shown.

	Post Self-Healing			
	Elastic Modulus (N/mm^2)	0.2% Offset Yield Strength (N/mm^2)	Ultimate Tensile Strength (N/mm^2)	Strain to Fracture (mm/mm)
Sample 8	421.5	0.5	0.6	0.0341
Sample 9	516.8	0.7	1.2	0.0812
Average	**469.2 +/- 67.4**	**0.6 +/- 0.1**	**0.9 +/- 0.4**	**0.0576 +/- 0.0333**

Researchers have proposed multiple definitions of healing efficiencies. We will measure healing by defining a recovery ratio (R). The recovery ratio is shown in Equation 7, where f is the partially healing material property and f_∞ is the virgin state material property.[106]

$$R(f) = \frac{f}{f_\infty} \qquad \textit{Equation 7}$$

Table 7 depicts the recovery ratios of the elastic moduli, the 0.2% offset yield strength, the UTS, and the strain to fracture from the 4 healed samples.

Table 7. The recovery ratio for each property examined for the resin samples after self-healing are shown.

	Elastic Modulus (N/mm^2)	0.2% Offset Yield Strength (N/mm^2)	Ultimate Tensile Strength (N/mm^2)	Strain to Fracture (mm/mm)
Sample 1	1.243	0.279	0.488	0.595
Sample 2	2.833	0.262	0.333	0.161
Sample 8	0.833	0.094	0.086	0.362
Sample 9	1.023	0.130	0.179	0.520

Two different resins were used in order to determine the self-healing efficiency to examine the plausibility of a dual-capsule self-healing system. Sample 1, the resin with monomer capsules and unencapsulated BPO, showed the most capacity for self-healing. By

examining the elastic modulus in this sample, one can determine that the sample became more elastic after self-healing. Although the 0.2% offset yield strength, the UTS, and the strain to fracture were all lower than the virgin Sample 1, the healed Sample 1 had values most similar to the original sample when compared to the other healed samples. However, the resins with initiator and monomer capsules (Samples 8 and 9) did display some degree of self-healing. To better understand the self-healing capacity of the dual capsule self-healing system, different ratios of capsules in the resin must be tested. Additionally, multiple healing times should be examined, and a larger overall sample size must be used.

5.4 CONCLUSION

By embedding PU nanocapsules encapsulating TEGDMA in West System Epoxy resins and comparing these resins to blank resins, the effects the monomer capsules have on the mechanical properties of a resin were determined. Tensile testing was used to determine the properties of both resin systems; the resin without monomer capsules proved to be stronger than the resin with the monomer capsules when the elastic modulus, 0.2% yield strength, UTS, and strain to fracture in both types of resins were compared. However, it is important to note that the monomer capsules did indeed crack during the resin fracture. This ultimately proved that the capsules have potential to have a self-healing effect in a resin when a crack propagates through the resin. Furthermore, after examining the self-healing capacity of resins with the monomer capsules and BPO and the monomer capsules and initiator capsules, a small degree of self-healing was present within the resins. Further testing must be pursued to fully understand the degree of self-healing possible in this dual-capsule system.

Chapter 6: Expanding the Possibilities of Polyurethane Capsules

6.1 INTRODUCTION

Due to the biocompatibility, mechanical flexibility, and thermal stability of polyurethane (PU), in tandem with the unique transport capabilities of nanocapsules, extending the use of these nanocapsules to other human health applications is highly desirable.[107] These other applications may include medicine or other therapeutic uses. However, some of these applications also require the nanocapsules to be suspended in some liquid media, as opposed to being fixed in a resin. Water intrusion/absorption into PUs plays a significant role in the degradation rate of the PU and the drug release profile of the PU system.[108] Hence, we must understand the rate at which encapsulated molecules will diffuse from the shell of these nanocapsules.

The size of the capsules is a key parameter that affects the ability of the capsules to interact with biological systems and influences the rate at which an encapsulated drug is released from the capsules.[109] Nanoencapsulation of drugs has been shown to improve drug stability, increase substance uptake by cells, increase efficacy and/or bioavailability, and decrease the adverse effects of drugs in the body.[110] Nanocapsules have a higher surface to volume ratio when compared with microcapsules.[111]

Nanocapsules were optimized to maintain structural integrity under physiological stress but were shown to burst when a simulated crack occurred in a resin matrix. When suspended in liquid media, however, PU nanocapsules function in a different way. In liquid media, PU nanocapsules release the encapsulated materials gradually; this is often referred

to as leaking. One common method to predict the rate of loss from a capsule is via time release study in which a detectable molecule is encapsulate in a shell and the free molecule (i.e. not contained in the shell) are quantified. For this study, the selected molecule was fluorescein. Fluorescein was used because its size is comparable to common drug molecules and can be quantified by fluorescence and absorption.[112]

6.2 MATERIALS AND METHODS

6.2.1 Materials

All materials were obtained from commercial suppliers and used without further purification. Sodium dodecyl sulfate (SDS) (BP166, Fisher Scientific) and 99% pure hexadecane (AC120465000, ACROS Organics) were the surfactant and costabilizer, respectively, used to form the polyurethane (PU) nanocapsules. Isophorone diisocyanate (IPDI) 98% (AC427602500, ACROS Organics) and 1,6-hexanediol (HDOH) 97% (AAA1243930, ACROS Organics) were the reactants from which PU was formed. Fluorescein (free acid, dye content 95%) (F2456, Sigma-Aldrich) was the fluorescent molecule that was encapsulated in the PU shell and used to quantify the total mass that the PU nanocapsules can encapsulate and release. Phosphate buffered solution (PBS) was used in the release study. One PBS tablet (P4417, MilliporeSigma) dissolved in 200 mL of deionized water yielded 0.01 M phosphate buffer, 0.0027 M potassium chloride, and 0.137 M sodium chloride, pH 7.4, at 25 °C.

6.2.2 Preparation of Fluorescent Capsules

PU nanocapsules encapsulating fluorescein were also synthesized referencing procedures previously published in literature to encapsulate triethylene glycol TEGDMA.[89-90] PU nanocapsules were formed via a poly-condensation in a two-phase system through mini-emulsions. Again, hexadecane and DI water formed the two phases, an oil phase and an aqueous phase. SDS was used as the surfactant to confer colloidal stability.[90]

Once 70 mL of water, 1.145 mL of HD, and 1.1 g of surfactant (SDS) were mixed together at 300 rpm and 40°C for 1 hour, 2.094 mL of IPDI was slowly dripped into the mixture and stirred; this step began the synthesis of the nanocapsules. By dripping the IPDI and monomers into the solution, the IPDI was evenly distributed throughout the oil phase. As the IPDI solution entered the pre-emulsification solution, the stirring speed was increased to 400 rpm. Once the IPDI solution was fully injected into the beaker, the solution was mixed at 400 rpm and 40°C for 10 minutes. During this step, the solution remained clear. Next, the solution was sonicated with a 130-Watt Ultrasonic Processor with Thumb-actuated Pulser at an amplitude of 38% to break up any IPDI molecules that had aggregated. During this step, emulsions formed, and the solution looked like milk. While sonication was still progressing, an aqueous solution of 0.0013 g of fluorescein and 5.9 g of HDOH and 10 mL of DI water was dripped into the system. Because of the high reactivity of the isocyanate, the IPDI reacted immediately with the HDOH at the interface of the two phases.[90] The synthesis process is portrayed in Figure 45, and Figure 46 shows a flow diagram to summarize the reaction.

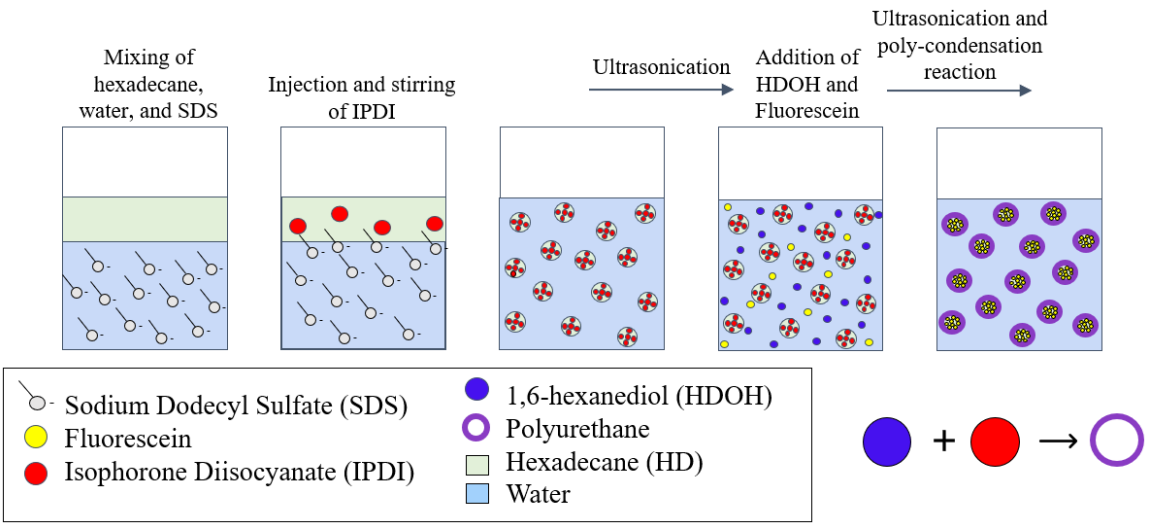

Figure 45. The synthesis method for the fluorescent capsule is depicted. Note that the SDS is a surfactant. It acts as a stabilizing agent and is always present; however, it is not be depicted fully in each step to avoid cluttering the image.

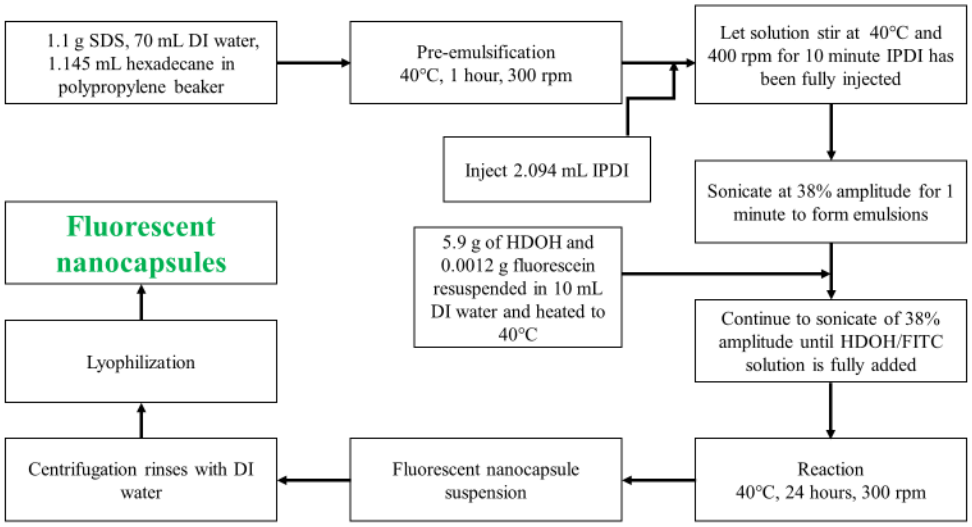

Figure 46. This flow diagram summarizes the synthesis method for the initiator capsules.

After sonication, the solution was left to react for 24 hours at 40°C and mixing at 300 rpm. After 24 hours, much of the solvent had evaporated and a clear, viscous solution was left

in the beaker. The solution was poured into a centrifuge tube and centrifuged with DI water for a total of 5 times at 10,000 rpm and 4 °C for 20 minutes each run. After each run, a distinct white pellet forms at the bottom of the tube. Additionally, after each run, the pale green supernatant was discarded, new DI water was added to the tube, and the pellet was resuspended. After the fifth centrifugation period, the supernatant was again discarded, new DI water was added, and the pellet was then resuspended. The resuspended pellet was frozen in liquid nitrogen and lyophilized. When fully dry, the capsules appeared to be a white powder.

6.2.3 Characterization of Nanocapsules

Capsule morphology and size. A vacuum sputter coater (Denton Desk II) was used to deposit a 20 nm layer of gold palladium onto the nanocapsule samples placed on carbon tape on a specimen stub for scanning electron microscopy (SEM) imaging using the Nova NanoSEM 450 from FEI. The surface morphology of the capsules was examined as well as the diameters of the capsules.

Capsule size and zeta potential. The Malvern ZetaSizer (Nano ZS90) was used to determine the diameter and calculated zeta potential of the nanocapsules via dynamic light scattering (DLS). The nanocapsules were placed in a 1mg/mL solution of 190 proof ethanol for sizing. This solution was pipetted into a cuvette (14955129, Fisher Scientific) which was placed into the ZetaSizer. The capsules were placed in a 1mg/mL solution of 10 mM potassium chloride (KCl) to determine the zeta potential. To measure the zeta potential, the solution was inserted into a folded capillary zeta cell (Malvern Store, DTS1070) which was

placed in the ZetaSizer. Both the size and zeta potential measurements were run in triplicates.

Capsule molecular components and structures. Fourier-transform infrared (FT-IR) (PerkinElmer Frontier Optica) spectroscopy was used to produce spectra to identify the molecular components and structures associated with the capsules. Gel Permeation Chromatography (GPC) (Viscotek, VE 2001) was used to measure the molecular weight and size of the components of the capsules. The GPC column (PL1110-6504) is of the Agilent Plgel MIXED family. Its phase is MIXED-D, its inner diameter is 7.5 mm, its length is 300 mm, and its particle size is 5 μm. To measure molecular weight and size, the reagents and capsule samples were first crushed via mortar and pestle. Then, a 10 mg of the crushed sample was resuspended in 1 mL of tetrahydrofuran (THF). This solution was filtered with PTFE membrane syringe filters (Fisher, 09-720-002) into GPC vials (VWR, 89239-024) which were placed in the machine for testing.

Characterization of Capsule Response to Sonication. 10 mg of the fluorescent capsules were suspended in PBS. First, the capsules were washed multiple times via centrifugation in a microcentrifuge for 10 minutes at 13.3 rpm. After each wash, the supernatant was removed and filtered through a 0.22 μm PTFE membrane syringe filter (0970002, Fisher Scientific). Fresh PBS was added to resuspend the pellet. The supernatant was then run on a fluorescent plate reader (Molecular Devices, SpectraMax M2) (excitation max: 485; emission max 525). This washing process was repeated until the fluorescence reading was below 20 to ensure that readings are not influenced by free fluorescein. At this point, the pellet was again resuspended in fresh PBS, and the solution was sonicated with a 130-Watt Ultrasonic Processor with Thumb-actuated Pulser at an amplitude of 76% for 30 seconds

to break the shells of the capsules. After sonication, the solution was centrifuged again, the supernatant was removed and tested, and new PBS was added to resuspend the pellet. Then, the solution was inserted into a rotator in an oven at 37°C for 15 minutes. After 15 minutes, the solution was again centrifuged, the supernatant was removed and tested, and new PBS was added to resuspend the pellet. The sonication and heating were repeated until the fluorescent readings were again below 20 after the sonication and all of the fluorescein was released from the capsules.

This entire process was repeated on another set of samples to determine the effect of the sonication time length. The only difference in this process was that the samples were sonicated at an amplitude of 76% for 1 minute.

Characterization of Capsule Release. 10 mg of the fluorescent capsules were suspended in PBS. First, the capsules were washed multiple times via centrifugation in a microcentrifuge for 10 minutes at 13.3 rpm. After each wash, the supernatant was removed and filtered through a 0.22 um PTFE membrane syringe filter (0970002, Fisher Scientific). Fresh PBS was added to resuspend the pellet. The supernatant was then run on a fluorescent plate reader (Molecular Devices, SpectraMax M2) (excitation max: 490; emission max 525). This washing process was repeated until the optical density was below 20. At this point, the pellet was again resuspended in fresh PBS and the solution was placed in a rotator in an oven at 37°C. At specific time points, the solution was centrifuged for 10 minutes at 13.3 rpm, the supernatant was removed and stored in darkness at 4°C, and the pellet was resuspended in fresh PBS.

6.3 RESULTS AND DISCUSSION

6.3.1 Capsule Characterization Results.

The resulting characteristics of the PU nanocapsules with fluorescein were similar to those of the monomer nanocapsules. Figure 47 and Figure 48 show the DLS results of the capsules. Figure 49 shows the FT-IR spectrum for the capsules, and Figure 50 presents the GPC data.

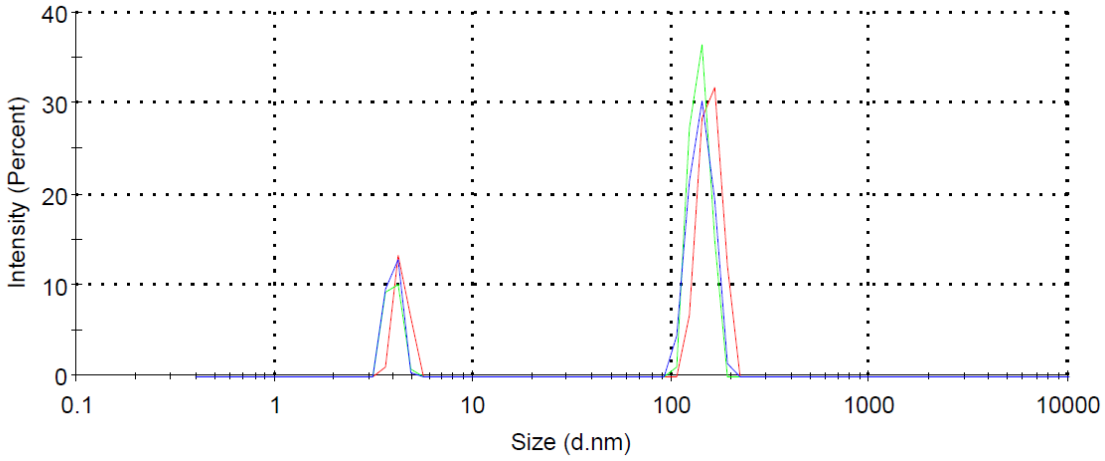

Figure 47. Three size replicates were collected. The first replicate had a diameter z-average of 438.4 nm with a polydispersity index (PDI) value of 0.838. The second replicate had a diameter z-average of 613.4 nm with a polydispersity index (PDI) value of 0.946. The third replicate had a diameter z-average of 472.8 nm with a polydispersity index (PDI) value of 0.917. The z-averages were very large due to aggregates of particles in the solution. The peak 1 values of the replicates were used to more accurately determine the size of the particles. The peak 1 value is the value that is measured most often during the scanning. The peak 1 value for the first reading was 156.6 nm. The second peak 1 value was 138.9 nm, and the third peak 1 value was 140.8 nm. The average of these peak values was 145.4 nm, meaning that the average size of the particles was 145.4 nm.

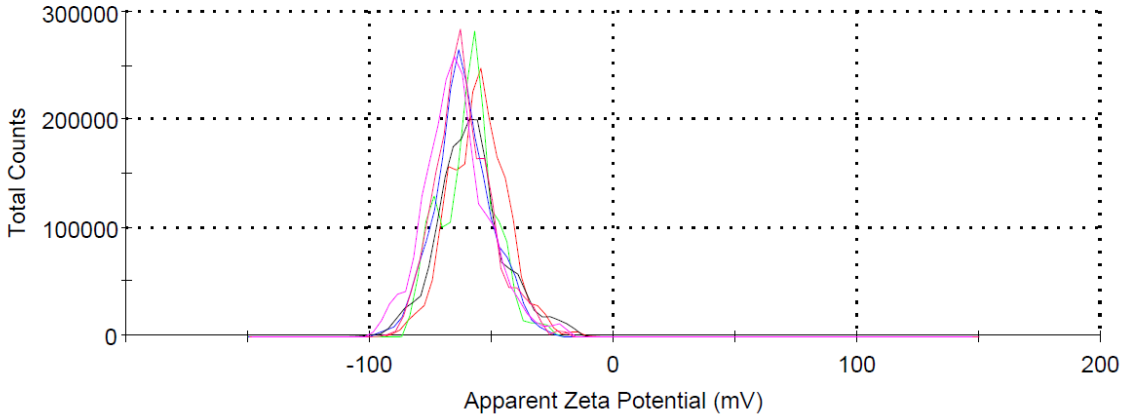

Figure 48. Six measurements were determined. The average zeta potentials aver the 6 replicates was -60.1 mV with an average zeta deviation of 12.4 mV.

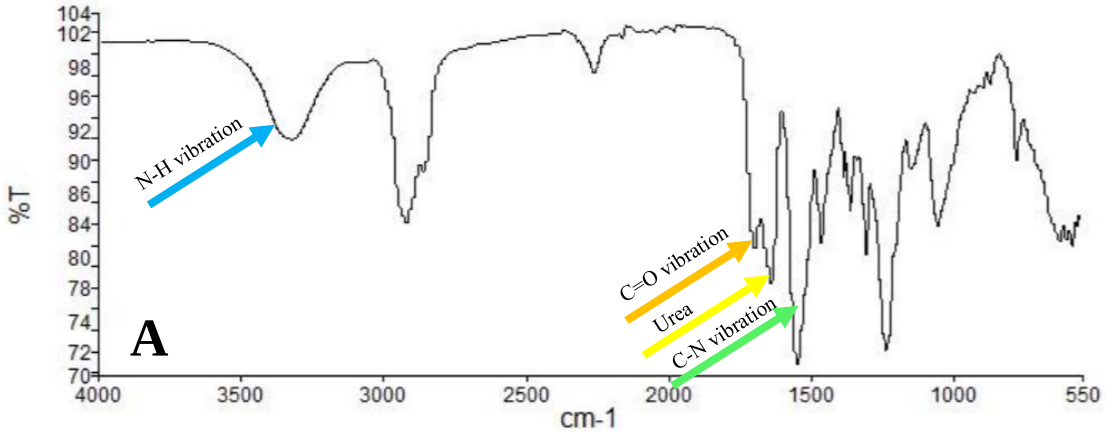

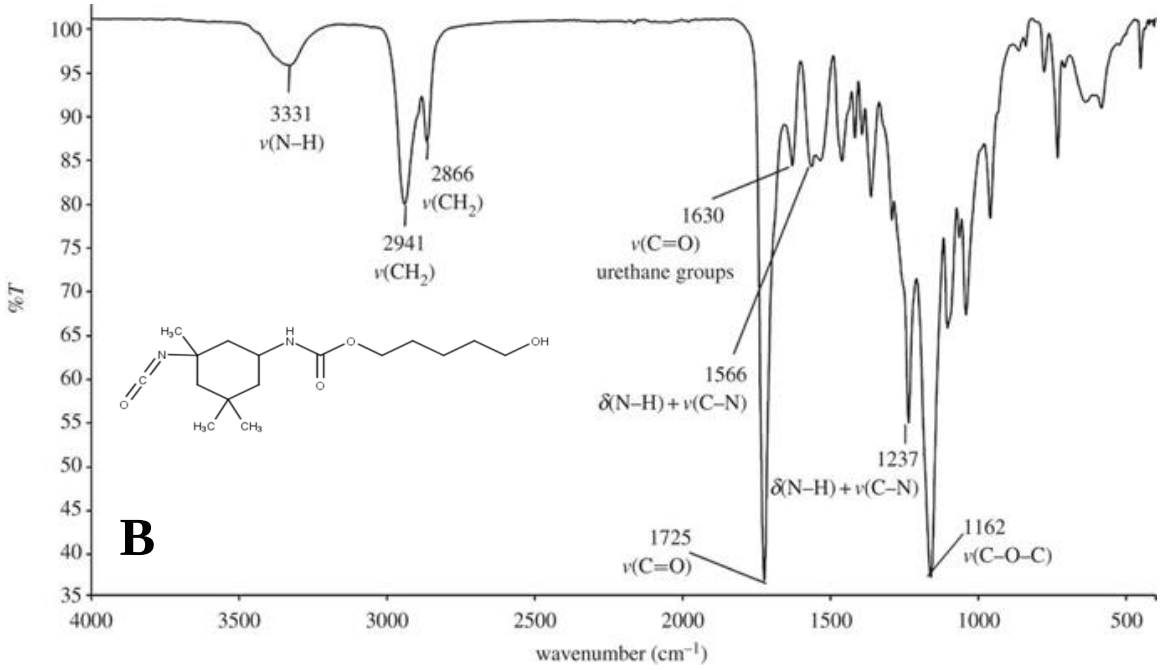

Figure 49. (A) The spectrum shows the peaks obtained from FT-IR for the PU nanocapsules encapsulating fluorescein. The peak at 1550 cm-1 represents the C-N vibration in the urethane present in each capsule. The peak at 1637 cm-1 appears due to the urea carbonyl presence in each capsule. The peak at 1720 cm-1 shows the C=O vibration, present in each capsule. Lastly, the peak at 3330 cm-1 depicts the N-H vibration present in each capsule.[77, 91-92] *(B) The spectrum is that of pure urethane along with the urethane molecule for reference, all taken from literature.*[93]

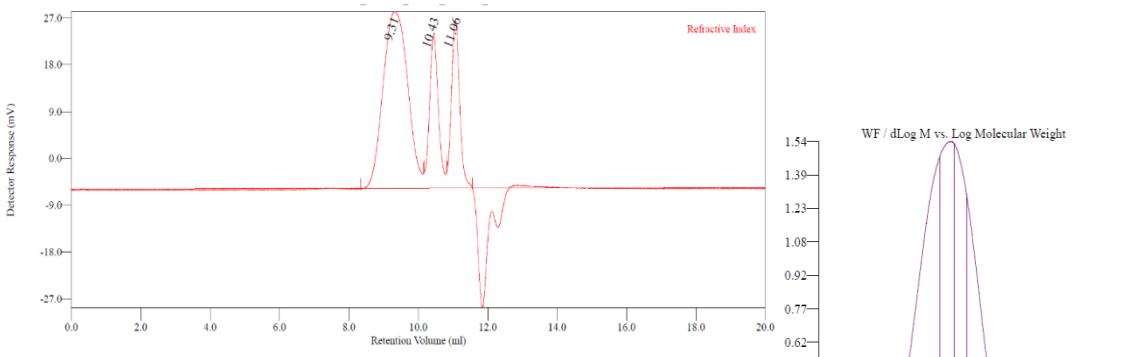

Conventional Calibration - Homopolymers : Results

Peak RV - (ml)	9.307	10.430	11.057
Mn - (Daltons)	1,462	212	64
Mw - (Daltons)	1,992	225	67
Mz - (Daltons)	2,627	238	71
Mp - (Daltons)	1,827	229	68
Mw / Mn	1.362	1.064	1.056
Percent Above Mw: 0	100.000	100.000	100.000
Percent Below Mw: 0	0.000	0.000	0.000
Mw 10.0% Low	639	134	42
Mw 10.0% High	4,396	328	95
Wt Fr (Peak)	0.613	0.194	0.193
RI Area - (mvml)	28.03	8.87	8.81
UV Area - (mvml)	0.00	0.00	0.00

Figure 50. The GPC data shows the molecular weight of the PU shell. The peak at 9.31 mL represents PU. The number average molecular weight (Mn) is 1,462 Da, and the weight-average molecular weight (Mw) is 1,992 Da. The polydispersity (Pd=Mw/Mn) of the PU is 1.362. The GPC column's operating range is 200 to 400,000 Da. The peak at 10.430 mL represents butylated hydroxytoluene. This is the stabilizer in the THF. The last peak (at 11.06 mL) is a solvent peak.

SEM images of the fluorescent capsules are shown in Figure 51.

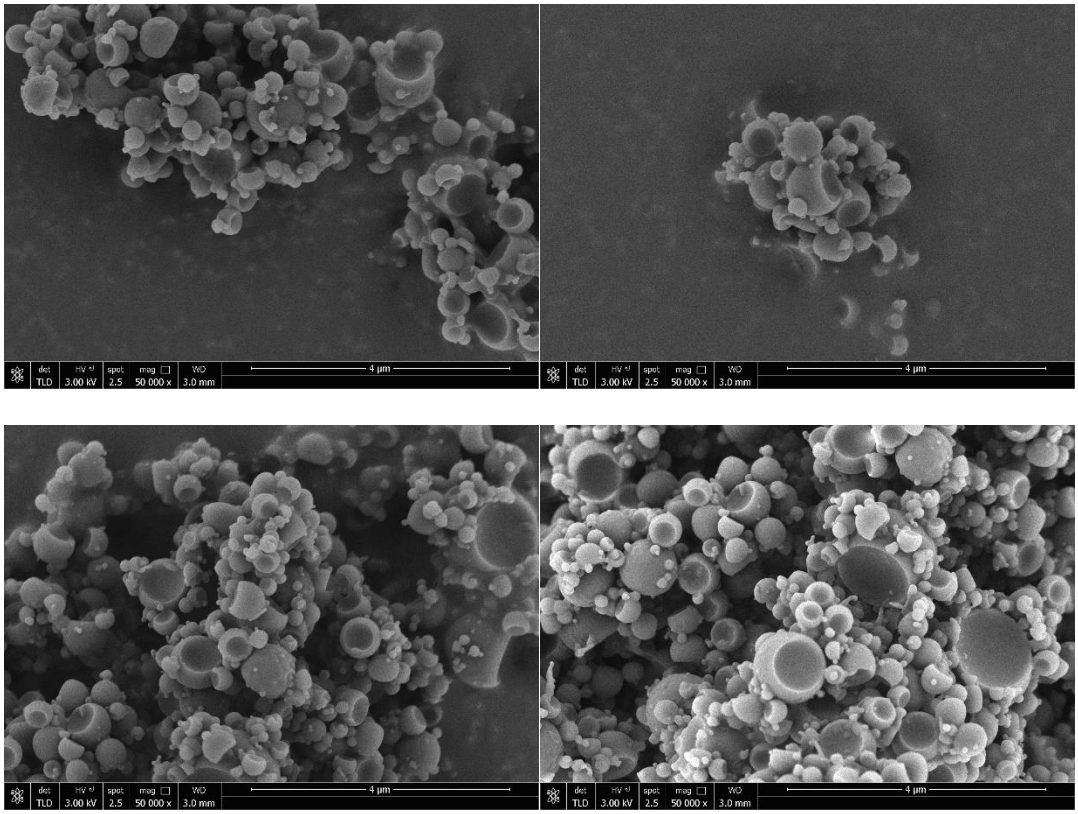

Figure 51. The SEM images show the fluorescent PU capsules before any fluorescein was released from them.

The characterization results proved that our fluorescent nanocapsules were indeed in the nano-size range with an average diameter of 145.4 nm. There were also smaller peaks around 4 nm. This is very common in PU syntheses.[75, 113] The capsules were negatively charged with a zeta potential of -60.1 mV. The FT-IR demonstrated that PU was present in the capsule composition. The GPC data showed that the polyurethane's weight average molecular weight was 1,992 Da. Although this is a relatively low Mw for polymers, it simply means the PU chains in the capsules were not as long. This could have resulted from crushing the capsule samples to prepare them for the GPC testing. The samples had to be crushed to ensure each part of the capsule could be measured appropriately; however,

in our efforts, only the PU was measured since fluorescein has a molecular weight that is on the edge of the GPC column's operating range. The SEM images help to further our understanding of the capsules. From the images, one can conclude the particles were polydisperse in size. The capsules also appear to have a concave edge. This suggests that the capsules were either deformed when they were lyophilized or required the reaction to proceed longer than 24 hours to further harder the shell.

6.3.2 Release Study Results

Figure 52 shows the standard curve used to determine the concentrations in the bursting study and release study. The standard curve was created by suspending fluorescein in PBS to form a 500 μM solution. Then, 2-fold serial dilutions were performed.

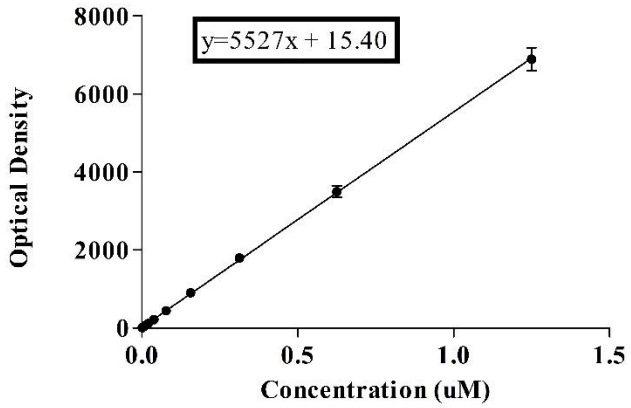

Figure 52. The standard curve used to determine the concentrations of the fluorescein released from the capsules due to sonication is shown. Fluorescence is plotted as a function of concentration measured in (μM). The equation of the line of best fit is y=5527x+15.40. Errors are STDEV, n=31.

Using a fluorescent plate reader, the loading (mg) of fluorescein per mass (mg) of capsules was determined to be 0.1.38E-09 mg/mg. From this, the loading efficiency was calculated to be 0.0013%. This was determined using the standard curve, shown in Figure 52. This loading was very low which suggested that the fluorescein was only trapped within the membrane of the PU shell rather than within the PU shell. This is a reasonable hypothesis considering the hydrophilicity of fluorescein. Because fluorescein is a more hydrophilic molecule, it is most probable that the molecule was not truly encapsulated within the PU shell. This is especially true considering that the interfacial polycondensation reaction scheme used is intended to encapsulate a hydrophobic molecule.

The results from the 30 second sonication study are shown in Figure 53 and the results from the 1-minute sonication study are shown in Figure 54. The concentration released from the capsules after each sonication period and 15-minute heating period were calculated using the equation of the line from the standard curve in Figure 52.

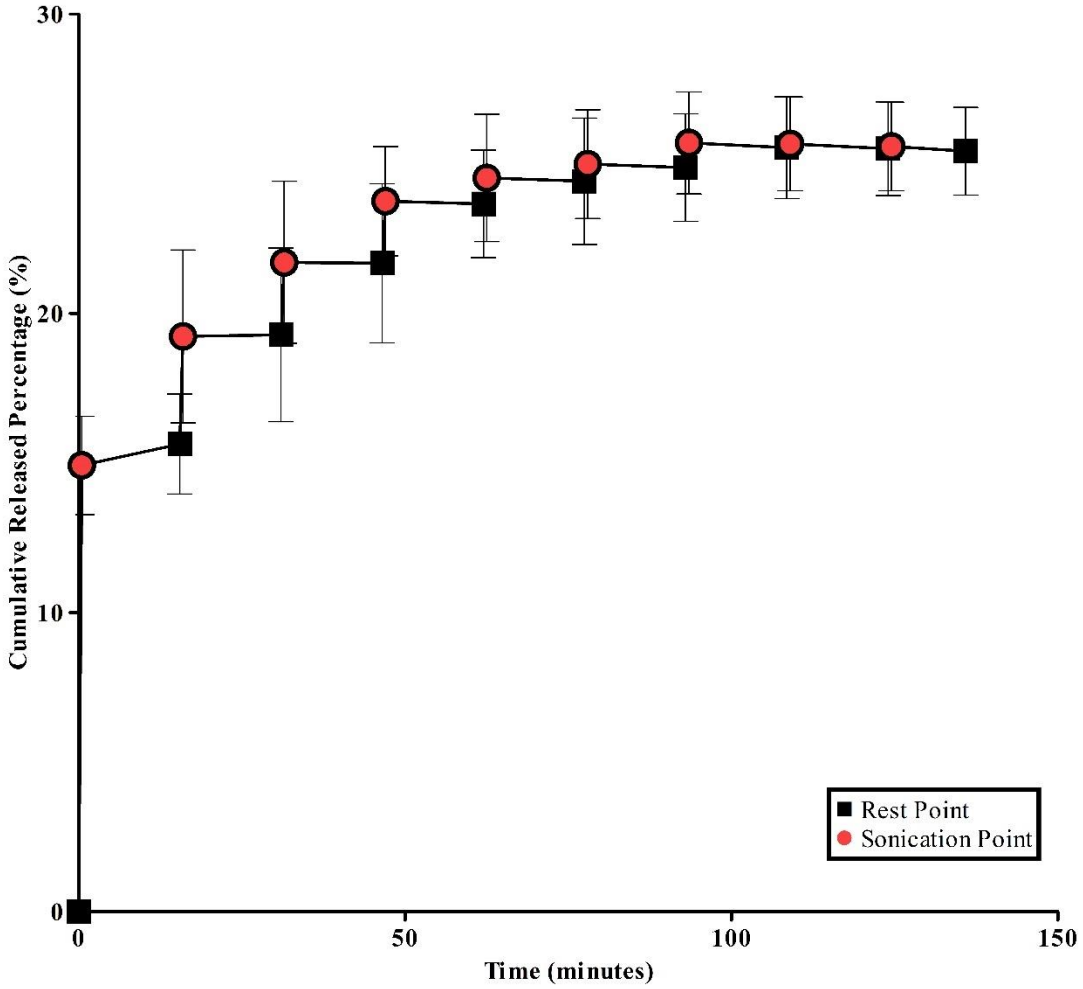

Figure 53. The percentages of the fluorescein released at each sonication point from the capsules due to sonication for 30 second increments and after each 15-minute wait period as functions of time are shown. Each of the samples tested were from the same bulk sample. Errors are STDEV, n=5. Note, the y-axis only reaches 30% to assure that the steps are evident in the graph.

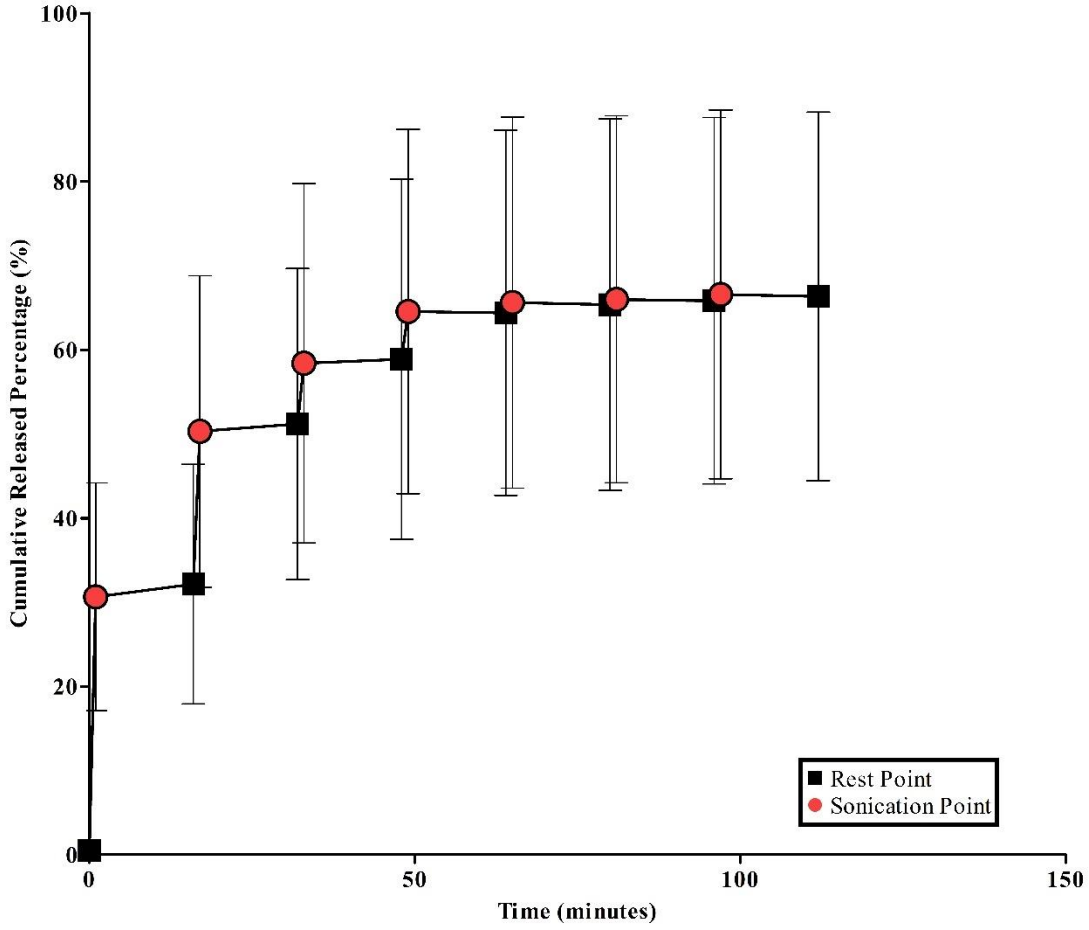

Figure 54. The percentages of the fluorescein released at each sonication point from the capsules due to sonication for 1-minute increments and after each 15-minute wait period as functions of time are shown. Each of the samples tested were from the same bulk sample. Errors are STDEV, n=3.

The sonication study, with the 15-minute heating periods, prove that sonication does break the capsules and releases the encapsulated contents. Figure 55 shows SEM images of the broken capsules caused by sonication during testing. Because after each 15-minute heating period, the concentration released from the capsules is essentially 0 μM, it was concluded it is not the heat from the sonication that weakens the capsules. Instead, the energy added

to the system via sonication breaks the urethane bonds. The amount of fluorescein released decreases as the number of sonication periods progress because the number of unbroken capsules is increasingly decreasing. In conclusion, from this study, we have proven that we can trigger release from our nanocapsules, thus these capsules show potential for use in drug release triggered by ultrasound.

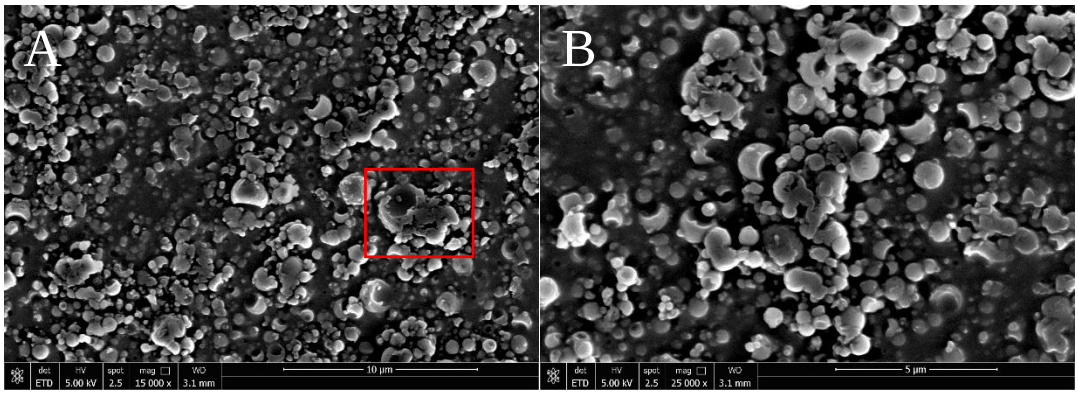

Figure 55. (A) This SEM image shows a less magnified image of the broken capsules. Note that not all the capsules are burst; however, an example of a broken capsule is designated by the box. (B) This SEM image is a higher magnified image of the broken capsules. In the middle of this image, it is evident that the capsules are broken.

The two sonication studies were compared by analyzing the percentage released from the capsules. The percentage was calculated by dividing the determined mass of fluorescein released at a certain time by the theoretical total encapsulated mass of fluorescein. This quotient was then multiplied by 100. The total amount encapsulated by the capsules was determined by continuously sonicating a sample of capsules until no more amount of fluorescence was detectable. By comparing the two different sonication studies, it is evident the length of time that the sample is sonicated makes a significant impact on the amount of fluorescein released from the capsules. During the first round of 1-minute

sonication, the amount of fluorescein released from the capsules was nearly double that released during the first round of 30 second sonication; however, the amount of fluorescein released during any sonication study was highly inconsistent, as observed from the large error bars in Figure 54. This is believed to be due to the difference in total encapsulation capacities for various capsules in the same batch of sample.

Figure 56 shows the results of the release study performed over a two-month span. Similarly, to calculating the total mass of fluorescein encapsulated in the capsules, at each time point, the mass of fluorescein released was calculated. The masses were then added together. It is important to note that fresh PBS was added at each time point to ensure an endless sink is maintained in the system. This ensured the amount of fluorescein in the supernatant did not limit the diffusion of the fluorescein from the capsules.

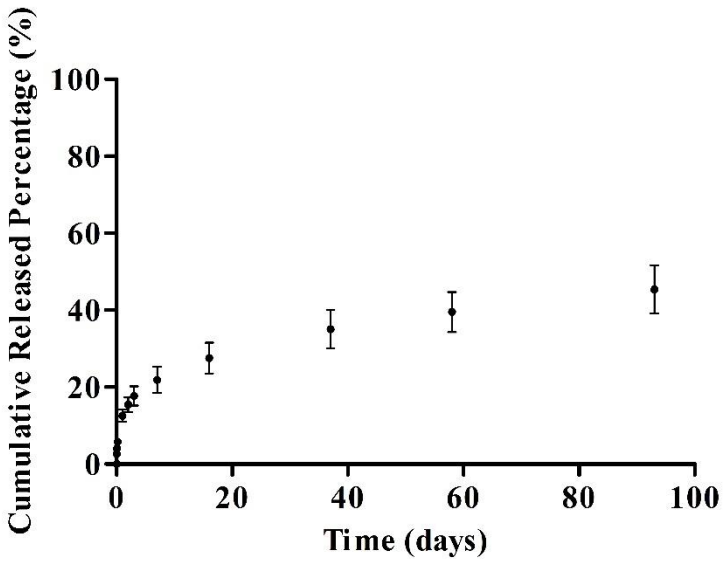

Figure 56. The cumulative concentrations of the fluorescein released at each time point from the capsules during the release study is shown. The percentage of fluorescein released from the capsules is plotted as a function of time in days. This study was run for over two months with 3 replicate samples. Each fluorescent reading was also determined by averaging 3 replicate readings from each sample. Errors are STDEV, n=3.

Our release study shows that the release of fluorescein from PU nanocapsules is very slow, and even after 3 months, not all of the encapsulated fluorescein has been released. This is evident as the percent released from the capsules is not yet 100%. The percentage was calculated by dividing the determined cumulative mass of fluorescein released at a certain time by the theoretical total encapsulated mass of fluorescein. This quotient was then multiplied by 100. The total amount encapsulated by the capsules was defined as the largest cumulative mass from a single capsule during the sonication study. Again, the loading (mg) of fluorescein per mass (mg) of capsules was determined to be 0.1.38E-09 mg/mg.

By comparing the 1-minute sonication study to the release study, as shown in Figure 57, it appears that while sonicating the capsules results in a quicker release of fluorescein, discharging fluorescein through sonication releases an unpredictable amount of fluorescein. This could be the result of how the fluorescein is probably not fully entrapped within the PU walls.

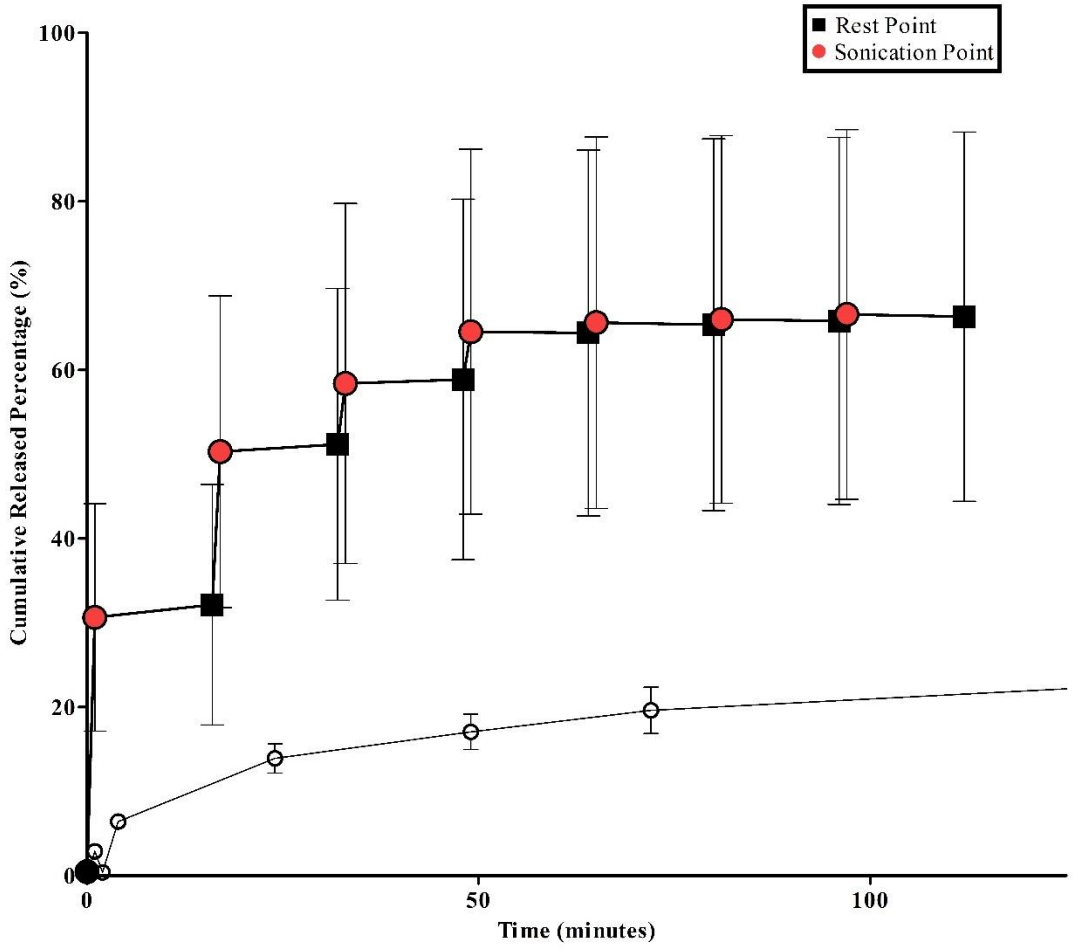

Figure 57. This graph depicts the 1-minute sonication study and the release study over-laid on the same plot. Note that the x-axis does not depict the full amount of time for which the release study occurred.

The study of PUs for controlled release of pharmaceuticals has been very limited, especially compared to the study of hydrogels.[114] The main driving forces for transport from a polymeric matrix are solute diffusion, polymer swelling, and degradation.[115] PUs are biodegrade and thus the capsules release the encapsulated contents (fluorescein) over time. Before understanding the modes of degradation in our PU, it is important to note that PU is made of two types of segments, the hard segments and the soft segments. In our PU, the hard segment consists of the IPDI and the soft segment consists of the polyol, HDOH.

Water intrusion and absorption into PUs play important roles in the degradation rate and in the drug release profile of the system.[108] PUs are susceptible to biodegradation because of the cleavage of hydrolytically sensitive bonds present in their soft segments. Oxidative degradation of urethane bonds in the hard segments into amines have also been noted to occur. The degradation kinetics highly depend on the structural composition of the PUs.[116] The polyol components control the in-vitro degradation rate.[117] PUs with hydrophilic soft segments demonstrate increased water uptake and a faster degradation rate, compared to those with hydrophobic soft segments.[117] Additionally, the molecular weight of the soft segment has an influence on PU's degradation.[118] Similarly, the degradation rate of the hard segment is highly dependent on the hard segment chemistry and size, in addition to the degree of hydrogen bonding.[119] The ratio of soft segments to hard segments affects the release rates. This is speculated to happen because the lower ratio is associated with increased cross-linking of the hard segments which ultimately results in a higher concentration of hard segments. This increased cross-linking reduces water penetration in the matrix and thus reduces drug diffusion out of the matrix.[120] PUs are decomposed in vivo through oxidative degradation. Specifically, it was reported that the α-hydrogen atom

in the R-group adjacent to the urethane reacts with reactive oxygen species to yield fragments of amines and carbon dioxide.[107]

Understanding the mechanisms of degradation and content release from the capsules is important. Studying the release of fluorescein from the capsules helps to demonstrate the potential effectiveness of our PU capsules in controlled drug release. Our release study in Figure 56 can be compared to a similar study performed by Feng et al.[121] In the study by Feng et al., PCL-PEG PCL triblock diols with various molecular weights were synthesized. Polyurethane acrylates (PUA) oligomers were obtained by reacting copolymer diols with 1,6-hexamethylene diisocyanate (HDI) or IPDI. The oligomers were end-capped with hydroxyethyl methacrylate (HEMA). These PUA films were loaded with tetracycline in PBS. Figure 58 shows the resulting release from the study.[121] Our release study, although not the same, can be compared to the profiles of the polymers containing IPDI. Our release study shows the same steep release over the first 200 hours of the study. Then, our release continues for over 3 months.

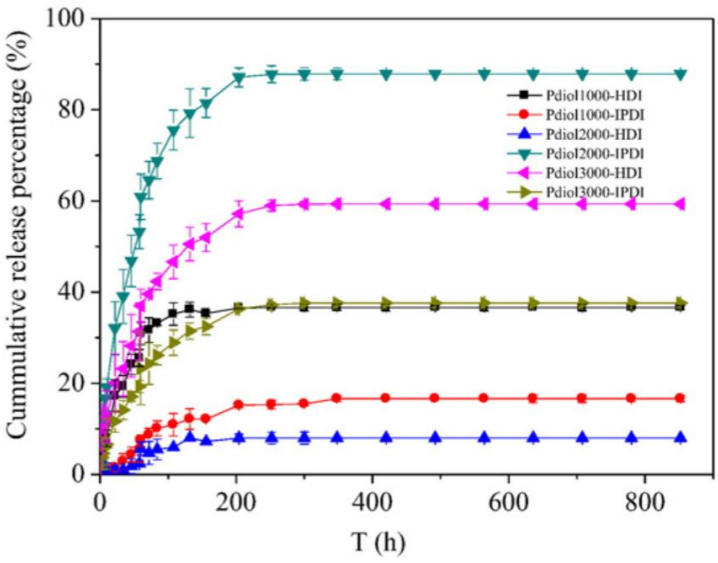

Figure 58. The drug releasing profile of cross-linked PUA films loaded with tetracycline in PBS. The errors are STDEV, n=3.[121]

6.4 CONCLUSION

The PU nanocapsules, averaging about 145 nm, were able to encapsulate fluorescein and proved to continuously release the fluorescein over a three-month span when placed in PBS. The capsules also proved to be able to burst upon command when sonication was induced. This testing provided evidence that these capsules have potential to be used as drug delivery systems; however, creating a more consistent release from the capsules is necessary. Further testing is needed in this study in order to determine how questions including how other molecules are released from these capsules and how the size of the capsules effects the release. Additionally, encapsulating a more hydrophobic molecule would increase our understanding of the encapsulation capacity of PU.

Chapter 7: Discussion

7.1 SUMMARY

In this project, we created polyurethane (PU) capsules that encapsulate monomers and initiators, intended for use to enhance the lifetime of both dental resins and bone cements. These capsules were of the nano-size range and had self-healing capabilities when both the monomer capsules and initiator capsules were broken and the monomer, triethylene glycol dimethacrylate (TEGDMA) was able to react with the initiator, benzoyl peroxide (BPO). The capsules were also proven to be able to be implemented into a resin and have been shown to break and heal a fracture when a crack propagates through the resin.

Not only do these capsules have potential for use in self-healing systems, we have also used PU capsules to encapsulate fluorescein. This allowed us to understand the encapsulation capacity of the PU capsules as well as study the potential for use of these capsules as drug delivery systems in liquid media.

7.2 FUTURE WORK

7.2.1 Improvement in Capsule Washing Process

Numerous variations were trialed to optimize the monomer capsules. Along the way, many issues were encountered. These issues included a vast size distribution, the capsules not being white, and the capsules not being obtained as a powder. These problems have been hypothesized to be the result of presence of unencapsulated triethylene glycol dimethacrylate (TEGDMA) on the outside of the capsules and the pre-mature

polymerization of TEGDMA. While the monomer capsules are functional, improvement in the washing process is still necessary. As can be seen from the SEM images in Figure 13, excess TEGDMA is present outside of the capsules. Many times, there was such a vast amount of excess TEGDMA in the system that it was difficult to locate the capsules. Many different methods were used to try to remediate this issue; however, none were truly successful.

Initially, the capsules were washed with solely water at a low centrifugation speed (4500 rpm) for 20 to 30 minutes per cycle. Then, the centrifugation was increased to 10,000 rpm for 20-minute periods. This increased speed helped increase the separation in the solution; however, it did not separate the capsules enough from the TEGDMA.

It was hypothesized that washing the capsules with ethanol instead of water would significantly reduce the amount of excess TEGDMA, since TEGDMA has a 10% solubility in ethanol.[122] To perform this washing, water was used in the first centrifugation period. Figure 59 shows how the monomer capsule sample looks after the first round of centrifugation.

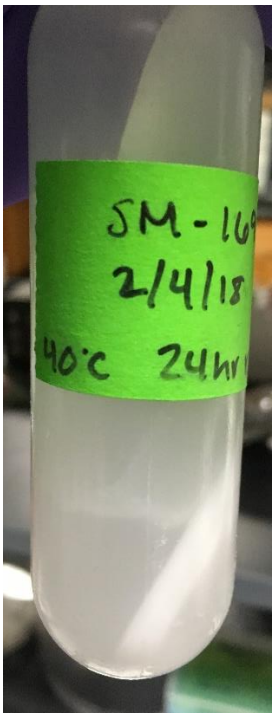

Figure 59. This is the resulting separation that occurred after the first round of centrifugation for the monomer capsules. The top layer in this image is the excess hexadecane from the reaction. The next layer is the water with a few particles suspended in it. The next layer, the white section in the bottom, right portion of the tube, is the monomer capsules; however, all of the capsules are stuck in the excess TEGDMA. The characterization of all of these layers was confirmed by FT-IR.

Then, after removing the supernatant, ethanol is used to resuspend the pellet. It is important to note that washing the capsules with ethanol first ultimately causes no separation in the solution. For this reason, water was used in the first centrifugation cycle. Ethanol was used for two centrifugation cycles. Then, water was used for the last two centrifugation cycles in order to remove the ethanol so that the sample was able to be lyophilized.

This change did not lead to significant improvements in the removal of TEGDMA. Figure 60 shows the SEM images from a sample in which this washing method was used.

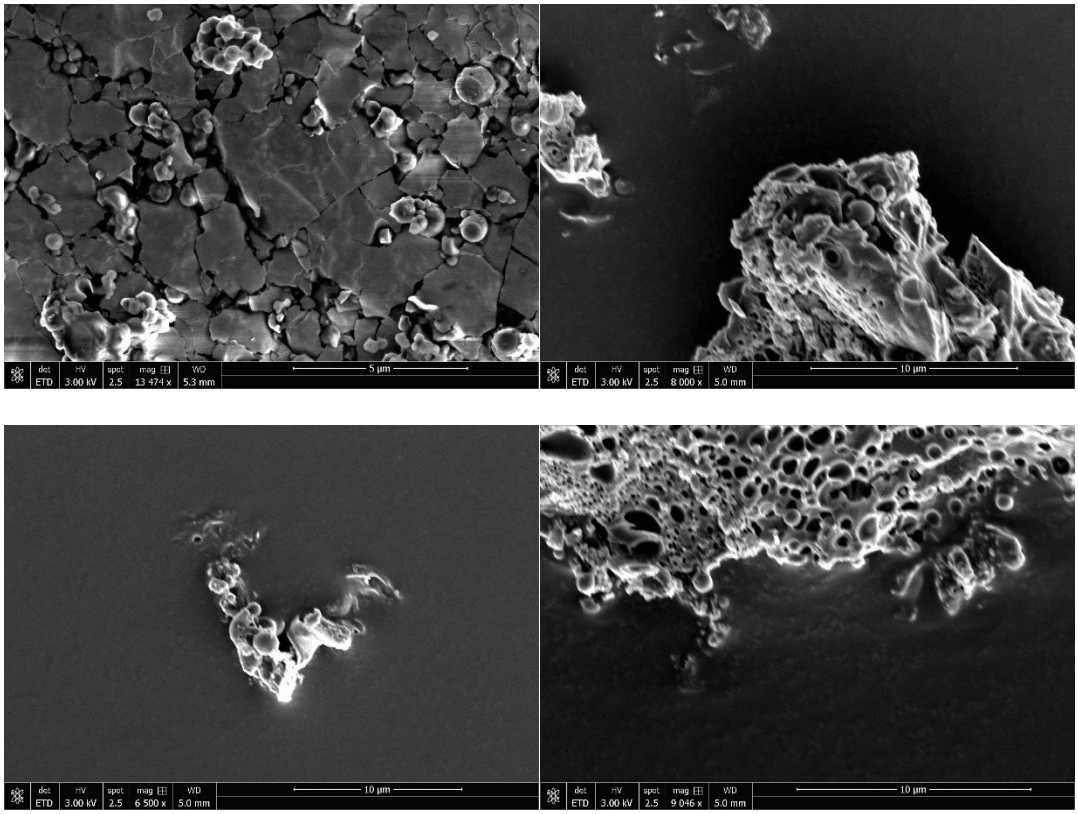

Figure 60. The SEM images portray the monomer capsules that were washed in ethanol along with the excess TEGDMA that is still present in the sample.

The means of addition and the amount of TEGDMA were next varied. First, TEGDMA was added by dripping the IPDI and monomer into the solution, as stated in Chapter 3 and shown in Figure 9. The IPDI was evenly distributed throughout the oil phase. As the IPDI and TEGDMA entered the pre-emulsification solution, the stirring speed was increased to 400 rpm. Once the IPDI and TEGDMA were fully injected into the beaker, the solution was left to mix at 400 rpm and 40°C for 10 minutes.[90]

To determine whether the injection of the TEGDMA had an influence on the reaction, the TEGDMA was instead poured into the pre-emulsification solution. More specifically, the 2.094 mL of IPDI and 6.1 mL of TEGDMA were heated to 40°C and vortexed together. Then, once the 70 mL of water, 1.145 mL of hexadecane (HD), and 1.1 g of surfactant (SDS) were mixed together at 300 rpm and 40°C for 1 hour, the mixture of IPDI and TEGDMA was poured into the pre-emulsification solution and stirred at 300 rpm for 1 minute. Then, the solution was sonicated as normal. This process is shown in Figure 61.

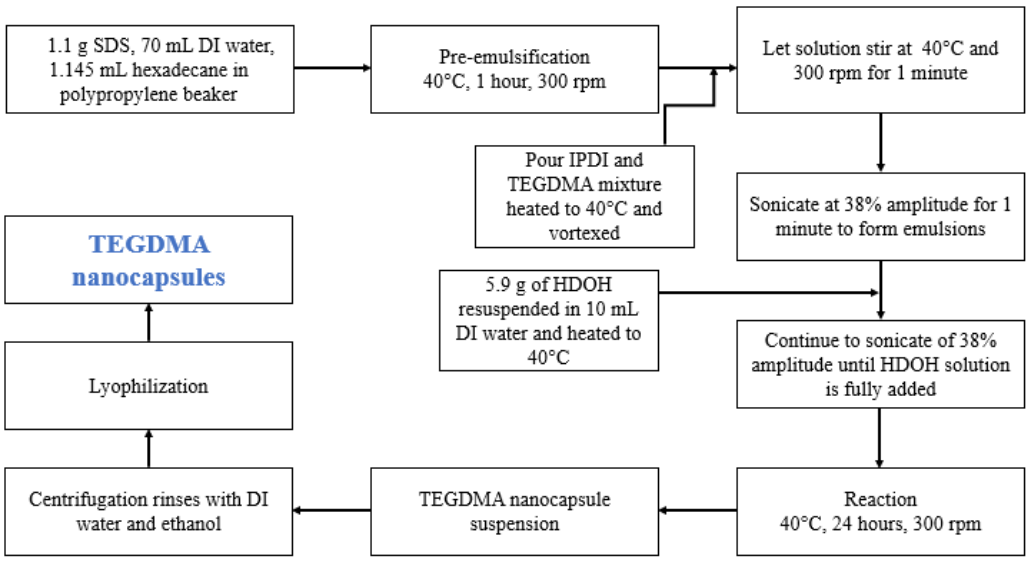

Figure 61. This flow diagram depicts the varied process by which the monomer capsules were synthesized.

The resulting capsules were again not improved. Figure 62 shows the SEM images of these capsules.

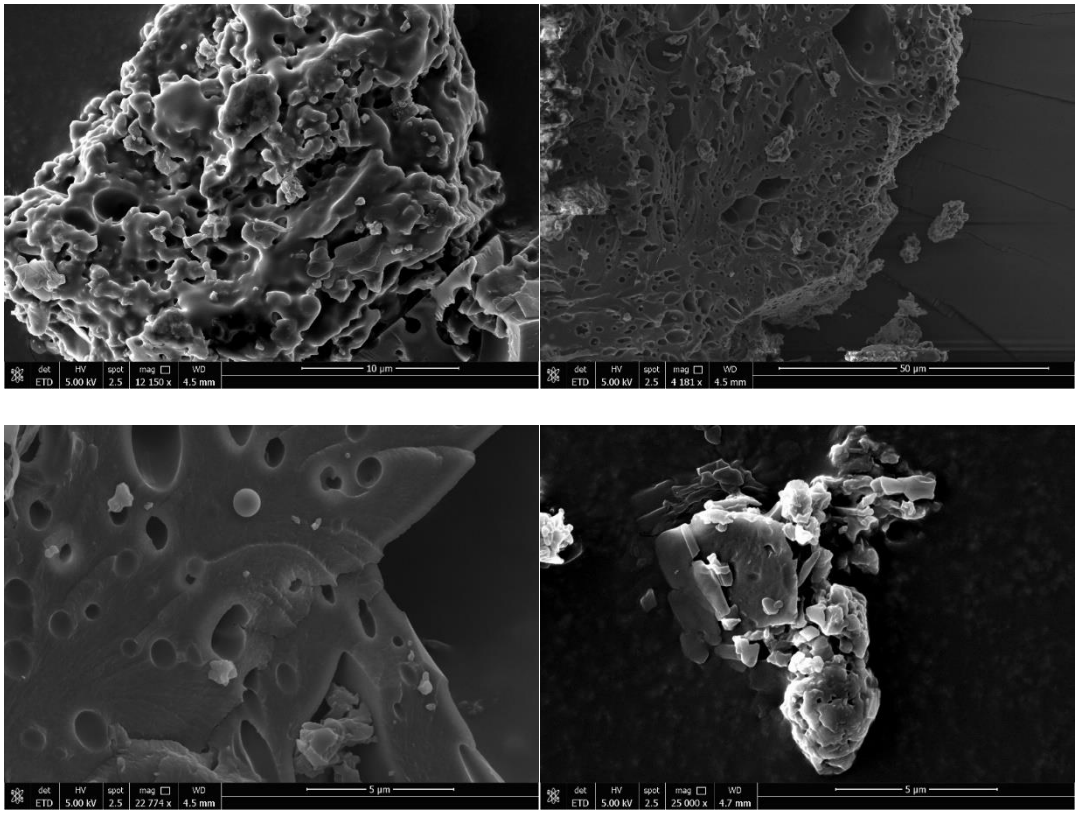

Figure 62. These SEM images depict samples created using the pouring technique with 6.1 mL of TEGDMA.

The amount of TEGDMA was next decreased, but the same pouring technique was used to add the TEGDMA. The amount of TEGDMA was decreased by 50% and 75% of the initial volume added. Figure 63 and Figure 64 portray SEM images for the capsules made with the pouring technique with 50% TEGDMA and the pouring technique with 25% TEGDMA. Note that in the images, the swiss cheese like structures are the excess TEGDMA that has polymerized outside of the capsules.

.

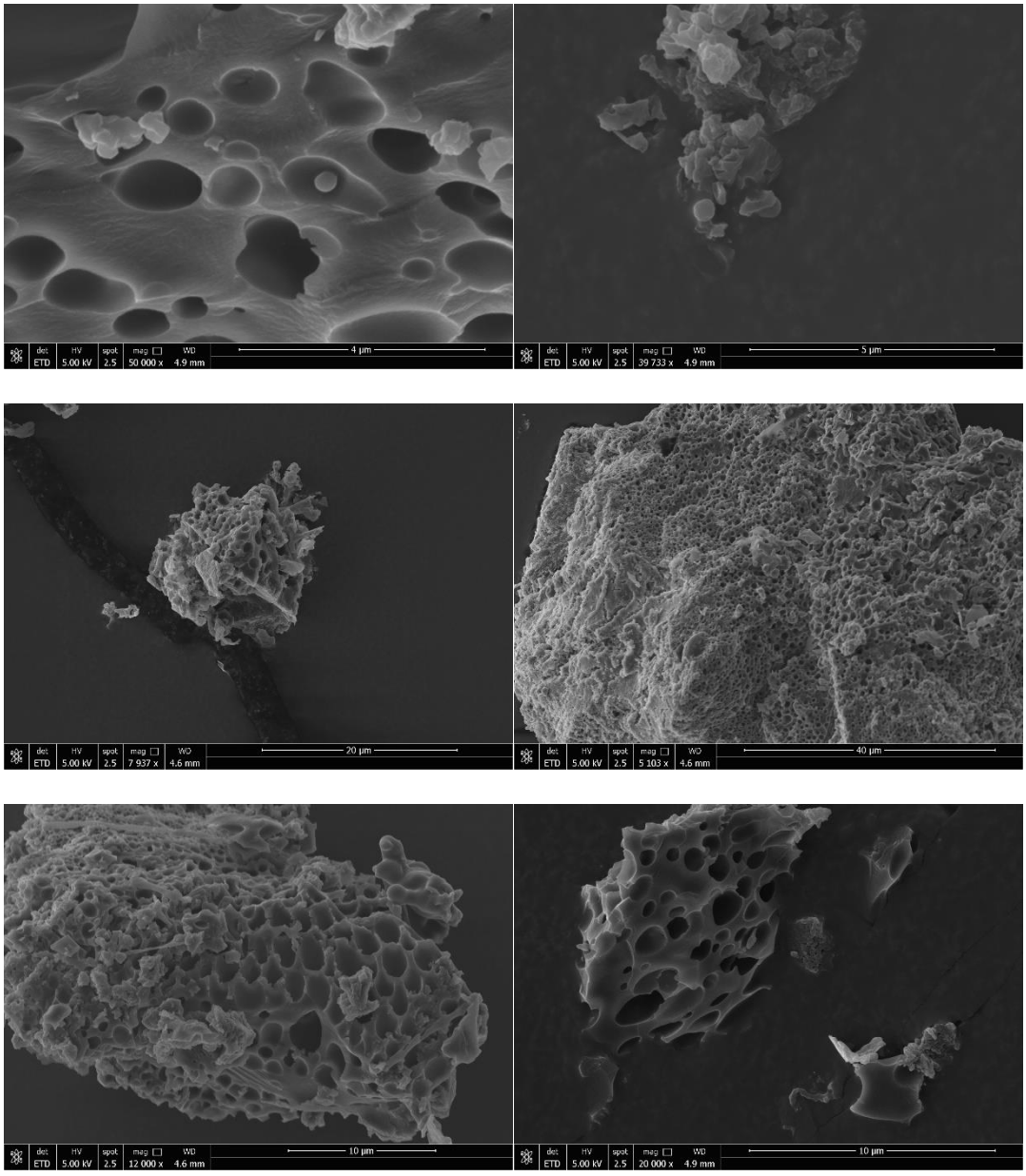

Figure 63. These SEM images depict samples created using the pouring technique with 3.05 mL of TEGDMA.

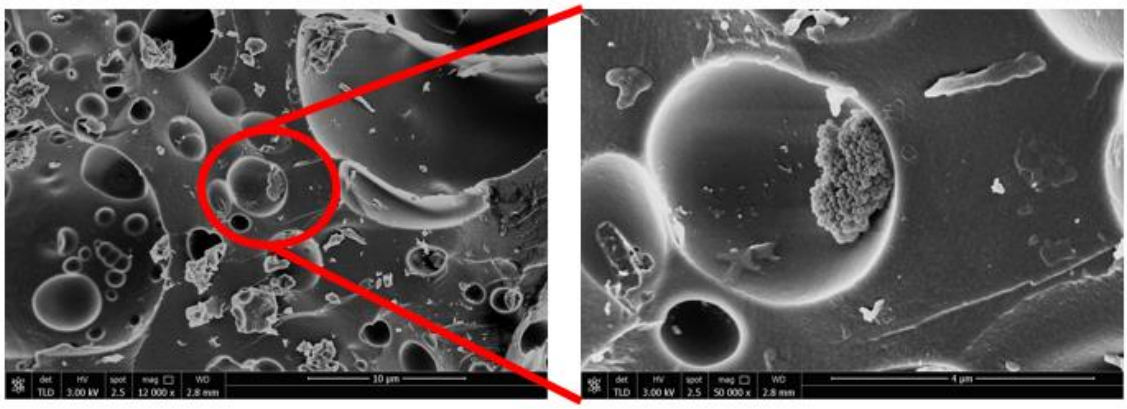

Figure 64. The SEM images show samples created using the pouring technique with 1.525 mL of TEGDMA. The image on the right is a magnification of the image on the left. Still in this image, it is evident that there is a large excess of TEGDMA.

All of the capsules created in the method variations were indeed PU capsules that encapsulated TEGDMA, as confirmed via FT-IR. Though many different methods were trialed, no conclusion resulted that led to a clear direction on how to lessen the amount of excess TEGDMA in the resulting monomer capsule sample. Comparing the results of the two synthesis methods showed that both methods create PU nanocapsules encapsulating TEGDMA; however, excess TEGDMA remains in the product. This means, the washing methodology must be improved in order to create a purer, more usable product.

7.2.2 Silica Coating

For capsules inserted into a resin, a dense silica shell can be incorporated around PU nanocapsules containing monomers and initiators to improve the strength of the self-healing system. It is important to address the stability of both the nanocapsules containing the initiator and the nanocapsules containing the monomers as well as the dispersion of the capsules in the matrix. The dense silica layer will not only protect the capsules from

prematurely bursting but will also limit the aggregation of the capsules when added to the resin matrix. The capsules will then be able to be dispersed at high concentrations and suffer little loss of reactivity.[123] Ultimately, the silica shell, when optimized, will increase the efficacy of the self-healing system to restore nearly all the strength of the virgin fracture toughness in a cracked resin.

Silica is a valuable shell material because it is chemically inert, optically transparent, porous in structure, and size-selectively permeable.[124] Coating colloidal particles with silica is very common in fields of colloid and material science; it adds both a protective and functional layer to the particle. Silica coating will not only increase the mechanical strength of the nanocapsules, but it will also allow manipulation of the interaction potential and make it possible for the capsules to disperse in a multitude of solvents in order to best heal any cracks that form in the resin.[125]

The Stöber method will be used to add silica to nanoparticles via the hydrolysis of tetraethyl orthosilicate (TEOS).[124] This procedure will result in a smooth silica shell because the growth will take place on a molecular level.[125] More specifically, TEOS will be added to an aqueous solution of the PU nanocapsules. Then, ammonium hydroxide will be added to the solution, and the solution will be stirred at room temperature for a various number of hours. Again, the particles will be washed by centrifugation in water.

The resulting nanocapsules with the dense silica shell will be larger than the nanocapsules without the silica shell. The capsules will also be more mechanically robust than the

nanocapsules without the silica shell, thus reducing the chance of premature bursting of the particle. Additionally, they will experience improved dispersion in the dental resin without the formation of large aggregates of particles. The silica-coated capsules will be examined using the same analytical methods that were used to determine the size, appearance, chemical composition, and loading efficiency of the capsules without the silica shell. Additionally, X-ray diffraction will be used to measure the crystalline structure of the silica coating. If the silica shell does not prove thick and durable during mechanical and analytical testing, the concentrations of TEOS and ammonium hydroxide will be altered to optimize the silica shell thickness while maintaining the nano-size of the capsules.

Some preliminary work has been performed to add silica to PU nanocapsules via the Stöber method. The time, the amount of catalyst, the amount of TEOS, the mass of capsules, the reaction time, the stirring speed, and the reaction temperature have all been varied and compared to the "standard" synthesis product. The "standard" reaction began with 1 gram of capsules resuspended in 20 mL of 190 proof ethanol. Then, a solution of 4 mL of TEOS, 50 mL of 190 proof ethanol, and 30 mL of DI water was quickly added. Then, 5 mL of NH_4OH was added to the solution that was stirring at room temperature on at 300 rpm. The reaction, at this point, was left for 21 hours. After 21 hours, the solution was washed with water via centrifugation to remove all the unreacted materials. The centrifugation occurred at 4500 rpm for 20 minutes for 3 cycles. A pellet formed at the bottom of the centrifuge tube after each centrifugation period. After the solution was washed, it was frozen in liquid nitrogen and lyophilized, so the sample became a white powder.

No clear optimal reaction method has been determined. The major issue seen in the product of the synthesis is the excess silica present that decreases the density of capsules that can be added to the resin. This ultimately lessens the potential for self-healing in the resin, the overall purpose of the capsules. Figure 65 displays silica coated initiator capsules created via the Stöber method using the "standard" protocol. Figure 66 again displays initiator capsules coated with silica using the "standard" protocol; however, this figure displays SEM images coupled with Energy Dispersive X-ray (EDX) Spectroscopy. Scanning electron microscopy with energy dispersive X-ray spectroscopy (SEM/EDX) is the best known and most widely-used of the surface analytical techniques.

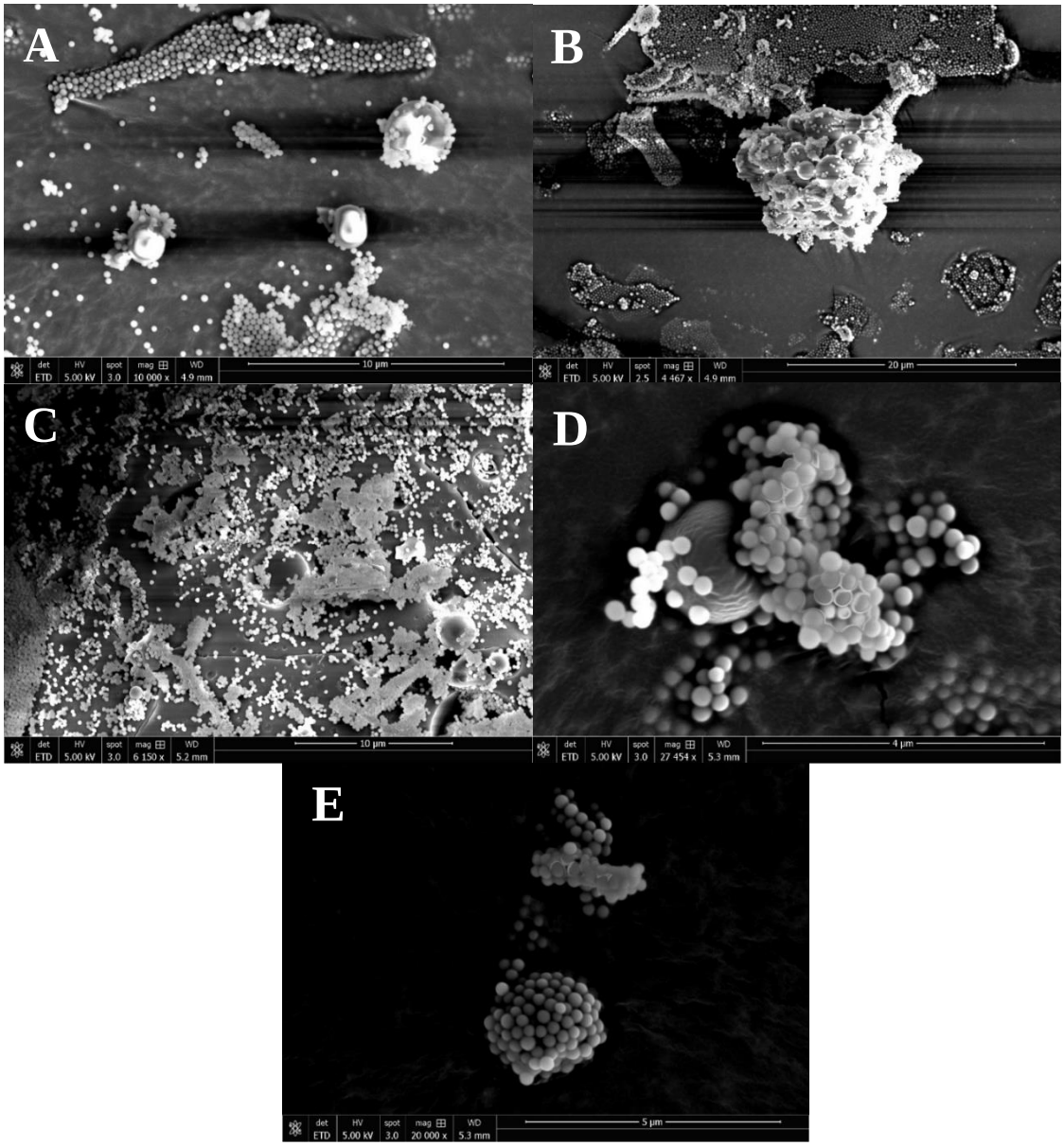

Figure 65. Images A and B are SEM images of silica encapsulating PU nanocapsules. Images C and D are SEM images of another PU nanocapsule sample coated in silica. In the images, the large spheres are PU nanocapsules and the smaller spheres are the silica. Image E is an SEM image of another initiator capsule coated in silica; however, in this image, the PU capsule is not visible because it is completely covered in silica. All the particles in these images were coated with 10 nm of platinum palladium.

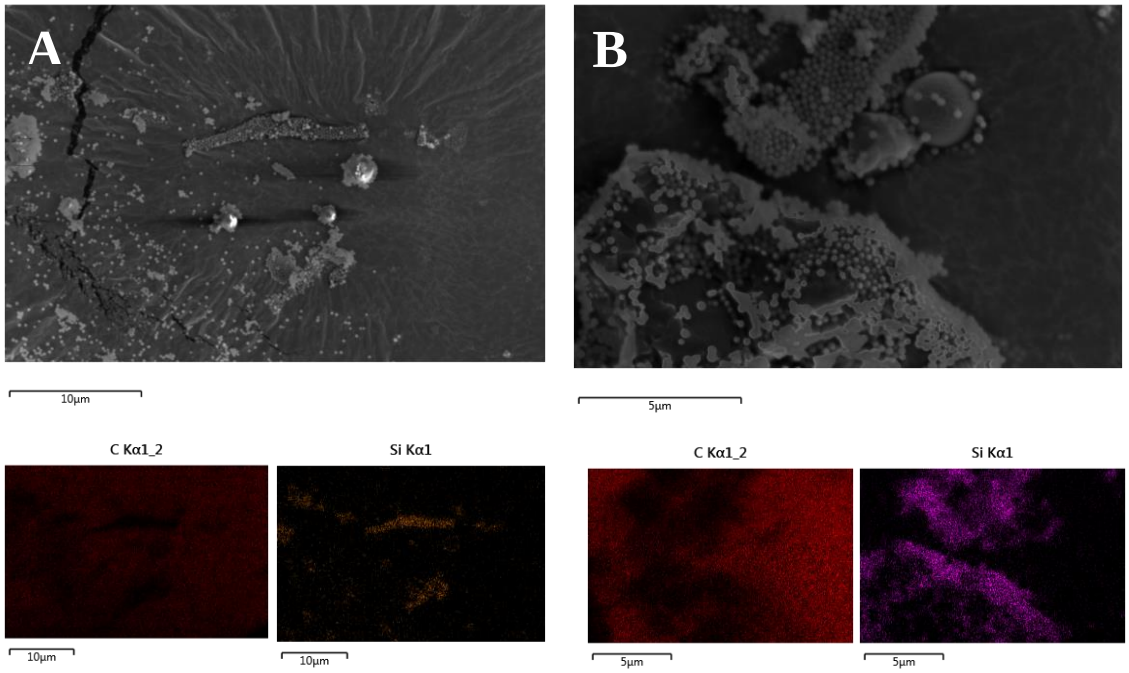

Figure 66. Image A is an SEM image of PU capsules coated with silica. Below this image are the EDX images. The EDX image on the left shows the carbon atoms and the image on the right shows the silicon atoms. Image B is an SEM image of another sample of PU capsules coated with silica. Below this image are the EDX images. The EDX image on the left shows the carbon atoms and the image on the right shows the silicon atoms. The particles in these images were coated with 10 nm platinum palladium.

Various syntheses methods were compared in a bar graph comparing the size of the coated capsules with the original size of the uncoated capsules. This data was collected via DLS and is shown in Figure 67. Note that no succinct conclusion pertaining to the best synthesis method can be drawn from this data. More trials for each method need to be analyzed and a smaller silica density must be present.

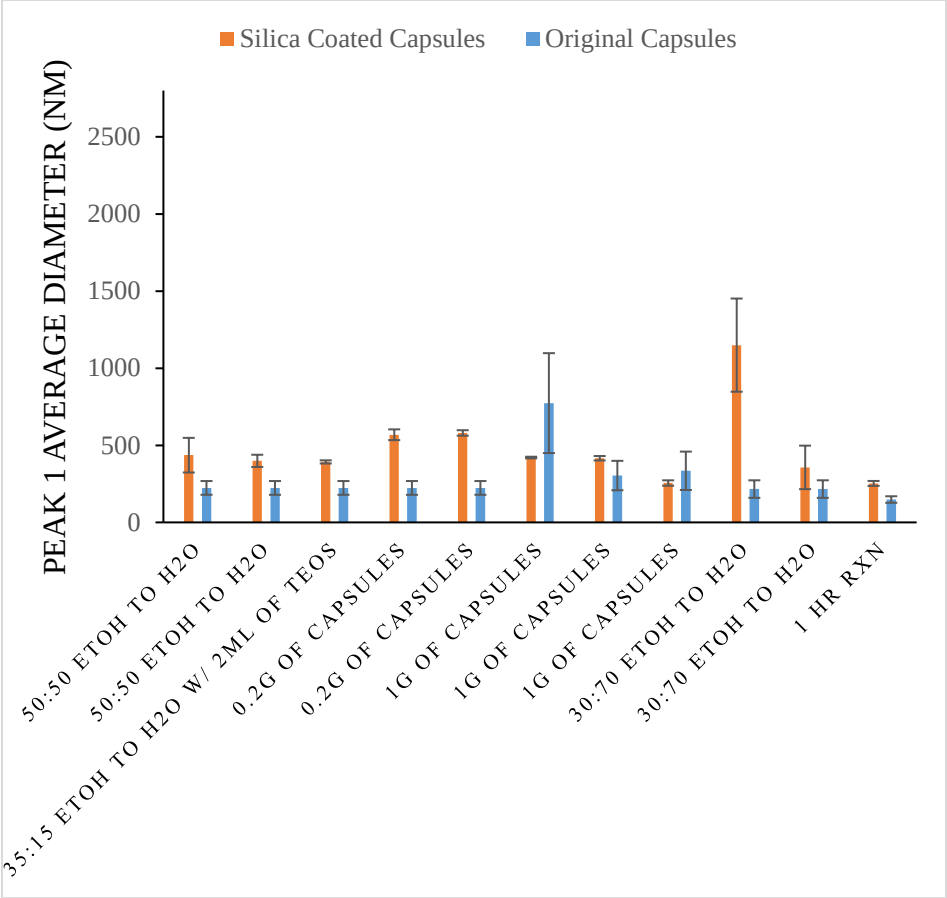

Figure 67. This figure portrays the size of the PU nanocapsules both before and after being coated with silica via the Stöber Method. The size of the particles increased when the silica was added to the outside of the capsules. This data was taken from the Peak 1 Average and not the overall average of the reading to prevent the large aggregates in the sample from skewing the data. It is important to note however that the raw data is mildly skewed due to aggregates of particles, both PU and silica, that were present when measuring the size. For this reason, the error bars in the figure are very large. It should be noted that there seems to be a decrease in the size of particles from original capsules in one of the syntheses methods. This is likely due to the fact that there were aggregates when the nanocapsules were sized initially. Another possibility is that there was a higher concentration of pure silica particles that did not coat nanocapsules that skewed the reading of the coated

capsules. Also, take note the variability among the error bars. They are adjusted to be one standard deviation of each of the three readings that were collected.

Biosilicification is similar to the Stöber method; however, weak basic amino acid (arginine) residues are used to control the reaction. Mahon et al. suggests that during the Stöber method, after nucleation, one is able to see a combination of aggregation and addition that contributes to particle growth rising.[126] This phenomenon then drops during the reaction due to the aggregation of the initial seeds. This process creates an incompletely condensed nano-porous core structure.[126] During biosilicification, small silica nanocapsules are formed in the water phase, and the TEOS is slowly hydrolyzed at the oil-water interface. The amino acid (arginine) is the catalyst for the silica condensation in the aqueous phase, and the TEOS is delivered heterogeneously. More specifically, TEOS will be added to an aqueous solution of the PU nanocapsules. Then, the amino acid will be added to the solution, and the solution will be stirred at room temperature for a various number of hours. Again, the particles will be washed by centrifugation in water. This process will ensure a very slow increase of the solution super-saturation and will allow particle growth through continuous monomer addition.[127]

The silica coated nanocapsules produced via biosilicification are expected to be denser and mechanically stronger than those synthesized by the Stöber method. The nanocapsules will be tested in the same way that those created with the Stöber method are tested. The concentrations of the amino acid and TEOS will be varied to find a ratio that will optimize the silica shell thickness while maintaining the nano-size of the capsules.

Some preliminary work has been performed to add silica to both the monomer and initiator capsules via the biosilicification method. Figure 68 shows PU capsules coated with silica using the method described in the previous paragraphs with a 3-hour reaction. More specifically, 0.5 g of capsules were resuspended in 50 mL of 190 proof ethanol. In a separate beaker, 4.4 g of arginine was resuspended in 50 mL of DI water. Then, 4 mL of TEOS was added to the capsule solution. Lastly, the arginine solution was poured into the capsule solution, and the solution was stirred at 300 rpm for 3 hours. After 3 hours, the solution was centrifuged at 10,000 rpm 3 times for 10 minutes each run. A defined and distinct pellet formed after each centrifugation. The supernatant was discarded after each wash and the pellet was resuspended in fresh DI water. After the centrifugation, the solution was frozen in liquid nitrogen and lyophilized until a white powder formed.

Notice in the TEM images in Figure 68, there is an abundant excess of silica. This amount of silica is detrimental in a resin because it decreases the capsule density in the system and thus decreases the number of capsules added to a resin. This essentially defeats the purpose of the self-healing system. The biosilicification synthesis is essentially two competing reactions. The trick in this synthesis is to find the optimal conditions in which the silica coats capsules and does not react with itself. To mitigate this issue, various components of the reaction must be varied to optimize the synthesis and decrease the amount of silica created while still allowing the silica to coat the capsules. The amount of arginine was varied to determine the optimal amount of arginine needed. Additionally, the amount of TEOS was varied as well as the mass of capsules.

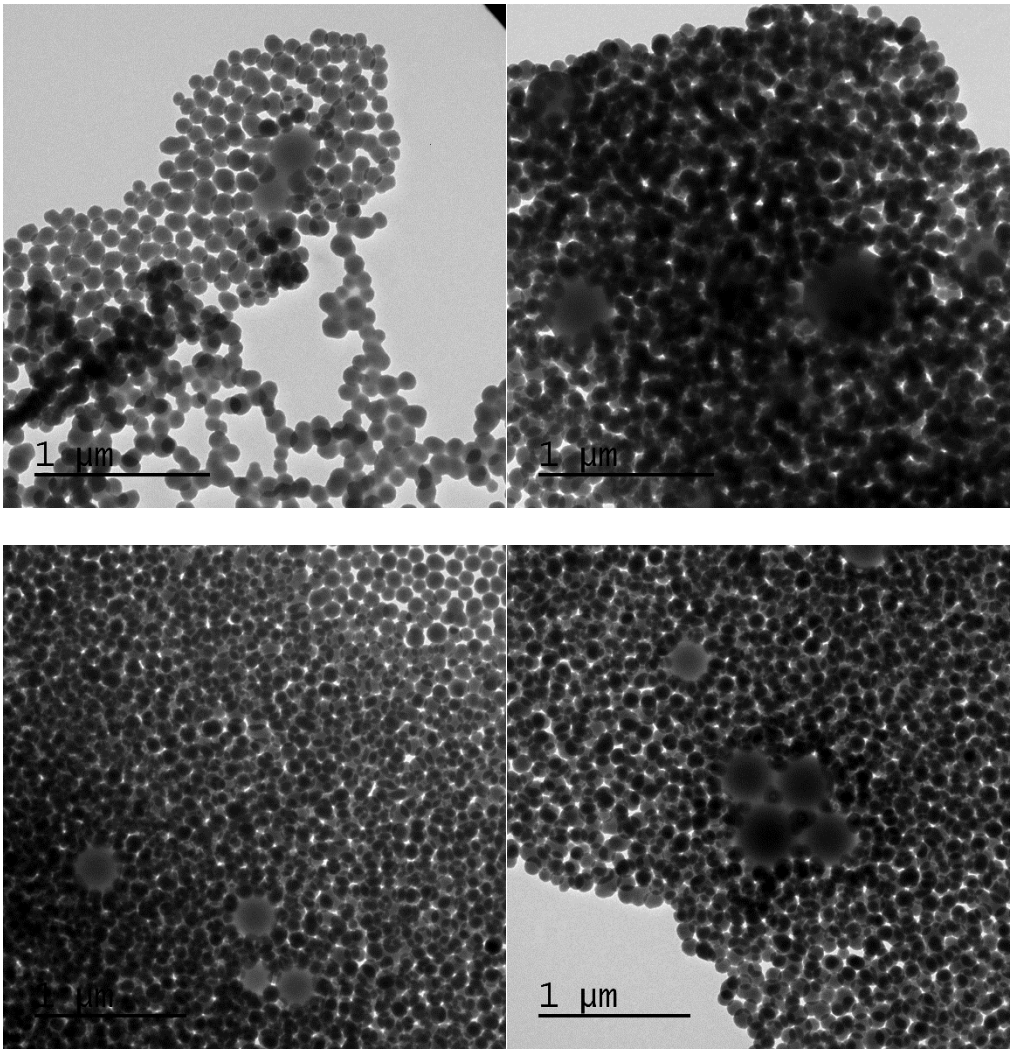

Figure 68. In these TEM images, the large spheres are the PU capsules and the small spheres are the silica that coat the capsules. Note that the darker regions in the images are locations where the silica is more densely populating the space.

The various syntheses methods were compared in a bar graph comparing the size of the coated capsules with the original size of the uncoated capsules. These syntheses included a 21-hour reaction, not a 3-hour reaction. It is important to note that the mass of capsules in all of the syntheses was held constant. In each method, 0.5 g of capsules were used, and a total of 100 mL of solvent was used. The data was collected via DLS and is shown in

Figure 69. Note that no succinct conclusion pertaining to the best synthesis method can be drawn from this data. More trials for each method need to be analyzed and better characterized and a smaller silica density must be present.

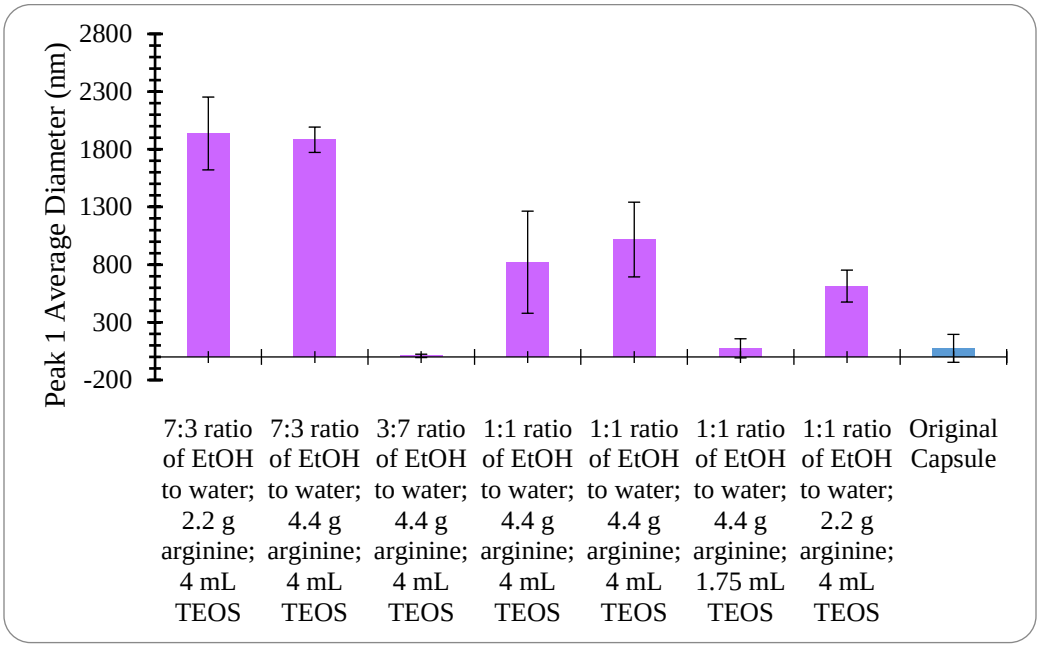

Figure 69. This figure portrays the size of the PU nanocapsules both before and after being coated with silica via biosilicification. The size of the particles mostly increased when the silica was added to the outside of the capsules. For the syntheses in which the capsules did not increase in size with the addition of silica, it is hypothesized that the large amount of pure silica in the sample skewed the data; in these sets, it can be assumed that only silica was characterized through DLS. All of the data was taken from the Peak 1 Average and not the overall average of the reading to prevent the large aggregates in the sample from skewing the data. It is important to note however that the raw data is mildly skewed due to aggregates of particles, both PU and silica, that were present when measuring the size. For this reason, the error bars in the figure are very large. They are adjusted to be one standard deviation of each of the three readings that were collected.

Using DLS, the size of the silica coated nanocapsules synthesized in both methods will be compared. Atomic force microscopy will be employed to determine the strength of the

silica shells, and X-ray diffraction will be used to measure the crystalline structure of the two types of silica shells. Lastly, to determine the encapsulation efficiency of the both types of silica-coated PU nanocapsules, fluorescent organic molecules, including fluorescein, will be used in place of the monomer/accelerator and initiator/stabilizer to measure the concentration of molecules released by the silica-coated capsules.

Mahon et al. suggests biosilicification is advantageous when compared to the Stöber method in terms of particle resistance to dissolution.[126] The silica shells synthesized via biosilicification are expected to be denser and therefore demonstrate higher strength properties when compared to the silica shells created via the Stöber method.

7.3 BROADER IMPACT

The broader impact of this project can be divided into 3 parts: the impact of dental health, the impact on orthopedic replacement longevity, and the impact of PU capsules in drug delivery. The project was originally begun to improve the longevity of dental resins. In recent years, dental resin-based composites have been replacing traditional mercury-containing amalgams for dental restorations. The amalgam's toxicity, both biologically and environmentally, has been debated for many years.[30] A dental resin is a type of synthetic composite filling. Unlike amalgams, composite fillings are bonded to the tooth and ultimately help to strengthen the weakened tooth.[128] However, the longevity of dental resins is limited, with half of all restorations failing in less than ten years.[129] Out of the 290-million cavities restored each year in the United States, 200-million are replaced due

to failed restorations.[130] Failed restorations are not only expensive but can also lead to life-threatening occurrences. If a crack in the resin is left untreated, infection can develop under the filling and trigger complications, such as an infection in the bloodstream or sepsis.[39] To combat the frequent failures in dental composites, self-healing techniques have been imparted.[84] These systems provide hope of autonomic repair to heal cracks and damages.[131] In recent years, a wide variety of self-healing chemistries have been developed, yet none have been employed in clinical studies due to a lack of biocompatibility and/or shortcomings in capsule mechanics and restoration abilities. This project, although not complete, has the potential to improve the lifespan of dental restorations that utilize dental resins by allowing dental resins to autonomously self-heal when the resins experience any type of degradation. Self-healing dental resins will reduce the cost of dental restorations and diminish the possibility of infection resulting from failure in dental resins.

Similar to use in dental resins, the self-healing capsule-based system created in this project has the potential to improve the longevity of orthopedic replacements. Mechanical failure in bone cement, used in orthopedic replacements, is postulated to be one of the main causes of mechanical failure in protheses, especially hip arthroplasties.[55] The fundamental problems associated with bone cement are fatigue and fracture of the cement and the osteolytic response to particulate debris.[79] The self-healing system created in this project has the potential to prevent and/or limit the amount of microcracking in the bone cement. This, in turn, would increase the lifetime of the cement and reduce the number of revision surgeries, thus decreasing the economic burdens these surgeries place on society and the potential of infection resulting from failure in the bone cement and/or from revision surgeries.

Moving in a completely different direction, the capsules intended for self-healing in resins have potential to have significant impacts in the drug delivery field. By understanding the rate at which encapsulated molecules will diffuse from the shell of the PU nanocapsules, the potential of these particles to be used for drug delivery is better understood. PU is one of the most common polymers currently used in medicine as they are biocompatible, thermally stable, biodegradable, and versatile.[69, 107] These capsules, while still requiring some modifications, have the potential to be used for sustained drug release or even controlled drug release. Drug delivery systems, if designed well, can influence patient adherence and tolerability of the drug. These systems offer steady blood level of the drug, which helps to avoid fluctuations which can lead to various side effects.[132]

Bibliography

1. Van Tittelboom, K.; De Belie, N., Self-Healing in Cementitious Materials—A Review. *Materials* **2013,** *6* (6), 2182.

2. P. Puska, D. P., P. E. Petersen, Dental Diseases and Oral Health. Organization, W. H., Ed. 2003.

3. Petersen, P. E.; Bourgeois, D.; Ogawa, H.; Estupinan-Day, S.; Ndiaye, C., The global burden of oral diseases and risks to oral health. *Bulletin of the World Health Organization* **2005,** *83* (9), 661-9.

4. *Future Use of Materials for Dental Restoration*; World Health Organization Geneva, Switzerland 2010; p 65.

5. Manhart, J.; Chen, H.; Hamm, G.; Hickel, R., Buonocore Memorial Lecture. Review of the clinical survival of direct and indirect restorations in posterior teeth of the permanent dentition. *Operative dentistry* **2004,** *29* (5), 481-508.

6. Bernardo, M.; Luis, H.; Martin, M. D.; Leroux, B. G.; Rue, T.; Leitao, J.; DeRouen, T. A., Survival and reasons for failure of amalgam versus composite posterior restorations placed in a randomized clinical trial. *Journal of the American Dental Association (1939)* **2007,** *138* (6), 775-83.

7. Shenoy, A., Is it the end of the road for dental amalgam? A critical review. *Journal of Conservative Dentistry : JCD* **2008,** *11* (3), 99-107.

8. White, S. R.; Sottos, N. R.; Geubelle, P. H.; Moore, J. S.; Kessler, M. R.; Sriram, S. R.; Brown, E. N.; Viswanathan, S., Autonomic healing of polymer composites. *Nature* **2001,** *409* (6822), 794-7.

9. Cluett, J. How Joint Replacement Implants Are Held in the Bone. https://www.verywellhealth.com/how-are-joint-replacements-held-in-the-bone-2549505 (accessed February 20, 2019).

10. Vaishya, R.; Chauhan, M.; Vaish, A., Bone cement. *Journal of clinical orthopaedics and trauma* **2013,** *4* (4), 157-163.

11. Lewis, G., Properties of acrylic bone cement: state of the art review. *Journal of biomedical materials research* **1997,** *38* (2), 155-82.

12. Pivec, R.; Johnson, A. J.; Mears, S. C.; Mont, M. A., Hip arthroplasty. *The Lancet* **2012,** *380* (9855), 1768-1777.

13. Sullivan, S. J. L.; Topoleski, L. D. T., Influence of initial component temperature on the apparent viscosity and handling characteristics of acrylic (PMMA) bone cement. *Journal of Biomedical Materials Research Part B: Applied Biomaterials* **2007,** *81B* (1), 224-230.

14. Topoleski, L. D.; Ducheyne, P.; Cuckler, J. M., The fracture toughness of titanium-fiber-reinforced bone cement. *Journal of biomedical materials research* **1992,** *26* (12), 1599-1617.

15. Aïssa, B.; Therriault, D.; Haddad, E.; Jamroz, W., Self-Healing Materials Systems: Overview of Major Approaches and Recent Developed Technologies. *Advances in Materials Science and Engineering* **2012,** *2012*, 17.

16. Brinkman, E. a. B. B., Self healing materials: concept and applications. 2 ed.; Agency, N., Ed. NL Agency: The Netherlands, 2011.

17. Jonkers, H. M., Self Healing Concrete: A Biological Approach. In *Self Healing Materials*, Springer Dordrecht: 2007; Vol. 100, pp 195-204.

18. Van Tittelboom, K.; Belie, N. D., Autogenous Healing of Cracks in Cementitious Materials with Varying Mix Compositions. In *Self-Healing Materials, 2nd International Conference, Proceedings*, 2009.

19. Yang, Y.; Ding, X.; Urban, M. W., Chemical and physical aspects of self-healing materials. *Progress in Polymer Science* **2015,** *49-50*, 34-59.

20. Brochu, A. B. W.; Craig, S. L.; Reichert, W. M., Self-healing biomaterials(). *Journal of biomedical materials research. Part A* **2011,** *96* (2), 492-506.

21. Malinskii, Y. M.; Prokopenko, V. V.; Ivanova, N. A.; Kargin, V. A., Investigation of self-healing of cracks in polymers. *Polymer Mechanics* **1970,** *6* (2), 240-244.

22. Ghosh, S. K., Self-Healing Materials: Fundamentals, Design Strategies, and Applications. In *Self-Healing Materials*, 2009.

23. Blaiszik, B. J.; Kramer, S. L. B.; Olugebefola, S. C.; Moore, J. S.; Sottos, N. R.; White, S. R., Self-Healing Polymers and Composites. *Annual Review of Materials Research* **2010**.

24. Diesendruck, C. E.; Sottos, N. R.; Moore, J. S.; White, S. R., Biomimetic Self-Healing. *Angewandte Chemie International Edition* **2015,** *54* (36), 10428-10447.

25. Alexander-Bryant, A. A.; Vanden Berg-Foels, W. S.; Wen, X., Bioengineering strategies for designing targeted cancer therapies. *Adv Cancer Res* **2013,** *118*, 1-59.

26. Kessler, M. R.; Sottos, N. R.; White, S. R., Self-healing structural composite materials. *Composites Part B: Engineering* **2003,** *A* (34), 11.

27. Diba, M.; Spaans, S.; Ning, K.; Ippel, B. D.; Yang, F.; Loomans, B.; Dankers, P. Y. W.; Leeuwenburgh, S. C. G., Self-Healing Biomaterials: From Molecular Concepts to Clinical Applications. *Advanced Materials Interfaces* **2018,** *5* (17), 1800118-n/a.

28. Brochu, A. B. W.; Craig, S. L.; Reichert, W. M., Self-healing biomaterials. *Journal of biomedical materials research. Part A* **2011,** *96* (2), 492-506.

29. National Center for Biotechnology Information.

30. Chin, G.; Chong, J.; Kluczewska, A.; Lau, A.; Gorjy, S.; Tennant, M., The environmental effects of dental amalgam. *Aust Dent J* **2000,** *45* (4), 246-9.

31. Habib, E.; Wang, R.; Wang, Y.; Zhu, M.; Zhu, X. X., Inorganic Fillers for Dental Resin Composites: Present and Future. *ACS Biomaterials Science & Engineering* **2016,** *2* (1), 1-11.

32. Spencer, P.; Ye, Q.; Misra, A.; Goncalves, S. E. P.; Laurence, J. S., Proteins, pathogens, and failure at the composite-tooth interface. *Journal of dental research* **2014,** *93* (12), 1243-1249.

33. Ferracane, J. L., Resin-based composite performance: are there some things we can't predict? *Dental materials : official publication of the Academy of Dental Materials* **2013,** *29* (1), 51-58.

34. Lee, J. J. W.; Kwon, J. Y.; Chai, H.; Lucas, P. W.; Thompson, V. P.; Lawn, B. R., Fracture Modes in Human Teeth. *Journal of Dental Research* **2009,** *88* (3), 224-228.

35. Taylor, T. D.; Agar, J. R., Twenty years of progress in implant prosthodontics. *The Journal of Prosthetic Dentistry* **2002,** *88* (1), 89-95.

36. Cramer, N. B.; Stansbury, J. W.; Bowman, C. N., Recent advances and developments in composite dental restorative materials. *Journal of dental research* **2011,** *90* (4), 402-416.

37. Opdam, N. J.; Loomans, B. A.; Roeters, F. J.; Bronkhorst, E. M., Five-year clinical performance of posterior resin composite restorations placed by dental students. *J Dent* **2004,** *32* (5), 379-83.

38. Murray, P. E.; Windsor, L. J.; Smyth, T. W.; Hafez, A. A.; Cox, C. F., Analysis of pulpal reactions to restorative procedures, materials, pulp capping, and future therapies. *Critical reviews in oral biology and medicine : an official publication of the American Association of Oral Biologists* **2002,** *13* (6), 509-20.

39. Staff, M. C., Cavities/tooth decay: Diagnosis. . In *Patient Care & Health Information* 2017.

40. Fugolin, A. P. P.; Pfeifer, C. S., New Resins for Dental Composites. *J Dent Res* **2017,** *96* (10), 1085-1091.

41. Bacchi, A.; Nelson, M.; Pfeifer, C. S., Characterization of methacrylate-based composites containing thio-urethane oligomers. *Dental Materials* **2016,** *32* (2), 233-239.

42. Moszner, N.; Fischer, U. K.; Angermann, J.; Rheinberger, V., Bis-(acrylamide)s as new cross-linkers for resin-based composite restoratives. *Dental Materials* **2006,** *22* (12), 1157-1162.

43. Gonzalez-Bonet, A.; Kaufman, G.; Yang, Y.; Wong, C.; Jackson, A.; Huyang, G.; Bowen, R.; Sun, J., Preparation of Dental Resins Resistant to Enzymatic and Hydrolytic Degradation in Oral Environments. *Biomacromolecules* **2015,** *16* (10), 3381-3388.

44. Song, H. B.; Sowan, N.; Shah, P. K.; Baranek, A.; Flores, A.; Stansbury, J. W.; Bowman, C. N., Reduced shrinkage stress via photo-initiated copper(I)-catalyzed cycloaddition polymerizations of azide-alkyne resins. *Dental Materials* **2016,** *32* (11), 1332-1342.

45. Podgorski, M.; Becka, E.; Chatani, S.; Claudino, M.; Bowman, C. N., Ester-free thiol-X resins: new materials with enhanced mechanical behavior and solvent resistance. *Polymer Chemistry* **2015,** *6* (12), 2234-2240.

46. Hoey, D.; Taylor, D., Quantitative analysis of the effect of porosity on the fatigue strength of bone cement. *Acta Biomater* **2009,** *5* (2), 719-26.

47. Stryker, Simplex P Bone Cement Products. *Stryker* **2006,** *2010*.

48. Deb, S., A review of improvements in acrylic bone cements. *Journal of biomaterials applications* **1999,** *14* (1), 16-47.

49. Total Knee Replacement Statistics 2017: Younger Patients Driving Growth. https://idataresearch.com/total-knee-replacement-statistics-2017-younger-patients-driving-growth/ (accessed February 20, 2019).

50. Kim, S., Changes in surgical loads and economic burden of hip and knee replacements in the US: 1997–2004. *Arthritis Care & Research* **2008,** *59* (4), 481-488.

51. Kindt-Larsen, T.; Smith, D. B.; Jensen, J. S., Innovations in acrylic bone cement and application equipment. *Journal of applied biomaterials : an official journal of the Society for Biomaterials* **1995,** *6* (1), 75-83.

52. Harrigan, T. P.; Harris, W. H., A three-dimensional non-linear finite element study of the effect of cement-prosthesis debonding in cemented femoral total hip components. *Journal of Biomechanics* **1991,** *24* (11), 1047-1058.

53. Spector, M., Biomaterial failure. *The Orthopedic clinics of North America* **1992,** *23* (2), 211.

54. Wilson, G. O.; Henderson, J. W.; Caruso, M. M.; Blaiszik, B. J.; McIntire, P. J.; Sottos, N. R.; White, S. R.; Moore, J. S., Evaluation of peroxide initiators for radical

polymerization-based self-healing applications. *Journal of Polymer Science Part A: Polymer Chemistry* **2010,** *48* (12), 2698-2708.

55. Deb, S.; Abdulghani, S.; Behiri, J. C., Radiopacity in bone cements using an organo-bismuth compound. *Biomaterials* **2002,** *23* (16), 3387-93.

56. Hill, J.; Orr, J.; Dunne, N., In vitro study investigating the mechanical properties of acrylic bone cement containing calcium carbonate nanoparticles. *Journal of materials science. Materials in medicine* **2008,** *19* (11), 3327-33.

57. Dunne, N. J.; Orr, J. F.; Mushipe, M. T.; Eveleigh, R. J., The relationship between porosity and fatigue characteristics of bone cements. *Biomaterials* **2003,** *24* (2), 239-245.

58. Topoleski, L. D. T.; Ducheyne, P.; Cukler, J. M., A fractographic analysis of in vivo poly(methyl methacrylate) bone cement failure mechanisms. *Journal of biomedical materials research* **1990,** *24* (2), 135-154.

59. James, S. P.; Jasty, M.; Davies, J.; Piehler, H.; Harris, W. H., A fractographic investigation of PMMA bone cenent focusing on the relationship between porosity reduction and increased fatigue life. *Journal of biomedical materials research* **1992,** *26* (5), 651-662.

60. Arora, M.; Chan, E. K.; Gupta, S.; Diwan, A. D., Polymethylmethacrylate bone cements and additives: A review of the literature. *World journal of orthopedics* **2013,** *4* (2), 67-74.

61. Awaja, F.; Zhang, S.; Tripathi, M.; Nikiforov, A.; Pugno, N., *Cracks, Microcracks and Fracture in Polymer Structures: Formation, Detection, Autonomic Repair*. 2016; Vol. 83.

62. Yuan, L.; Liang, G.-z.; Xie, J.-q.; He, S.-B., Synthesis and characterization of microencapsulated dicyclopentadiene with melamine–formaldehyde resins. *Colloid and Polymer Science* **2007,** *285* (7), 781-791.

63. Jin, H.; Mangun, C. L.; Stradley, D. S.; Moore, J. S.; Sottos, N. R.; White, S. R., Self-healing thermoset using encapsulated epoxy-amine healing chemistry. *Polymer* **2012,** *53* (2), 581-587.

64. Brown, E. N.; Kessler, M. R.; Sottos, N. R.; White, S. R., In situ poly(urea-formaldehyde) microencapsulation of dicyclopentadiene. *Journal of microencapsulation* **2003,** *20* (6), 719-730.

65. Yang, J.; Keller, M. W.; Moore, J. S.; White, S. R.; Sottos, N. R., Microencapsulation of Isocyanates for Self-Healing Polymers. *Macromolecules* **2008,** *41* (24), 9650-9655.

66. Yuan, Y. C.; Rong, M. Z.; Zhang, M. Q.; Chen, J.; Yang, G. C.; Li, X. M., Self-Healing Polymeric Materials Using Epoxy/Mercaptan as the Healant. *Macromolecules* **2008,** *41* (14), 5197-5202.

67. Liu, X.; Sheng, X.; Lee, J. K.; Kessler, M. R., Synthesis and Characterization of Melamine-Urea-Formaldehyde Microcapsules Containing ENB-Based Self-Healing Agents. *Macromolecular Materials and Engineering* **2009,** *294* (6-7), 389-395.

68. Huang, M.; Yang, J., Facile microencapsulation of HDI for self-healing anticorrosion coatings. *Journal of Materials Chemistry* **2011,** *21* (30), 11123-11130.

69. Santerre, J. P.; Woodhouse, K.; Laroche, G.; Labow, R. S., Understanding the biodegradation of polyurethanes: From classical implants to tissue engineering materials. *Biomaterials* **2005,** *26* (35), 7457-7470.

70. Simon, J.; Barla, F.; Kelemen-Haller, A.; Farkas, F.; Kraxner, M., Thermal stability of polyurethanes. *Chromatographia* **1988,** *25* (2), 99-106.

71. Zhu, D. Y.; Rong, M. Z.; Zhang, M. Q., Self-healing polymeric materials based on microencapsulated healing agents: From design to preparation. *Progress in Polymer Science* **2015,** *49-50*, 175-220.

72. Brochu, A. B. W.; Matthys, O. B.; Craig, S. L.; Reichert, W. M., Extended fatigue life of a catalyst free self-healing acrylic bone cement using microencapsulated 2-octyl cyanoacrylate. *Journal of biomedical materials research. Part B, Applied biomaterials* **2015,** *103* (2), 305-312.

73. Wertzberger, B. E.; Steere, J. T.; Pfeifer, R. M.; Nensel, M. A.; Latta, M. A.; Gross, S. M., Physical characterization of a self-healing dental restorative material. *Journal of Applied Polymer Science* **2010,** *118* (1), 428-434.

74. Biggs, P.; Jones, L.; Wellborn, B.; Lewis, G. In *A Self-healing PMMA Bone Cement: Influence of Crystal Size of Grubbs' Catalyst*, 25th Southern Biomedical Engineering Conference 2009, 15 – 17 May 2009, Miami, Florida, USA, Berlin, Heidelberg, 2009//; McGoron, A. J.; Li, C.-Z.; Lin, W.-C., Eds. Springer Berlin Heidelberg: Berlin, Heidelberg, 2009; pp 147-150.

75. Wu, J.; Weir, M. D.; Zhang, Q.; Zhou, C.; Melo, M. A. S.; Xu, H. H. K., Novel self-healing dental resin with microcapsules of polymerizable triethylene glycol dimethacrylate and N,N-dihydroxyethyl-p-toluidine. *Dental materials : official publication of the Academy of Dental Materials* **2016,** *32* (2), 294-304.

76. Caruso, M. M.; Delafuente, D. A.; Ho, V.; Sottos, N. R.; Moore, J. S.; White, S. R., Solvent-Promoted Self-Healing Epoxy Materials. *Macromolecules* **2007,** *40* (25), 8830-8832.

77. Ouyang, X.; Huang, X.; Pan, Q.; Zuo, C.; Huang, C.; Yang, X.; Zhao, Y., Synthesis and characterization of triethylene glycol dimethacrylate nanocapsules used in a self-healing bonding resin. *J Dent* **2011,** *39* (12), 825-33.

78. Dailey, M. M. C.; Silvia, A. W.; McIntire, P. J.; Wilson, G. O.; Moore, J. S.; White, S. R., A self-healing biomaterial based on free-radical polymerization. *Journal of Biomedical Materials Research Part A* **2014,** *102* (9), 3024-3032.

79. Gladman, A. S.; Celestine, A.-D. N.; Sottos, N. R.; White, S. R., Autonomic Healing of Acrylic Bone Cement. *Advanced Healthcare Materials* **2015,** *4* (2), 202-207.

80. Huyang, G.; Debertin, A. E.; Sun, J., Design and development of self-healing dental composites. *Materials & design* **2016,** *94*, 295-302.

81. Dewhirst, F. E.; Chen, T.; Izard, J.; Paster, B. J.; Tanner, A. C. R.; Yu, W.-H.; Lakshmanan, A.; Wade, W. G., The Human Oral Microbiome. *Journal of Bacteriology* **2010,** *192* (19), 5002.

82. The Anthropology of Modern Human Teeth. In *The Anthropology of Modern Human Teeth: Dental Morphology and Its Variation in Recent and Fossil Homo sapiens*, 2 ed.; Turner Ii, C. G.; Scott, G. R.; Townsend, G. C.; Martinón-Torres, M., Eds. Cambridge University Press: Cambridge, 2018; pp i-ii.

83. Ruben, J. L.; Roeters, F. J. M.; Montagner, A. F.; Huysmans, M. C. D. N. J. M., A multifunctional device to simulate oral ageing: the "Rub&Roll". *Journal of the Mechanical Behavior of Biomedical Materials* **2014,** *30*, 75-82.

84. Bekas, D. G.; Tsirka, K.; Baltzis, D.; Paipetis, A. S., Self-healing materials: A review of advances in materials, evaluation, characterization and monitoring techniques. *Composites Part B: Engineering* **2016,** *87*, 92-119.

85. C, C. J.; Bharat, B., Bioinspired self-healing materials: lessons from nature. *Beilstein Journal of Nanotechnology* **2018,** *9*, 907-935.

86. Brochu, A. B. W.; Chyan, W. J.; Reichert, W. M., Microencapsulation of 2-octylcyanoacrylate tissue adhesive for self-healing acrylic bone cement. *Journal of Biomedical Materials Research Part B: Applied Biomaterials* **2012,** *100B* (7), 1764-1772.

87. Joseph, C.; Jefferson, A. D.; Isaacs, B.; Lark, R.; Gardner, D., Experimental investigation of adhesive-based self-healing of cementitious materials. *Magazine of Concrete Research* **2010,** *62* (11), 831-843.

88. Srinivasan, P. K.; Sperber, V.; Afify, M.; Tanaka, H.; Fukushima, K.; Kögel, B.; Gremse, F.; Tolba, R., Novel synthetic adhesive as an effective alternative to Fibrin based adhesives. *World journal of hepatology* **2017,** *9* (24), 1030-1039.

89. Torini, L.; Argillier, J. F.; Zydowicz, N., Interfacial Polycondensation Encapsulation in Miniemulsion. *Macromolecules* **2005,** *38* (8), 3225-3236.

90. GUO Jinxin, P. Q., HUANG Cui, ZHAO Yanbing, OUYANG Xiaobai, HUO Yonghong, and DUAN Sansan, The Role of Surfactant and Costabilizer in Controlling Size of Nanocapsules Containing TEGDMA in Miniemulsion. **2009,** *24* (6).

91. Hung, W. C.; Shau, M. D.; Kao, H. C.; Shih, M. F.; Cherng, J. Y., The synthesis of cationic polyurethanes to study the effect of amines and structures on their DNA transfection potential. *Journal of Controlled Release* **2009,** *133* (1), 68-76.

92. Sobczak, M., Synthesis and Characterization of Polyurethanes Based on Oligo(ϵ-caprolactone) Prepared by Free-Metal Method. *Journal of Macromolecular Science, Part A* **2011,** *48* (5), 373-380.

93. Asefnejad, A.; Khorasani, M. T.; Behnamghader, A.; Farsadzadeh, B.; Bonakdar, S., Manufacturing of biodegradable polyurethane scaffolds based on polycaprolactone using a phase separation method: physical properties and in vitro assay. *International journal of nanomedicine* **2011,** *6*, 2375-2384.

94. Achilias, D. S.; Sideridou, I. D., Kinetics of the Benzoyl Peroxide/Amine Initiated Free-Radical Polymerization of Dental Dimethacrylate Monomers: Experimental Studies and Mathematical Modeling for TEGDMA and Bis-EMA. *Macromolecules* **2004,** *37* (11), 4254-4265.

95. Mrzezo Polymerization Reactions. https://pocketdentistry.com/5-acrylic/.

96. Reusch, W. Synthesis of Addition Polymers. https://chem.libretexts.org/Textbook_Maps/Organic_Chemistry/Supplemental_Modules_(Organic_Chemistry)/Polymers/Synthesis_of_Addition_Polymers.

97. Young, R. J.; Lovell, P. A., *Introduction to Polymers : Second Edition*. Chapman & Hall: London, 1991; p 443.

98. Yehye, W. A.; Rahman, N. A.; Ariffin, A.; Abd Hamid, S. B.; Alhadi, A. A.; Kadir, F. A.; Yaeghoobi, M., Understanding the chemistry behind the antioxidant activities of butylated hydroxytoluene (BHT): A review. *European Journal of Medicinal Chemistry* **2015,** *101*, 295-312.

99. Wu, J.; Weir, M. D.; Melo, M. A. S.; Xu, H. H. K., Development of novel self-healing and antibacterial dental composite containing calcium phosphate nanoparticles. *Journal of Dentistry* **2015,** *43* (3), 317-326.

100. Sideridou, I. D.; Achilias, D. S.; Karava, O., Reactivity of Benzoyl Peroxide/Amine System as an Initiator for the Free Radical Polymerization of Dental and Orthopaedic Dimethacrylate Monomers: Effect of the Amine and Monomer Chemical Structure. *Macromolecules* **2006,** *39* (6), 2072-2080.

101. Schroeder, W. F.; Vallo, C. I., Effect of different photoinitiator systems on conversion profiles of a model unfilled light-cured resin. *Dental Materials* **2007,** *23* (10), 1313-1321.

102. Keller, M.; Sottos, N., *Mechanical Properties of Microcapsules Used in a Self-Healing Polymer*. 2006; Vol. 46, p 725-733.

103. Jesson, D. A.; Watts, J. F., The Interface and Interphase in Polymer Matrix Composites: Effect on Mechanical Properties and Methods for Identification. *Polymer Reviews* **2012,** *52* (3), 321-354.

104. Lv, L.; Schlangen, E.; Yang, Z.; Xing, F., Micromechanical Properties of a New Polymeric Microcapsule for Self-Healing Cementitious Materials. *Materials (Basel, Switzerland)* **2016,** *9* (12), 1025.

105. Dowling , N. E., *Mechanical Behavior of Materials: Engineering Methods for Deformation, Fracture, and Fatigue*. 3 ed.; Pearson Prentice Hall: Upper Saddle River, 2007.

106. Wool, R. P.; O'Connor, K. M., A theory crack healing in polymers. *Journal of Applied Physics* **1981,** *52* (10), 5953-5963.

107. Cherng, J. Y.; Hou, T. Y.; Shih, M. F.; Talsma, H.; Hennink, W. E., Polyurethane-based drug delivery systems. *International Journal of Pharmaceutics* **2013,** *450* (1), 145-162.

108. Guo, Q.; Knight, P. T.; Mather, P. T., Tailored drug release from biodegradable stent coatings based on hybrid polyurethanes. *Journal of controlled release : official journal of the Controlled Release Society* **2009,** *137* (3), 224-33.

109. Shimanovich, U.; Bernardes, G. J. L.; Knowles, T. P. J.; Cavaco-Paulo, A., Protein micro- and nano-capsules for biomedical applications. *Chemical Society Reviews* **2014,** *43* (5), 1361-1371.

110. Frank, L. A.; Contri, R. V.; Beck, R. C. R.; Pohlmann, A. R.; Guterres, S. S., Improving drug biological effects by encapsulation into polymeric nanocapsules. *Wiley Interdisciplinary Reviews: Nanomedicine and Nanobiotechnology* **2015,** *7* (5), 623-639.

111. Musyanovych, A.; Landfester, K., Polymer Micro- and Nanocapsules as Biological Carriers with Multifunctional Properties. *Macromolecular Bioscience* **2014,** *14* (4), 458-477.

112. Preiß, T.; Zimpel, A.; Wuttke, S.; Rädler, J. O., Kinetic Analysis of the Uptake and Release of Fluorescein by Metal-Organic Framework Nanoparticles. *Materials (Basel, Switzerland)* **2017,** *10* (2), 216.

113. Su, J. F.; Wang, L. X.; Ren, L.; Huang, Z.; Meng, X. W., Preparation and characterization of polyurethane microcapsules containing n-octadecane with styrene-maleic anhydride as a surfactant by interfacial polycondensation. *Journal of Applied Polymer Science* **2006,** *102* (5), 4996-5006.

114. Vermonden, T.; Censi, R.; Hennink, W. E., Hydrogels for protein delivery. *Chemical reviews* **2012,** *112* (5), 2853-88.

115. Arifin, D. Y.; Lee, L. Y.; Wang, C. H., Mathematical modeling and simulation of drug release from microspheres: Implications to drug delivery systems. *Advanced drug delivery reviews* **2006,** *58* (12-13), 1274-325.

116. Storey, R. F.; Hickey, T. P., Degradable polyurethane networks based on d,l-lactide, glycolide, ε-caprolactone, and trimethylene carbonate homopolyester and copolyester triols. *Polymer* **1994,** *35* (4), 830-838.

117. Guan, J.; Sacks, M. S.; Beckman, E. J.; Wagner, W. R., Biodegradable poly(ether ester urethane)urea elastomers based on poly(ether ester) triblock copolymers and putrescine: synthesis, characterization and cytocompatibility. *Biomaterials* **2004,** *25* (1), 85-96.

118. Huang, S. J., Biodegradation of polyurethanes derived from polycaprolactonediols. *Am. Chem. Soc. Symp. Ser.* **1981,** *172*, 471-487.

119. Tang, Y. W.; Labow, R. S.; Santerre, J. P., Enzyme-induced biodegradation of polycarbonate-polyurethanes: Dependence on hard-segment chemistry. *Journal of biomedical materials research* **2001,** *57* (4), 597-611.

120. Shoaib, M.; Bahadur, A.; Iqbal, S.; Rahman, M. S. U.; Ahmed, S.; Shabir, G.; Javaid, M. A., Relationship of hard segment concentration in polyurethane-urea elastomers with mechanical, thermal and drug release properties. *Journal of Drug Delivery Science and Technology* **2017,** *37*, 88-96.

121. Feng, X.; Wang, G.; Neumann, K.; Yao, W.; Ding, L.; Li, S.; Sheng, Y.; Jiang, Y.; Bradley, M.; Zhang, R., Synthesis and characterization of biodegradable poly(ether-

ester) urethane acrylates for controlled drug release. *Materials Science and Engineering: C* **2017,** *74*, 270-278.

122. Weast, R. C.; Astle, M. J., *CRC handbook of data on organic compounds*. CRC Press: Boca Raton, Fla., 1985.

123. Jackson, A. C.; Bartelt, J. A.; Marczewski, K.; Sottos, N. R.; Braun, P. V., Silica-Protected Micron and Sub-Micron Capsules and Particles for Self-Healing at the Microscale. *Macromolecular Rapid Communications* **2011,** *32* (1), 82-87.

124. Wong, Y. J.; Zhu, L.; Teo, W. S.; Tan, Y. W.; Yang, Y.; Wang, C.; Chen, H., Revisiting the Stöber Method: Inhomogeneity in Silica Shells. *Journal of the American Chemical Society* **2011,** *133* (30), 11422-11425.

125. Graf, C.; Vossen, D. L. J.; Imhof, A.; van Blaaderen, A., A General Method To Coat Colloidal Particles with Silica. *Langmuir* **2003,** *19* (17), 6693-6700.

126. Mahon, E.; Hristov, D. R.; Dawson, K. A., Stabilising fluorescent silica nanoparticles against dissolution effects for biological studies. *Chem Commun (Camb)* **2012,** *48* (64), 7970-2.

127. Fouilloux, S.; Daillant, J.; Thill, A., Single step synthesis of 5–30nm monodisperse silica nanoparticles: Important experimental parameters and modeling. *Colloids and Surfaces A: Physicochemical and Engineering Aspects* **2012,** *393*, 122-127.

128. Nejad, M., Should Amalgam (Silver) Fillings be replaced? Biomimetic Dentistry, 2014; Vol. 2018.

129. Sakaguchi, R. L., Review of the current status and challenges for dental posterior restorative composites: clinical, chemistry, and physical behavior considerations. Summary of discussion from the Portland Composites Symposium (POCOS) June 17-19,

2004, Oregon Health and Science University, Portland, Oregon. *Dental materials : official publication of the Academy of Dental Materials* **2005,** *21* (1), 3-6.

130. Goldberg, M., In vitro and in vivo studies on the toxicity of dental resin components: a review. *Clin Oral Investig* **2008,** *12* (1), 1-8.

131. Wu, D. Y.; Meure, S.; Solomon, D., Self-healing polymeric materials: A review of recent developments. *Progress in Polymer Science* **2008,** *33* (5), 479-522.

132. Leahy, L. G., From Immediate Release to Long Acting Drug Delivery Systems What Do They Mean and Why Do They Matter? *JOURNAL OF PSYCHOSOCIAL NURSING AND MENTAL HEALTH SERVICES* **2017,** *55* (5), 19-23.